

Aus dem Institut für Schlaganfall- und Demenzforschung (ISD)

Institut der Ludwig-Maximilians-Universität München

Vorstand: Prof. Dr. med. Martin Dichgans



The Role of MIF-2 in Obesity-induced Wound Healing Disorder

Dissertation
zum Erwerb des Doktorgrades der Naturwissenschaften
an der Medizinischen Fakultät der
Ludwig-Maximilians-Universität München

vorgelegt von

Kevin Arnke

aus

Rheine

Jahr

2022

Mit Genehmigung der Medizinischen Fakultät
der Universität München

Betreuer: Prof. Dr. Jürgen Bernhagen

Zweitgutachter: Prof. Dr. Christian Ries

Dekan: Prof. Dr. med. Thomas Gudermann

Tag der mündlichen Prüfung: 13. April 2023

Table of content

Table of content	I
Abstract	VI
Zusammenfassung.....	VIII
List of figures.....	X
List of tables	XII
List of abbreviations	XIII
1. Introduction	1
1.1 Cutaneous wound healing mechanism and its pathophysiology	1
1.1.1 Structure of the skin.....	1
1.1.2 Fundamentals of the wound healing process	3
1.1.3 Wound healing disorder.....	6
1.1.4 Obesity-induced chronic wounds.....	7
1.2 Mouse wound model to mimic human skin reconstruction	8
1.2.1 Murine skin vs human skin	8
1.2.2 Differences in murine and human wound healing.....	9
1.3 Fibroblasts.....	10
1.3.1 Fibroblasts in the human body.....	10
1.3.2 Fibroblasts and their role in wound repair.....	11
1.3.3 Myofibroblast differentiation signaling cascades.....	12
1.4 Macrophage migration inhibitor factor (MIF) protein family	13
1.4.1 MIF and its receptors	13
1.4.2 MIF-2, a new member of MIF-protein family.....	14
1.4.3 MIF protein family in adipose tissue and obesity	15
1.4.4 MIF protein family in inflammation	16
1.4.5 The MIF protein family in wound healing	17

Table of content

2.	Aims	19
3.	Materials	20
3.1	Mouse strains.....	20
3.2	Mouse chows	20
3.3	Patient characteristics	21
3.4	Chemicals, reagents, media and drugs.....	21
3.5	Cell culture media and buffers.....	24
3.5.1	Cell culture media	24
3.5.2	Buffer for the gel contraction assay.....	24
3.6	Primers.....	25
3.7	Antibodies	26
3.8	Consumables	27
3.9	Devices	28
3.10	Software.....	30
4.	Methods	31
4.1	<i>in vivo</i> techniques.....	31
4.1.1	High fat diet (HFD) and weight measurement.....	31
4.1.2	Wound healing model.....	31
4.1.3	Macroscopic analysis of the wounds and wound scoring	32
4.1.4	Sample collection	33
4.2	Histology and immunohistochemistry.....	33
4.2.1	Masson-Goldner's trichrome staining	33
4.2.2	Immunohistochemical staining.....	34
4.3	Molecular biological analyses of the wound tissue.....	35
4.3.1	RNA isolation from mouse wound tissue	35
4.3.2	Reverse transcription and real-time quantitative polymerase chain reaction (RT-qPCR)	36

Table of content

4.4	Murine fibroblast cell line NIH/3T3 differentiation	36
4.4.1	FACS-flow cytometry	37
4.4.2	Collagen gel contraction assay	37
4.5	Human primary cells	38
4.5.1	Isolation and culture of human fibroblasts	38
4.5.2	Isolation of human stromal vascular fraction (SVF)	39
4.5.3	Producing of SVF-conditioned medium (SVF-CM)	40
4.5.4	Viability assay with SVF-CM and rMIF-2 treatment	40
4.6	Statistics.....	41
5.	Results	42
5.1	<i>In vivo</i> experiments	42
5.1.1	Weight gain of C57BL/6 wild type and <i>Mif-2^{-/-}</i> mice under RD or HFD	42
5.1.2	Wound size measurement.....	44
5.2	Immunohistochemical and immunocytochemical staining of wound tissue.....	49
5.2.1	Collagen determination in wound tissue via Masson-Goldner's trichrome staining.....	50
5.2.2	Myofibroblast determination in wound tissue via expression of α -smooth muscle actin	53
5.2.3	Cell proliferation in wound area via expression of Ki-67	55
5.2.4	Inflammation and macrophage infiltration via expression of TNF- α and F4/80	55
5.2.5	Angiogenesis via expression of CD31	57
5.3	Wound tissue analysis on genetic level via RT-qPCR.....	58
5.3.1	Expression of genes coding for collagen types.....	58
5.3.2	Expression of various genes related to extracellular matrix.....	60
5.3.3	Expression of genes related to growth factors that activate fibroblast differentiation.....	61

Table of content

5.3.4	Expression of genes related to re-epithelization	62
5.3.5	Expression of genes related to macrophages.....	63
5.3.6	Expression of genes coding for macrophage migration inhibitor factor protein family.....	64
5.4	CD74 receptor expression during differentiation of NIH/3T3 cells.....	65
5.5	Collagen gel contraction assay	66
5.6	Impact of rMIF-2 on primary human dermal fibroblast (HDF) proliferation	68
6.	Discussion.....	72
6.1	Obesity and <i>Mif-2</i> ^{-/-} results in delayed wound healing.....	72
6.2	Consequences of impaired <i>Mif-2</i> expression	73
6.2.1	Influence of MIF-2 on the differentiation of myofibroblasts.....	73
6.2.2	MIF-2 and the myofibroblast differentiation pathway.....	74
6.2.3	Direct consequences of diminished myofibroblast differentiation.....	75
6.2.4	Further consequences of a delayed myofibroblast differentiation	76
6.2.5	Impact on re-epithelialization and keratinocytes associated growth factors	77
6.3	Increased wound tissue inflammation caused by low MIF-2 levels	78
6.4	Obesity-induced secretion changes without MIF-2 influence	79
6.5	The right amount of MIF-2.....	80
6.5.1	Inhibitory alternative pathway of MIF-2 in myofibroblast differentiation	80
6.5.2	The positive and negative influence of MIF-2 on cell viability.....	81
6.6	Conclusion and outlook.....	82
7.	References.....	85
Appendix	97
Score Sheet	97
Score Legend	98
Acknowledgements	99

Table of content

Affidavit	100
Confirmation of congruency	Fehler! Textmarke nicht definiert.
Curriculum vitae	101
List of publications.....	103

Abstract

Wounds that do not undergo sufficient healing or even become chronic wounds represent a major challenge for medicine. Obese individuals are prone to non-healing wounds. In this context, the adipose tissue can become chronically inflamed, causing a pathological alteration at the molecular and cellular level. This results in impaired cell migration, proliferation and differentiation, as well as a reduced angiogenesis. Since the adipose tissue is located in immediate vicinity of cutaneous wounds and is involved in wound healing, the obesity-induced cellular and molecular changes also negatively influence the wound healing process. Although obesity-induced chronic wounds have been studied for a long time and a lot is known, there our understanding of the mechanisms is still limited.

One pathologically altered protein family is the macrophage migration inhibitor factor (MIF) family, in human encompassing MIF and MIF-2. While MIF has been well studied, MIF-2 was only recently discovered as a homologue of MIF. Both bind to the same receptor, CD74, while only MIF interacts with CXCR2, and they differ in various systemic conditions e.g. in obesity, in which MIF is increased and MIF-2 is decreased. In inflammation, MIF polarizes macrophages towards a pro-inflammatory M1-like phenotype and MIF-2 towards an anti-inflammatory M2-like subtype. The role of MIF in wound healing is still controversially discussed, but it seems that its function differs in distinct phases and tissue types. MIF-2 was recently reported to exhibit a positive effect on wound healing.

Thus, in this thesis, the role of MIF-2 in wound healing was investigated in a murine wound healing model employing *Mif-2^{-/-}* mice, accompanied by mechanistic *in vitro* experiments. Both mice groups, the obese wild type as well as the *Mif-2^{-/-}* mice showed a delayed wound healing when compared to the control lean wild type mice. Their wound sizes became even wider during the first days. Immunohistochemical analysis confirmed the impaired healing process in obese and *Mif-2^{-/-}* mice. Furthermore, tissue examinations and genetic analysis showed reduced collagen production and granulation tissue formation as well as a diminished myofibroblast differentiation, which was most pronounced in the *Mif-2^{-/-}* mice. In *in vitro* experiments, NIH/3T3 cells were differentiated into myofibroblasts when treated with recombinant MIF-2 or a MIF-2 inhibitor. When MIF-2 was inhibited, differentiation potential

decreased sharply even at low doses. At higher concentrations of recombinant MIF-2, cell differentiation was also partially reduced.

My experiments revealed that MIF-2 is crucial for the differentiation from “wound fibroblasts” into myofibroblasts, which are primarily responsible for collagen production and formation of granulation tissue. In an *in vivo* wound model characterized by obese and *Mif-2^{-/-}* mice as well as applying *in vitro* pathway analyses, the deletion of MIF-2 resulted in an impaired differentiation and wound closure. It appeared that MIF-2 influenced the canonical TGF- β /Smad pathway, the main pathway for myofibroblasts differentiation, via an ERK1/2-MAPK downstream cascade and a so far unknown key protein. However, I also obtained evidence in my thesis that an excess of MIF-2 leads to a partial inhibition of the differentiation, most likely also via ERK1/2, suggestive of a differential dose behavior.

In conclusion, the obesity-induced downregulation of MIF-2 seems to be one major reason for a delayed and insufficient wound healing process in obese individuals. Furthermore, my results indicates that this impairment is caused by diminished myofibroblast differentiation resulting in delayed granulation tissue formation.

Zusammenfassung

Nicht ausreichend heilende Wunden und chronische Wunden stellen eine große Herausforderung für die Medizin dar. Übergewichtige Personen sind anfälliger für nicht heilende Wunden. Ihr Fettgewebe ist chronisch entzündet, was eine pathologische Veränderung auf molekularer und zellulärer Ebene zur Folge hat. Dies führt zu einer beeinträchtigten Zellmigration, -proliferation und -differenzierung sowie einer verminderten Angiogenese. Da sich das Fettgewebe in unmittelbarer Nähe zu kutanen Wunden befindet und an der Wundheilung beteiligt ist, beeinflussen durch Fettleibigkeit bedingte zelluläre und molekulare Veränderungen auch die Wundheilung negativ. Obwohl Adipositas-induzierte chronische Wunden seit langem untersucht werden und bereits einiges darüber bekannt ist, fehlt noch viel, um den gesamten Mechanismus zu verstehen.

Eine pathologisch veränderte Protein Gruppe ist die Makrophagen Migration Inhibition Faktor (MIF) Familie, MIF und MIF-2. Während MIF seit langem gut erforscht ist, wurde MIF-2 erst kürzlich als MIF-Homolog entdeckt. Beide binden an denselben Rezeptor, CD74, unterscheiden sich jedoch in verschiedenen systemischen Zuständen wie bei Fettleibigkeit, MIF ist erhöht und MIF-2 erniedrigt. Bei Entzündungen polarisiert MIF Makrophagen zum pro-inflammatorischen M1 und MIF-2 zum anti-inflammatorischen M2 Phänotypen. Die Rolle von MIF in der Wundheilung wird noch kontrovers diskutiert, aber seine Funktion scheint sich in verschiedenen Phasen und Gewebetypen zu unterscheiden. Kürzlich gab es Hinweise für einen positiven Effekt von MIF-2 auf die Wundheilung.

Daher wurde in dieser Arbeit die Rolle von MIF-2 bei der Wundheilung in einem murinen Wundheilungsmodell mit *Mif-2^{-/-}* Mäusen untersucht und mit *in-vitro* Experimenten zum Mechanismus untermauert. Sowohl die adipösen Wildtypen als auch die *Mif-2^{-/-}* Mäuse wiesen eine verzögerte Wundheilung auf im Vergleich zu den normalgewichtigen Kontrollmäusen. Während den ersten Tagen hat sich das Wundareal sogar erweitert. Immunhistologische Analysen bestätigten den verschlechterten Heilungsprozess in der adipösen und in der *Mif-2^{-/-}* Gruppe. Zusätzlich wiesen Gewebeanalysen und genetische Untersuchungen eine reduzierte Produktion von Kollagen und des Granulationsgewebes auf, sowie eine verminderte Myofibroblastendifferenzierung, welche am stärksten bei den *Mif-2^{-/-}* Mäusen

vorhanden war. NIH/3T3 Zellen wurden in *in-vitro* Experimenten zu Myofibroblasten differenziert unter der Behandlung von rekombinantem MIF-2 oder einem MIF-2 Inhibitor. Wenn die Zellen mit dem MIF-2 Inhibitor behandelt wurden, sank das Differenzierungspotential bereits bei geringer Konzentration rapide ab. Ebenso hatten hohe Dosen vom rekombinantem MIF-2 eine partielle Reduzierung der Differenzierbarkeit zur Folge.

In meiner Arbeit konnte ich zeigen, dass MIF-2 eine zentrale Rolle für die Differenzierung von "Wund-Fibroblasten" zu Myofibroblasten hat, welche hauptverantwortlich sind für die Kollagenproduktion und für die Bildung des Granulationsgewebes. Sowohl in dem *in-vivo* Wundheilungsmodell als auch in den *in-vitro* Mechanismusanalysen führte die Deletion von MIF-2 zu einer beeinträchtigten Differenzierung und Wundschliessung. Es scheint, dass MIF-2 den kanonischen TGF- β /Smad-Weg, den Hauptweg für die Differenzierung von Myofibroblasten, über die ERK1/2-MAPK-Downstream-Kaskade beeinflusst und ein bisher unbekanntes Schlüsselprotein ist. Allerdings wurde in der Dissertation auch gezeigt, dass ein Überschuss an MIF-2 auch zu einer teilweisen Hemmung der Differenzierung führt, höchstwahrscheinlich auch über ERK1/2.

Zusammengefasst scheint die durch Fettleibigkeit induzierte Herunterregulation von MIF-2 ein Hauptfaktor für die verzögerte und unzureichende Wundheilung zu sein, welche bei Adipositas beobachtet werden kann. Weiterhin geben meine Ergebnisse Hinweise darauf, dass die Beeinträchtigung durch eine verminderte Differenzierung von Myofibroblasten herführt, wodurch die Bildung von Granulationsgewebe verzögert wird.

List of figures

Figure 0.1: Anatomical structure and cell composition of human skin.	3
Figure 1.2: Temporal description of the four wound healing phases.	6
Figure 1.3: Comparison of human (left) and murine (right) skin morphology.	9
Figure 1.4: TGF- β initiated signaling pathways for gene transcription.	12
Figure 1.5: X-ray structure of human MIF superfamily members; (A) D-DT/ MIF-2, (B) MIF.	15
Figure 4.1: Incisional and excisional wound model.	32
Figure 4.2: Picture of the designed device to ensure always the same distance from camera to the wound.	33
Figure 4.3: Phases of digested fat tissue after centrifugation.	40
Figure 5.1: Weight gain of (A) wild type (WT) and (B) <i>Mif-2</i> ^{-/-} C57BL/6 male mice under regular diet (RD) and high fat diet (HFD).	43
Figure 5.2: Weight gain of wild type (WT) and <i>Mif-2</i> ^{-/-} C57BL/6 male mice under (A) regular diet and (B) high fat diet.	43
Figure 5.3: Representative wound photos from one mouse in each group in an excisional wound model.	44
Figure 5.4: Wound area in an excisional wound model in wild type (WT) and <i>Mif-2</i> ^{-/-} C57BL/6 male mice under regular diet (RD) and high fat diet (HFD).	45
Figure 5.5: Wound size in an excisional wound model in wild type C57BL/6 male mice under regular diet (RD) and high fat diet (HFD).	46
Figure 5.6: Wound size in an excisional wound model in <i>Mif-2</i> ^{-/-} C57BL/6 male mice under regular diet (RD) and high fat diet (HFD).	47
Figure 5.7: Wound area in an excisional wound model in wild type (WT) and <i>Mif-2</i> ^{-/-} C57BL/6 male mice under regular diet.	48
Figure 5.8: Wound area in an excisional wound model in wild type (WT) and <i>Mif-2</i> ^{-/-} C57BL/6 male mice under high fat diet.	49
Figure 5.9: Representative tissue slights stained by the Masson-Goldner's trichrome procedure.	51
Figure 5.10: Quality of newly formed granulation tissue in an incisional murine wound model.	52
Figure 5.11: Determination of tissue thickness of newly formed granulation tissue in an incisional murine wound healing model.	52

Figure 5.12: Representative tissue slights stained by anti- α -smooth muscle actin (α -SMA).	54
Figure 5.13: Expression of α -SMA protein in wound tissue by IHC.	54
Figure 5.14: Expression of Ki67 protein in healthy skin tissue and wound tissue by IHC.	55
Figure 5.15: Expression of TNF- α protein in healthy skin tissue and wound tissue by IHC.	56
Figure 5.16: Expression of F4/80 protein in wound tissue by IHC.	57
Figure 5.17: Blood vessel production in newly formed granulation tissue.	58
Figure 5.18: Relative mRNA expression of three collagen types in wound tissue from an incisional wound model.	59
Figure 5.19: Relative mRNA expression of extracellular matrix related proteins in wound tissue from an incisional wound model.	61
Figure 5.20: Relative mRNA expression of proteins triggering fibroblast differentiation in wound tissue from an incisional wound model.	62
Figure 5.21: Relative mRNA expression of proteins related to re-epithelialization in wound tissue from an incisional wound model.	63
Figure 5.22: Relative mRNA expression of proteins related to macrophages in wound tissue from an incisional wound model.	64
Figure 5.23: Relative mRNA expression of macrophage migration inhibitor factor (MIF) protein family in wound tissue from an incisional wound model.	65
Figure 5.24: CD74 receptor on undifferentiated and differentiated NIH/3T3 cells.	66
Figure 5.25: Contractile activity after myofibroblasts differentiation under different treatments.	68
Figure 5.26: Viability assay of HDFs treated with SVF-CM derived from 4 obese patients (BMI > 25) and additional rMIF-2.	69
Figure 5.27: Viability assay of HDFs treated with SVF-CM derived from 4 lean patients (BMI \leq 25) and additional rMIF-2.	70
Figure 5.28: Viability assay of HDFs treated with SVF-CM derived from 4 lean patients (BMI \leq 25) and 4 obese patients (BMI > 25) with or without additional rMIF-2.	71
Figure 6.1: Two postulated mechanisms for the regulation of the TGF- β /Smad signaling pathway by MIF-2 via Erk1/2.	81

List of tables

Table 3.1: Mouse strains used in this thesis.	20
Table 3.2: Various mouse chows for the regular and high fat diet used in this thesis.	20
Table 3.3: Details of patient characteristics from which the stromal vascular fraction (SVF) was isolated to generate SVF conditioned media.	21
Table 3.4: Chemicals, reagents, media and drugs used in this thesis.	21
Table 3.5: Components of the various media used in this thesis.	24
Table 3.6: Components of the buffer for the gel contraction assay.	24
Table 3.7: Primers used in this thesis.	25
Table 3.8: Primary antibodies used in this thesis.	26
Table 3.9: Secondary antibodies used in this thesis.	26
Table 3.10: Consumables used in this thesis.	27
Table 3.11: Devices used in this thesis.	28
Table 3.12: Software used in this thesis.	30
Table 3.1: Antibodies used for immunohistochemical staining.	35
Table 5.1: n-value of wounds of each mice group on the specific days of the wound size measurement.	45

List of abbreviations

4-CPPC	4-(3-Carboxyphenyl)-2,5-pyridinedicarboxylic acid
°C	Degree Celsius
µg	Microgram
µL	Microliter
µm	Micrometer
µM	Micromolar
µ	Micro
<i>al.</i>	<i>“altera”</i>
AMPK	AMP-activated protein kinase
Arg	Arginine
ASC	Adipose-derived stromal cells
ATM	Adipose tissue macrophages
AU	Arbitrary unit
bFGF	Basic fibroblast growth factor
BM	Basic medium
BMI	Body mass index
BSA	Bovine serum albumin
<i>C-terminal</i>	Carboxyl-terminal
<i>ca.</i>	<i>“circa”</i>
CD	Cluster of differentiation
CDK	Cyclin-dependent kinase
cDNA	Complementary deoxyribonucleic acid
C/EBP	CCAAT/enhancer binding protein
<i>Col</i>	Collagen
CM	Conditioned medium
CO ₂	Carbon dioxide
CXCL	CXC ligand
CXCR	CXC chemokine receptor
dH ₂ O	Distilled water
D-DT	D-dopachrome tautomerase
DAB	3,3-Diaminobenzidine tetrahydrochloride
DMEM	Dulbecco's Modified Eagle's Medium

List of abbreviations

DNA	Deoxyribonucleic acid
dNTP	Nucleoside triphosphate
DTT	Dithiothreitol
E	Glutamine
<i>e.g.</i>	For example (" <i>exempli gratia</i> ")
ECM	Extra cellular matrix
EDTA	Ethylenediaminetetraacetic acid
EGF	Endothelial growth factor
<i>Eln</i>	Elastin
ELR	Glutamine-Leucine-Arginine
em	Emission
EMT	Endothelial-mesenchymal transition
ERK	Extracellular signal-regulated kinase
<i>etc.</i>	" <i>et cetera</i> "
EtOH	Ethanol
ex	Excitation
FACS	Fluorescence associated cell sorting
FGF	Fibroblast growth factor
<i>Fn</i>	Fibronectin
g	Gram
<i>g</i>	Gravitational acceleration
G-CSF	Granulocyte-colony stimulating factor
GM-CSF	Granulocyte-macrophage colony stimulating factor
HEPES	4-(2-hydroxyethyl)-1-piperazineethanesulfonic acid
HFD	High fat diet
HLA	Human leukocyte antigen system
HRP	Horse reddish peroxidase
IFN	Interferon
IgG	Immunoglobulin G
IL	Interleukin
KGF	Keratinocyte growth factor
kJ	Kilo joule
Leu	Leucine
LPS	Lipopolysaccharide

List of abbreviations

Lys	Lysine
M	Molar
MAPK	Mitogen-activated protein kinase
mg	Milligram
MIF	Macrophage migration inhibitor factor
min	Minute
mL	Milliliter
MMP	Matrix metallo-protease
mRNA	Messenger ribonucleic acid
MSC	Mesenchymal stem cell
<i>N-terminal</i>	Amino-terminal
NaCl	Sodium chloride
NF- κ B	nuclear factor kappa-light-chain-enhancer of activated B cells
ng	Nanogram
OD	Optical density
PAT	Patient
PBS	Phosphate buffered saline
PCR	Polymerase chain reaction
PDGF	Platelet derived growth factor
pen/strep	Penicillin-streptomycin
pH	<i>"Potentia hydrogenii"</i>
PI3K	Phosphatidylinositol-3-kinase
PM	Proliferation medium
PPAR γ	Peroxisome proliferator-activated receptor γ
Pro	Proline
r	recombinant
RBC	Red blood cells
RD	Regular diet
RLR	Arginine-Leucine-Arginine
ROS	Reactive oxygen species
rpm	Rounds per minute
RPMI	Roswell Park Memorial Institute
RPS29	Ribosomal protein S29
RT	Real time

List of abbreviations

q	Quantitative
SDF	Stromal cell-derived factor
SMA	Smooth muscle actin
SVF	Stromal vascular fraction
T β R	TGF- β receptor
TGF- β	Transforming growth factor- β
TIMP	Tissue inhibitor of metalloproteinase
TNF- α	Tumor necrosis factor- α
U	Unit
US/USA	United states of America
UV	Ultra violet
VEGF	Vascular endothelial growth factors
v/v	Volume/volume
WT	Wild type

1. Introduction

1.1 Cutaneous wound healing mechanism and its pathophysiology

1.1.1 Structure of the skin

The skin takes up to 16 % of the total body mass in humans. This makes it the largest organ with versatile functionality [1, 2]. One function of the skin is the regulation of the body temperature through sweat and hair as well as by adjusting peripheral blood flow and fluid homeostasis [2-4]. In addition, the skin is also a sensory organ with different external sensory receptors for temperature, vibration, pain or pressure [2-5]. The major function of the skin, however, is to separate the underlying tissue from the external environment. It serves as a physical barrier protecting from invasion of microorganisms and pathogens, physical and chemical trauma and injuries, as well as from UV-light-induced damage due [1-4, 6].

Three layers make up the skin: the epidermis, dermis, and the supporting subcutaneous layer (Figure 1.1). The epidermis is the outermost layer and can be subdivided in four sublayers: *stratum basale*, *stratum spinosum*, *stratum granulosum* and *stratum corneum*. The major cell types in the whole epidermis are keratinocytes, which appear in various states of differentiation in the single layers [1, 3, 4, 6].

The *stratum basale* is the first layer of the epidermis. It consists mainly of undifferentiated, mitotically active keratinocytes able to proliferate, superficially migrate and differentiate forming the upper layers of the epidermis. The undifferentiated keratinocytes can be characterized by keratin 14 [3, 4]. Keratinocytes moving up the *stratum* towards the upper epidermis layers start to differentiate forming the spinous layer, *stratum spinosum*. In this early differentiation state, the cells make an expression switch from keratin 14 to keratin 10, lose their mitotic ability, grow and form robust, intercellular spine-like desmosomes. [1, 3, 4, 7, 8]. In the upper *stratum granulosum*, the cells transform to an elongated, flatten shape. Intracellular keratohyalin granules are produced containing electron dense proteins like profilaggrin and keratin intermediate filaments. These proteins mainly form the cornified envelope of the terminally differentiated keratinocytes [1, 3, 4, 7]. The *stratum corneum*, 10 – 20 µm thick, forms the outermost part of the epidermis, and is in direct contact to

the environment making it mainly responsible for the physical protection barrier. In this layer, keratinocytes lose their nuclei and most of the organelles and release lipids into the intercellular space. Through interaction with the matrix protein filaggrin, the cells are aligned in a highly condensed order and a strong, hard polymer of lipids and proteins is formed and envelopes the cell. The keratinocytes are differentiated into anucleate, “dead” corneocytes. Next to the cells, the *stratum corneum* is composed of keratin [1, 3, 4, 6, 9].

Below the epidermis lies a thin collagen membrane. This layer, also called basal membrane is made up of collagen type IV, endothelial cells and podocytes and separates the epidermis and dermis [10-12]. The dermis is a mainly fibrous connective tissue layer made of extra cellular matrix (ECM) and different cells. It can be subdivided into the upper papillary and the lower reticular dermis. While the papillary layer is softer, more vascular and composed of loose connective tissue, the reticular one consists of a thick dense connective tissue making up the majority of the dermis [4, 13]. The primary cell type of the dermis are fibroblasts, which produce chiefly ECM components including different types of collagens, particularly type I and III, which make the biggest part of the layer, as well as elastin and fibrillin, which form elastic fibers and are responsible for the elasticity of the skin. The space between these fibrous components is filled with an aqueous, heterogenic, amorphous “ground substance” containing glycosaminoglycans and proteoglycans like hyaluronic acid or dermatan and keratan sulfate as well as adhesion proteins like fibronectin or vitronectin [4, 13-15]. Other common cell types are macrophages, adipocytes, mast cells and stem cells. Next to the cells and ECM, the dermis hosts blood vessels, nerve endings, sensory receptors and hair follicles [1, 4, 16]. The dermis provides the elasticity and tensile strength of the skin and supplies the epidermis with nutrients and oxygen [1, 4, 14].

The subcutaneous tissue or hypodermis forms the bottom layer primarily composed of adipose tissue and connective tissue consisting of collagen and elastin. It is not only a heat insulator and mechanical cushion, but also is home to blood vessels, nerves and regulates the dermis/epidermis with cytokines. Apart from adipocytes, mature fat cells (ASC), other important cell types of the hypodermis are adipose-derived stromal

cells, fibroblast, macrophages, keratinocytes and other progenitor cells, which migrate through the subcutaneous layer to the dermis and epidermis [4, 17-19].

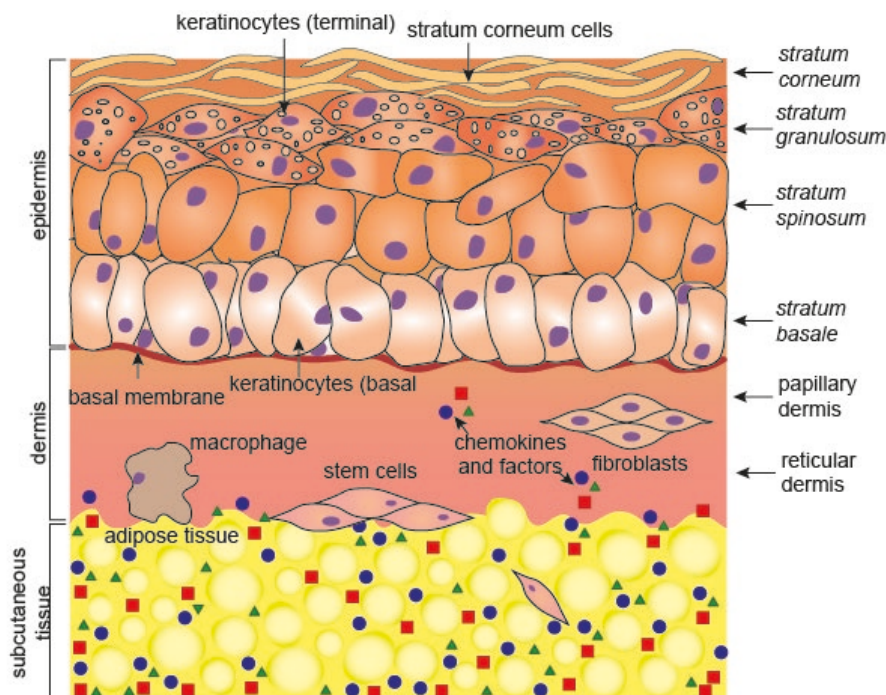


Figure 1.1: Anatomical structure and cell composition of human skin. The skin consists of three layers: the outer epidermis, the dermis and the subcutaneous tissue. The epidermis can be subdivided in basal, spinous, granular and cornified layer. Keratinocyte is the major cell type in the epidermis and they are in various stages of differentiation; from undifferentiated keratinocytes in the basal layer to terminal differentiated corneocytes in the *stratum corneum*. The dermis is below the epidermis separated by the basal membrane and consists of fibroblast producing the extra cellular matrix. The underlying subcutaneous tissue is mostly constructed from adipose tissue (adipocytes and pre-adipocytes) and connective tissue.

1.1.2 Fundamentals of the wound healing process

In general, cutaneous wound healing is a complex process of skin restoration. Although the mechanisms have been studied for a long time, several aspects remain controversial. In particular, chronic wounds that do not undergo a physiological healing course represent a major challenge for medicine and have therefore become for a research focus [8-10].

Upon skin injury, the epidermis, serving as a natural protection barrier, is disrupted and several cytokines, growth factors, proteases and inflammatory proteins are released from the surrounding tissue initiating the reparative body response. Classically, the repair process, is separated into four overlapping stages: hemostasis

(or blood clotting), inflammation, proliferation, and remodeling of the tissue and skin (Figure 1.2) [19, 20].

Immediately after injury, the initial vascular response encompasses vasoconstriction of the damaged blood vessels. The endothelium and platelets in the vicinity of the wound area release cytokines, growth factors and inflammatory proteins (such as interleukin (IL)-1, thromboxane A₂, fibrin-stabilizing factor XIII, tumor necrosis factor (TNF)- α and transforming growth factor (TGF)- β) and activate the intrinsic coagulation cascade [19, 21]. Once the platelets have changed to an amorphous shape providing clotting, they coagulate with fibronectin, fibrinogen, thrombin and collagen to a clot, which adheres to the endothelium of the damaged vessels aiming for primary hemostasis [19, 21, 22]. By that, thrombin is activated to cross-link fibrinogen to fibrin strands. These fibrin strands improve the clotted thrombus by acting as a glue and form a scaffold for other migrating cells. This whole hemostasis phase can last from a few minutes until an hour and in cases of severe deep injuries up to several hours or even 2 – 3 days [19, 21-23].

Towards the end of the first vascular response when the clot closes the wound, the inflammatory phase takes place. The blood vessels widen again (vasodilation), so that leukocytes, mainly neutrophils and monocytes migrate into the wounded area. The recruited neutrophils release proteolytic enzymes such as proteases and create reactive oxygen species (ROS) to kill bacteria and degrade non-viable tissue by digesting collagen with matrix metallo-proteases (MMPs). Furthermore, monocytes differentiate to macrophages, absorb and remove damaged cells, cell debris, as well as bacteria and other invading pathogens. Via this way in addition with exudation, the leakage of fluid, the wound is cleansed and protected against infections through pathogens [19-21]. Macrophages also release growth factors like platelet derived growth factors (PDGF) or vascular endothelial growth factors (VEGF), cytokines like TNF- α , IL-1 and IL-6 to attract further macrophages and other cells that are necessary for repairing like fibroblast, keratinocytes and stem cells [24]. Vasodilation also ensures a better influx of nutrients and antibodies and outflux of lymph from damaged lymphocytes. As a result, the wound area is reddened (erythema) and swollen, finally causing an edema [19, 21, 25].

After approximately 1 - 7 days, new tissue is established by migration, proliferation and differentiation of pro-healing cells [21]. During the up to several weeks lasting proliferation stage, fibroblasts migrate to the damaged area where their proliferation rate is increased by stimulation through IL-1 and IL-6. Macrophages secrete cytokines such as PDGF and TGF- β 1 activating fibroblasts to differentiate into “wound fibroblast” and subsequently into myofibroblasts. Myofibroblasts are the major producer of collagen, fibronectin and elastin making them responsible for the formation of ECM and mainly the new formed tissue, also called granulation tissue. Newly built ECM serves as a scaffold for blood vessels and promotes angiogenesis [26-29]. Thus, the hemostasis clot is replaced by a temporary granulation tissue to ensure an adequate supply of nutrients and oxygen. The remodeling of the epithelial layer, a process labeled as reepithelization, does simultaneously occur on the surface of the wound to restore a protective layer against bacteria and other pathogens. In order to decrease the wound size, myofibroblasts “anchor” at the wound and contract. Superfluous cells get eliminated through apoptosis [19, 20, 25-27, 30].

The proliferation phase results in a closed wound with a scar atop. At first, the scar is light reddish and bulging but the excrescence decreases with time. The remodeling stage is the longest period and can last years. In this process, the amorphous collagen fibers realign along the underlying muscle fibers forming the so called Langer lines (tension lines). The tissue adjusts to the surrounding environment, inelastic collagen is exchanged by elastin for a higher elasticity of the tissue and new hair follicle and sweat glands are formed [19, 20].

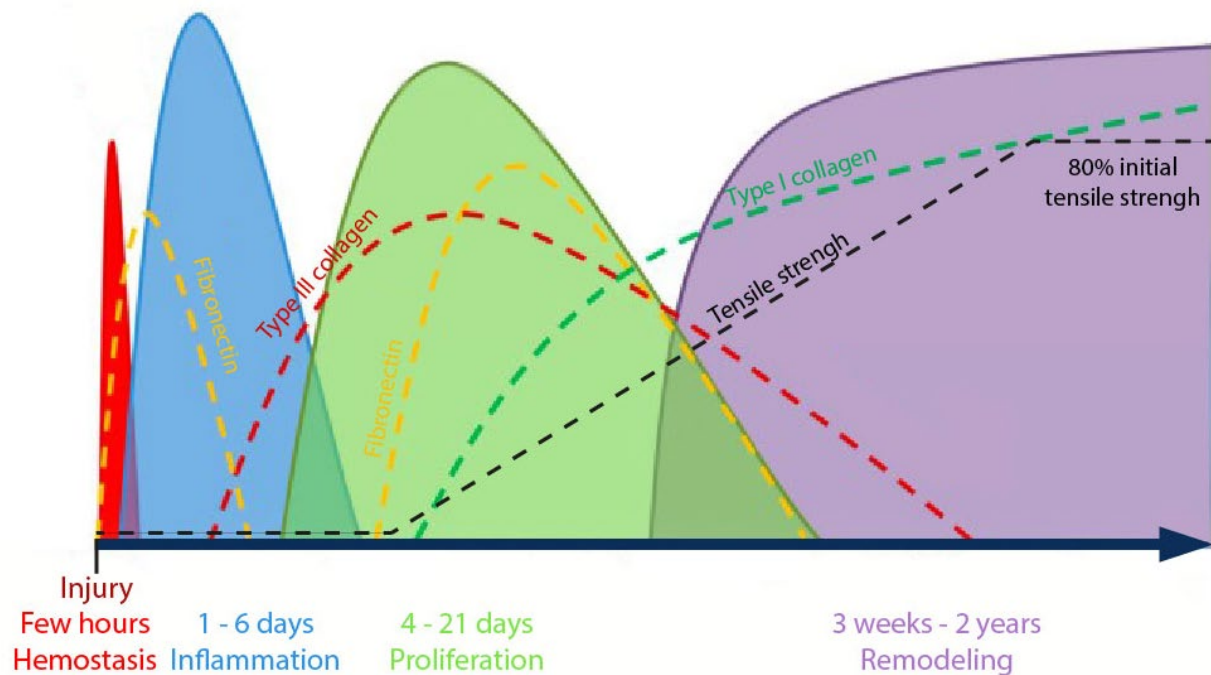


Figure 1.2: Temporal description of the four wound healing phases. Hemostasis occurs immediately after the injury to stop the bleeding with a fibrin-platelet-clot. At the same time, cytokines are released to recruit various leukocytes such as neutrophils and monocytes. The recruited different leukocytes clean up the wound area from cell debris, non-viable tissue, bacteria, and other invaded pathogens by several mechanisms. In the later phase of the inflammation phase, further chemoattractants are secreted, so that tissue-rebuilding cells migrate into the wound area. During the proliferation stage, the granulation tissue, a transitional tissue, is formed primarily by myofibroblasts. At the same time, the reconstruction of the epidermis, reepithelialization, takes place resulting in a scar. Remodeling is the last and longest lasting phase, sometimes over several years. The amorphous collagen is cross linked and partially exchanged by more elastic elastin resulting in an increase of the tensile strength. Adapted from Przekora [31]

1.1.3 Wound healing disorder

Alone in western industrialized countries approximately 1 – 2 % of adult patients suffer from chronic wounds which are difficult to heal or do not heal at all [32-35]. Next to the physiological harm of the patients, the long term treatment of chronic wounds is a financial burden to the global healthcare system, e.g. in the United States (US) these are reported to reach up to US\$ 25 billion annually [34, 36].

Chronic wounds are wounds that do not physiologically complete the entire repair process, do not heal sufficiently in a reasonable period of time and often cause complications such as keloids, ulcers, fistula, septic wounds and others [35, 37-39]. They mainly remain in the inflammatory phase and the expression of pro-inflammatory cytokines is higher when compared to normal wounds leading to an increased level of

ROS produced in neutrophils. In low concentrations, ROS eliminate and protect from microorganisms, but superphysiological ROS concentrations caused by a hypoxic and inflammatory environment damage cells and ECM proteins. Thereby the pro-inflammatory cytokine levels stay high with a concomitant increase of proteases [40]. In acute wounds, proteases remain balanced with regulation of their inhibitors and the degradation of the damaged ECM. However, this homeostasis is disrupted by the increased level of proteases by which ECM is more strongly digested. This loop prevents the wound from transitioning from the inflammatory to the proliferation phase [41].

Besides the molecular level, chronic wounds are also impaired on a cellular level with cells experiencing early senescence. Numerous studies have shown that fibroblasts, keratinocytes, macrophages and endothelial cells lose their proliferation ability caused through oxidative stress by ROS [42-45].

1.1.4 Obesity-induced chronic wounds

Obesity in particular has been an underestimated factor in the delay and disruption of physiological wound healing. Several studies have demonstrated that obesity leads to impaired wound repair [36-39, 46, 47]. Next to the epidermis and dermis, the underlying subcutaneous tissue also influences the healing process of a cutaneous wound (Figure 1.1). The subcutaneous layer is mainly composed of adipose tissue, which is therefore in immediate vicinity to the wound area. It participates in wound healing through the release of growth factors and cytokines like PDGF, VEGF, TNF- α , IL-1 and IL-6 attracting progenitor and stromal cells such as fibroblasts, keratinocytes and endothelial cells. A multitude of various cells migrates from the adipose tissue into the wound area, where they proliferate and differentiate. This cell recruitment and stimulation is essential for a proper tissue reconstruction [19, 39, 48, 49].

However, in obese patients, the adipose tissue is chronically inflamed with pathological alteration in the secretion of chemokines and growth factors whereby the reparative function of the subcutaneous layer is disturbed. The altered cytokine expression leads to diminished cell migration, proliferation and differentiation resulting in a modified cellular composition of the wound area. Furthermore, it leads to decreased angiogenesis, *i.e.* an insufficient supply with oxygen and nutrients. An

additional impaired glucose metabolism, as it often is associated with obesity, enhances these negative effects. The pathological cytokine secretion and cell composition, the reduced vascularity and oxygen tension ultimately lead to diminished wound healing in obese patients [19, 36, 39, 46-50].

1.2 Mouse wound model to mimic human skin reconstruction

Mus musculus, the house mouse is the most common laboratory animal to investigate cutaneous wound healing [51-54]. The basic structure and composition of the skin and functions of the various layers - as described above - are similar between species [55, 56]. Still, it is important to be aware of the interspecies differences and specializations in skin evolution between the different species [57].

1.2.1 Murine skin vs human skin

Mice and humans share over 95 % genetic identity with 40 % alignment, even though the genome of the mice is 14 % smaller [58]. In general, skin of both species is 30.2 % identical. Genes related to structure and barrier function, structure proteins such as type I and III collagen, and cytokines for cell proliferation are highly conserved. Despite the well-analyzed genomics, the function of 15 conserved genes is still unknown [52]. Nevertheless murine and human skin still differ (Figure 1.3). Beside the fact that the human skin is more than 4 times thicker than mouse skin (human: ~100 µm; mouse: <25 µm), mice do also have less epidermal layers, by which the function of protection is reduced and percutaneous absorption is increased [52, 54, 59-61]. Furthermore, mice have an additional muscle layer, the *panniculus carnosus*, within the subcutaneous tissue. The *panniculus carnosus* causes the skin to contract and changes the biomechanics compared to humans, in whom this layer is missing [52]. Another obvious difference is the amount of hair follicles. Mice have fur and are covered in hair follicles, while in humans the hair follicles are sparse and irregularly distributed [52, 61]. In contrast, human skin is permeated with eccrine sweat glands, which are involved in body temperature control and innate immune system [52]. While mice – like most mammals – solely have apocrine glands in breasts [54, 55].

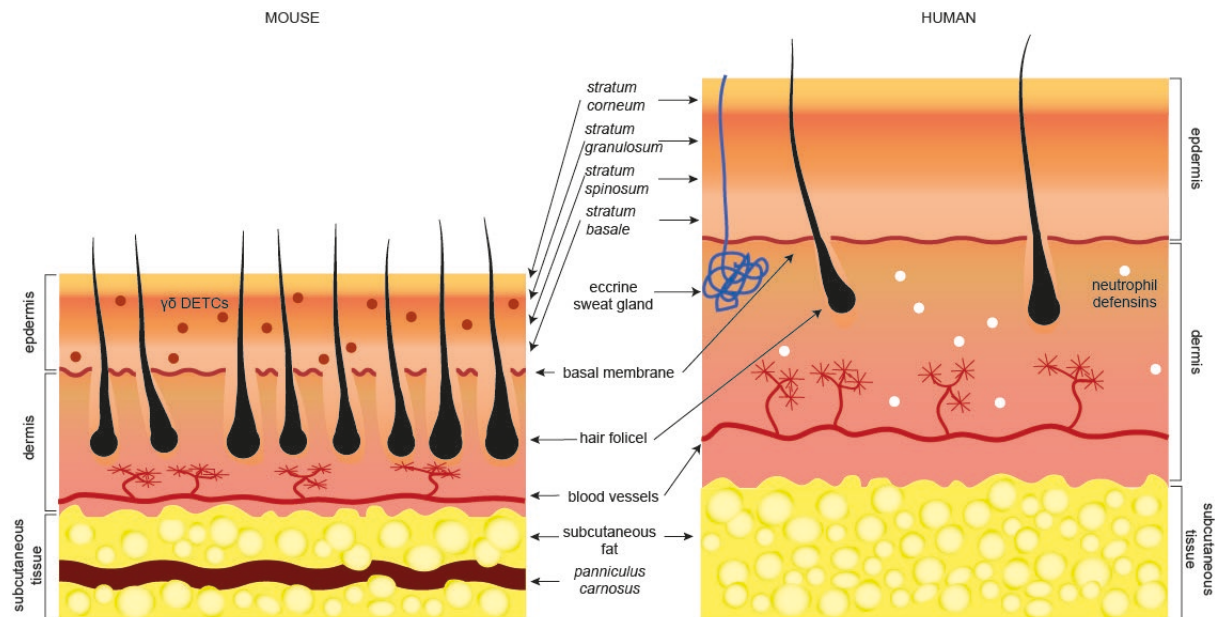


Figure 1.3: Comparison of human (left) and murine (right) skin morphology. At the cellular level, different layers of skin are shown and compared between humans and mice. Human skin is 4-times thicker than murine skin and has more epidermal layers. On the other hand, mice have an additional muscle layer, *panniculus carnosus*, within the subcutaneous tissue and the skin is rich on hair follicle. While the *panniculus carnosus* is absent in humans and they have only a few hair follicles spread over the body. Furthermore, humans have eccrine sweat glands, which are absent in mice. They have apocrine sweat glands only in the breast.

1.2.2 Differences in murine and human wound healing

The skin of mice and humans is not identical. Thus, particular consideration should be given to the regeneration of the skin after an injury - the process in mice is similar but not identical to that in humans, but the basic 4 overlapping phases are mostly the same on molecular and cellular levels [19, 51, 62, 63]. The primary difference is wound contraction. The *panniculus carnosus*, which is absent in humans, has a great contraction potential. This plays an important role in wound closure in mice. Large excisional wounds are closed up to 90 % by skin contraction. The contraction in human skin varies and is minimal when compared with that of mice [52, 64]. Wounds of men, on the other hand, heal only by granulation tissue formation and reepithelialization [19, 26, 27, 30, 65]. Despite the wound contraction in mice, the formation of granulation tissue and epithelial layer is highly conserved and identical in both species [52]. In mice, hair follicles regenerate in renewed tissue after an injury, while humans do not rebuild hair follicles, so that scars remain hairless [51, 63].

Furthermore, the source of stem cells partially differ between mice and humans. Mice have two kinds of epidermal stem cells: heterogeneous progenitor cells in the basal

membrane, which differentiate into keratinocytes during wound healing, and quiescent undifferentiated stem cells at hair follicles that are activated after injury [66]. The presence of epidermal stem cells in human skin and their role in wound repair process is controversy discussed [55, 67, 68]. On the other hand human have stem cells, which participate in reepithelialization, near sweat glands, which are lacking in mice [69]. However, the participation of these epidermal stem cells and mesenchymal stem cells (MSC) derived from fat tissue or skin is not yet clarified [70].

At the immunological level, there are also some differences between wound healing in human and mouse. Contribution of the various leucocytes already varies between both species: humans have 50 % – 70 % neutrophils and 30 % – 50 % lymphocytes, while mice have 10 % – 25 % neutrophils and 90 % – 25 % lymphocytes [71]. Furthermore, only mice skin harbors $\gamma\delta$ dendritic epidermal T cells (DETCs), which are crucial for murine wound healing and skin homeostasis [61, 72]. They secrete fibroblast growth factor (FGF)-9 that subsequently activates secretion of more FGF-9 by dermal fibroblasts resulting in regeneration of hair follicle [73]. In contrast, human neutrophils and eccrine sweat glands produce antimicrobial peptides, defensins, such as dermoccidin. They prevent pathogens to invade wounds and trigger cells to migrate, proliferate and differentiate [74, 75]. These defensins are not secreted by mice [52].

1.3 Fibroblasts

1.3.1 Fibroblasts in the human body

Fibroblasts are the major cell type in connective tissue and found in several tissues such as the dermis of the skin, lung or heart [1, 14, 76, 77]. They belong to the group of embryonic, mesenchymal cells that are derived from three sources: epithelial-mesenchymal transition (EMT), bone marrow- and tissue-derived MSC [14, 26, 76, 78-81]. While fibroblast differentiate directly from bone marrow- and tissue-derived MSCs through stimulation mainly by TGF- β , in the EMT process fibroblasts arise through dedifferentiation from epithelial cells [81-83].

Although fibroblasts have different origins and are found in various tissues, the main function is the same. They are responsible for the synthesis of ECM. This is made up of different collagen types, elastin, fibronectin and proteoglycans [13, 15]. An additional function is maintaining the homeostasis of ECM by degradation through

release of proteases like MMPs and their inhibitors like tissue inhibitors of metalloproteinase (TIMPs). The whole production and homeostatic mechanism is regulated by cell-cell and cell-matrix interactions [14, 26, 82]. Fibroblasts also take part in regulation of volume and pressure of interstitial tissue fluid. The cells interact via $\beta 1$ integrin receptors with the ECM and anchor themselves to the endothelium of blood vessels whereby they narrow the lumen of the vessels [26, 77, 84].

1.3.2 Fibroblasts and their role in wound repair

As fibroblasts form ECM, they play also a crucial role in wound repair after an injury when the connective tissue composed mainly of ECM is damaged. Already in the early state after injury, fibroblasts are recruited through chemotaxis caused by cytokines and growth factors like platelet factor IV released by platelets [22]. Endothelial cells secrete IL-1 stimulating macrophages to express more chemoattractant cytokines and growth factors like TNF- α , IL-6, granulocyte-colony stimulating factor (G-CSF) and granulocyte-macrophage colony-stimulating factor (GM-CSF) as well as PDGF which is the most important macrophage-derived growth factor for fibroblast proliferation. Also fibroblasts themselves stimulated by IL-1 release growth factors and cytokines which activate fibroblasts from surrounding tissue to migrate to the wound in an autocrine manner [24, 27, 85, 86]. A secondary function of fibroblasts during inflammatory state is to support monocyte differentiation to macrophages through the expression of interferon (IFN)- γ and the production of MMPs to clean the wound [14, 26, 87].

Fibroblasts are mainly activated in the proliferation state. Triggered by IL-1 and TNF- α fibroblasts produce IL-6 and FGF-7 and -10, previously known as keratinocyte growth factor (KGF)-1 and -2, stimulating keratinocytes to migrate to the wound site, proliferate and differentiate to the different stages to build a new epithelial layer [3, 88, 89]. Fibroblasts, however, play also a direct role in wound healing. After migration and proliferation in the wound area fibroblasts get stimulated by PDGF and endothelial growth factor (EGF) derived from anti-inflammatory M2 macrophages and platelets to change their phenotype to so called "wound fibroblasts". The wound fibroblasts form a provisional matrix made of fibronectin, collagen III and glycosaminoglycans and reduce their ability to proliferate [29, 90, 91]. Further triggered by TGF- $\beta 1$ released by macrophages, fibroblasts differentiate to myofibroblasts, which can be characterized

through α -smooth muscle actin (α -SMA). Myfibroblasts produce collagen I and III, enhance the synthesis of TIMPs and cell adhesion proteins and decrease the MMP production. In addition, myfibroblasts also contract the collagen rich ECM and promote the wound healing through mechanically wound closure [27, 28, 92-94].

1.3.3 Myfibroblast differentiation signaling cascades

TGF- β is the principal factor for myfibroblast differentiation. It stimulates differentiation via the canonical TGF- β /Smad signaling pathway. TGF- β activates TGF- β receptors (T β Rs), serine (T β RI) and threonine (T β RII) kinases. The activated T β Rs phosphorylate Smad2 and Smad3 at C-terminal SSXS motif. The phosphorylated Smad proteins subsequently build heterotrimers with Smad4. The so activated Smad-complex translocates into the nucleus, binds at the specific promotor region on the DNA, and activates transcription [95-97]. Next to the Smad pathway there are other non-Smad pathways in TGF- β signaling such as the Rho-like GTPase pathway, the phosphatidylinositol-3-kinase (PI3K) AKT pathway, and the mitogen-activated protein kinase (MAPK) downstream cascaded through either JNK, p38, or extracellular signal-regulated kinase (ERK) 1 and 2 (Figure 1.4) [83, 95, 98].

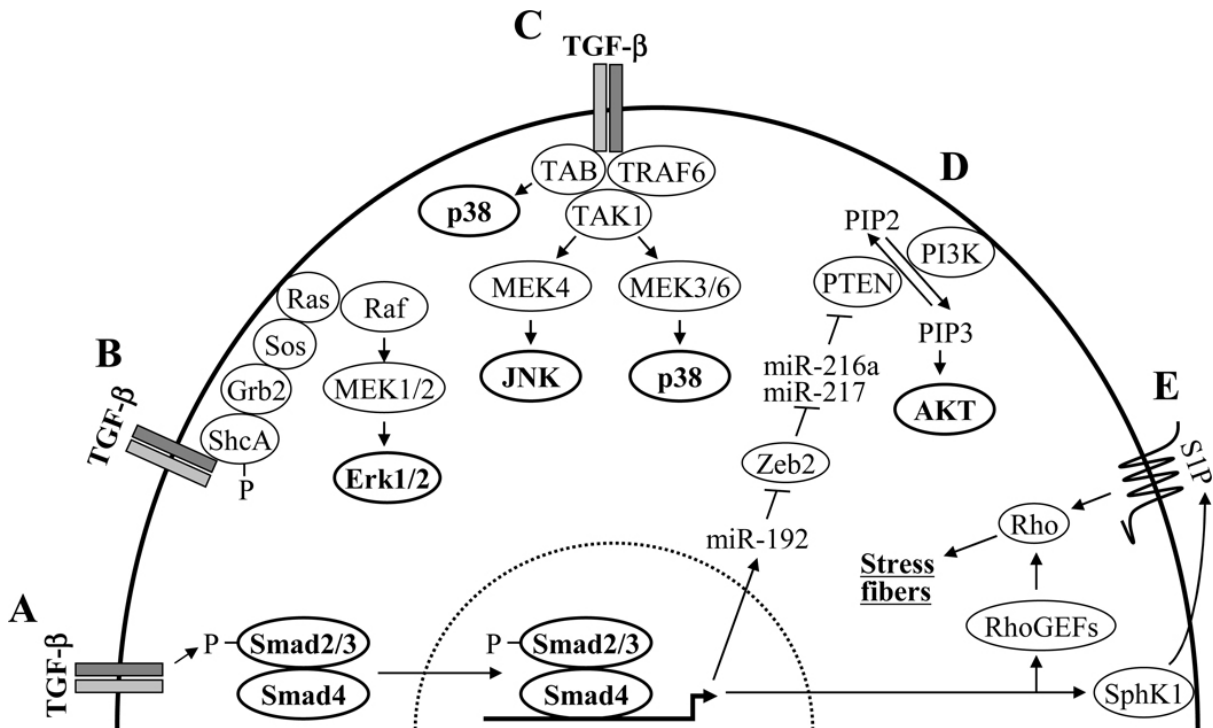


Figure 1.4: TGF- β initiated signaling pathways for gene transcription. (A) Solely canonical TGF- β /Smad pathway; MAPK activated pathways through (B) Erk1/2 or (C) JNK and p38; (D) activation through phosphatidylinositol-3-kinase (PI3K) AKT pathway and (E) activation through Rho pathway. [95]

1.4 Macrophage migration inhibitor factor (MIF) protein family

1.4.1 MIF and its receptors

When macrophage migration inhibitor factor (MIF) was first described in 1966, it was initially thought to be a soluble factor that is solely expressed in T leukocytes and inhibits macrophage migration [99, 100]. More detailed investigations of the crystal structure and biological function revealed that, MIF in fact is a highly conserved, ubiquitously expressed, pleiotropic inflammatory chemokine-like protein [101, 102]. MIF appears in equilibrium as a monomer, dimer and trimer, while monomeric and dimeric forms predominate [102-107]. Next to T leukocytes, macrophages, monocytes, neutrophils and endothelial cell and many more cell types produce MIF [108-112]. MIF is a crucial upstream regulator of innate immunity and regulates essential inflammatory mediators like IFN- γ or TNF- α . An overexpression of MIF correlates with excessive inflammation and immunopathology. In addition, MIF has an impact on cell proliferation and survival [101, 113-118].

MIF binds to four cell membrane receptors and thereby activates paracrine and autocrine cellular processes [119-124]. The first known receptor for MIF was the cluster of differentiation 74 (CD74), also known as human leukocyte antigen system (HLA) class II histocompatibility antigen gamma chain. Once MIF binds to CD74, it forms a complex with CD44 and initiates the extracellular signal-regulated kinase (ERK) cascade that belongs to the mitogen-activated protein kinase (MAPK) pathway (ERK1/2-MAPK). Further pathways activated by the CD74/CD44 complex are the PI3K-Akt signal transduction cascade, tyrosine kinase c-Src, AMP-activated protein kinase (AMPK) and nuclear factor kappa-light-chain-enhancer of activated B cells (NF- κ B) pathway. All aforementioned pathways are important for cell proliferation and survival [118, 124-126].

The remaining three MIF receptors belong to the CXC chemokine receptor (CXCR) class: CXCR2, CXCR4 and CXCR7. These receptors have a high ligand specificity and are G-protein coupled chemokine receptors [119, 120]. CXCR2 and CXCR4 stimulate the recruitment of leukocytes like T cells, neutrophils and monocytes [120]. Numerous ligands of CXCR2 such as CXC ligand (CXCL)8 incorporate the identical N-terminal Glu-Leu-Arg (ELR) motif. This sequence facilitates the binding of the ligand

to its receptor [127]. MIF, by contrast, does not show an ELR sequence but includes a similar Asp-44-X-Arg-11 motif that is named *pseudo-(E)LR* [123]. CXCR4 has two known chemokine ligands, stromal cell-derived factor (SDF-1 α), also called CXCL12, and MIF [120, 128]. SDF-1 α has an *N*-terminal sequence Lys-1-Pro-2 which is necessary to activate CXCR2. MIF interacts with CXCR4 through an N-like-loop with an *N*-terminal proline and the specific amino acid sequence Arg-Leu-Arg (RLR) similar to the ERL motif [128-130]. The interaction between CXCR7 and MIF was previously described to be important the migration of B-lymphocytes [119].

Various studies have demonstrated that two or three receptors build complexes that are required to stimulate specific signaling cascades. In these cases, CD74 appears to play a pivotal role as it is a mandatory part of these receptor complexes. Next to the already mentioned CD74/CD44 complex, CD74 establishes complexes with the CXCR receptors. CD74/CXCR2 and CD74/CXCR4 have shown to trigger inflammatory and atherogenic monocyte and T cell recruitments [120, 123, 131]. The three receptor complex CD74/CXCR4/CXCR7 activates ERK1/2 and ZAP70 pathway as well as enhances lymphocyte chemotaxis [119].

1.4.2 MIF-2, a new member of MIF-protein family

For many years, MIF was considered the only member of its protein class. Recently, D-dopachrome tautomerase (D-DT) has been identified as a homolog of MIF due to its similar structural and functional properties. D-DT was first described in 1993 as a tautomerase converting D-dopachrome to 5,6-dihydroxyindole. MIF also is able to catalyze tautomerization of D-dopachrome but in contrast to D-DT without decarboxylation [132, 133]. While more precise crystallographic examinations of MIF and D-DT demonstrated a shared homotrimeric structure (Figure 1.5). Due to its similarities to MIF, D-DT was assigned to the MIF superfamily and henceforth labeled "MIF-2" [102, 107, 133, 134]. Next to the same three-dimensional structure, the gene sequence of MIF-2 is 50 % identical to the sequence of MIF [132]. Furthermore, the two proteins also share similarities on the protein level with 35 % identity in humans and 27 % identity in mice [135]. One important property both family members have in common is the *N-terminal* proline, which is essential for the highly conserved tautomerase activity [136]. Nevertheless, they also differ greatly in some points in the

amino acid sequence. One major difference is MIF-2's absence of the *pseudo (E)LR* motif, which facilitates MIF to activate its CXC receptors like CXCR2 [132, 134].

Even though the structure of MIF-2 is well studied, little is known about its expression and biological functions. MIF-2 is expressed in immune cells, adipocytes and many other tissue types [137]. The circulating serum MIF-2 level is increased in septic tissue and cancer [132, 137]. Merk *et al.* have demonstrated that CD74 also is a receptor for MIF-2 through which MIF-2 initiates the ERK1/2-MAPK and other inflammatory signaling pathways [132]. So far, MIF and MIF-2 are the only known signal activating ligands for CD74. Due to the lack of the *pseudo (E)LR* sequence MIF-2 may not interact with CXCR2 [132]. There is evidence for interaction of MIF-2 with the chemokine receptors CXCR2, CXCR4 and CXCR7 (personal communication).

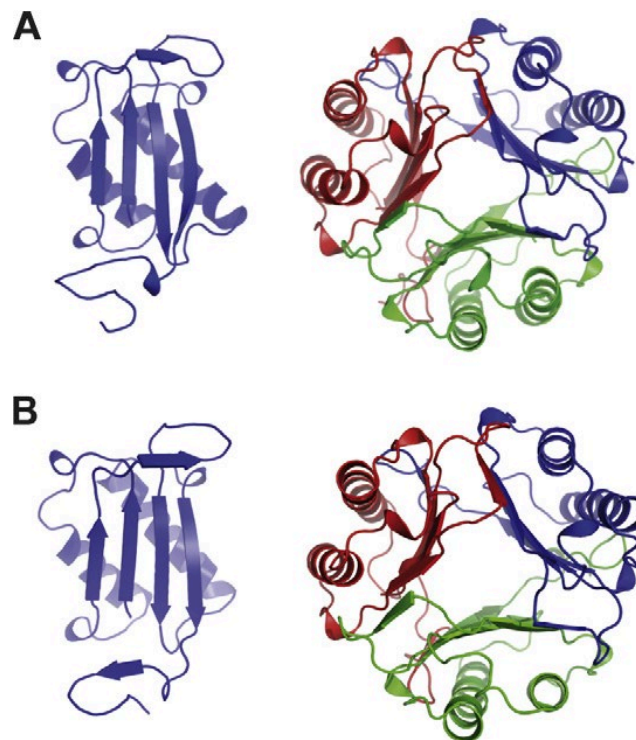


Figure 1.5: X-ray structure of human MIF superfamily members; (A) D-DT/MIF-2, (B) MIF. On the left side are monomeric panel structures and on the right side are homotrimeric structures of MIF and MIF-2. The 3D structures show clearly the structural homology from MIF and MIF-2 [134].

1.4.3 MIF protein family in adipose tissue and obesity

In the late 90s, Hirokawa *et al.* first described MIF expression in adipose tissue of rodents. The authors also demonstrated that MIF level increased after TNF- α stimulation in 3T3L-1 cells, a murine preadipocyte cell line [138]. Several years later

MIF was also detected in human adipose tissue. It was mainly secreted in cultured pre-adipocytes and freshly isolated adipocytes where it was localized in the cytoplasm in both cases. The amount of MIF varied depending on the harvest location [139]. For instance, MIF mRNA levels in visceral fat depots were twofold higher than in deep and superficial depots, and adipocytes from subcutaneous fat tissue secrete more MIF when compared to mammary adipocytes [139, 140].

The expression of MIF-2 in adipose tissue has only recently been reported [141]. In contrast to MIF, it was only found to be secreted by adipocytes from subcutaneous and visceral fat tissue. Additional MIF-2 was also found to be secreted from immune cells in septic adipose tissue [132, 141]. Ishimoto *et al.* have shown in *in vitro* experiments with a human preadipocyte cell line, that MIF-2 levels are increased during adipogenic differentiation but only in the differentiated adipocytes [142].

Although MIF and MIF-2 are structural and partially functionally homologs and are secreted from adipose tissue, they seem to play different roles in adipogenesis and obesity. MIF initiates clonal expansion and higher expression of the intracellular receptor peroxisome proliferator-activated receptor (PPAR) γ and transcription factors for adipogenesis such as CCAAT/enhancer binding protein (C/EBP) α and δ whereby MIF promotes adipogenesis [143]. While Ishimoto *et al.* have shown that MIF-2 treated pre-adipocytes had a reduced expression of the adipogenic transcription factors C/EBP α , β and δ , of PPAR γ 2 as well as of the adipokine peptide hormone adiponectin [142]. Via this way, MIF-2 diminishes the adipogenic differentiation. An additional difference was found in the correlation between the serum level of MIF and MIF-2 in the body mass index (BMI) of patients. While MIF levels were increased in patients with a higher BMI, MIF-2 levels were negatively correlated [141, 144-146]. Interestingly, MIF plasma levels in obese patients were investigated earlier in patients before and after weight loss. The authors demonstrated that the MIF plasma level decreased with weight loss [144].

1.4.4 MIF protein family in inflammation

MIF is a pro-inflammatory protein produced in different immune cells [108-112]. MIF regulates pro-inflammatory cytokines such as TNF- α and IFN- γ in a paracrine and autocrine way [147]. In addition, MIF is also chemoattractant to leukocytes and

influences macrophage polarization and activation as well as their survival. These biological functions cause MIF to promote inflammation in several diseases such as rheumatoid arthritis, sepsis, type 2 diabetes and atherosclerosis [148, 149]. An additional unique function of MIF was reported by Calandra *et al.* Glucocorticoids in low levels induce MIF expression following by a counter regulation of the immunosuppressive effect of glucocorticoids [150]. In a murine model, Bernhagen *et al.* have shown that MIF was secreted by the pituitary gland after lipopolysaccharide (LPS) treatment [114]. In a murine wound healing model with MIF knockout (*Mif*^{-/-}) mice and recombinant MIF treated mice, it was shown that TNF- α levels were increased in MIF treated mice and decreased in *Mif*^{-/-} mice [151].

Similar to MIF, MIF-2 is a pro-inflammatory cytokine but in contrast, its precise role in the pathology and immune physiology is unclear. MIF-2 also interacts with the CD74/CD44 complex initiating inflammatory signaling cascades whereby it counter-regulates the immunosuppressive function of glucocorticoids. In clinical studies, MIF-2 serum level was increased in systemic inflammation, sepsis or metastatic cancer [132]. Furthermore, it was shown that upon LPS stimulation MIF-2 expression also was enhanced [114, 132, 152]. The immune inhibition of MIF and MIF-2 solely or combined lead to a diminished, not lethal endotoxemia [132, 152, 153].

However, Kim *et al.* recently discovered a different behavior of MIF and MIF-2 in an LPS induced murine endotoxemia model [152]. In the visceral fat depot, MIF expression was increased according to previous results, but MIF-2 was reduced when compared to the control group. An additional difference was the polarization of adipose tissue macrophages (ATM). Deletion of *Mif-2* polarized ATMs towards the pro-inflammatory M1 phenotype whereas ATMs of *Mif*^{-/-} mice were skewed towards the anti-inflammatory M2 phenotype. As MIF is increased while MIF-2 is decreased in septic visceral adipose tissue, ATMs are driven towards an M1 polarization ending in excessive pro-inflammatory cytokine expression.

1.4.5 The MIF protein family in wound healing

As an important pro-inflammatory cytokine, MIF also was intensely investigated in the context of cutaneous wound healing. MIF is expressed in mature and developing skin

and shows increased cutaneous expression in pathologies such as carcinogenic, autoimmune and allergic skin diseases. Most importantly, the expression of MIF is increased in skin during wound repair, although its exact role is controversial [154]. There are several studies showing a beneficial effect of MIF during wound healing. Abe *et al.* have demonstrated that female rats treated with anti-rat MIF antibody showed delayed wound healing. Moreover, harvested keratinocytes treated with recombinant MIF had an increased migration tendency [155]. Built on that, the effect of MIF on fibroblast was examined by Zhao *et al.*. *Mif*^{-/-} mice showed diminished wound healing as in the study of Abe *et al.*. Furthermore, fibroblast isolated from *Mif*^{-/-} mice proliferated less upon LPS treatment when compared to fibroblast from wild type mice [156]. A positive effect of MIF could also be demonstrated in wound healing in other tissues such as lung or cornea [157, 158]. By contrast, there are also several groups claiming a negative effect of MIF in skin during the healing process of incisional wounds [154, 159, 160]. Interestingly, Kim *et al.* could show that the healing of excisional wounds of *Mif*^{-/-} mice was improved when compared to the control group. Wound healing of wild type mice treated with recombinant murine MIF, by contrast, delayed [151]. In general, we can postulate that the role of MIF in wound healing is still unclear and might differ in distinct phases and different tissue types.

With regards to MIF-2, there are only two reported studies of skin damage. Sonessen *et al.* radiated healthy human skin with ultra violet (UV) B-light to induce a cutaneous inflammation and collected the fluids of the blisters. MIF and MIF-2 levels in the fluids were elevated [161]. In the most recent *in vitro* study, human dermal fibroblasts were treated with recombinant MIF-2 protein leading to an improved proliferation [162]. As already described above, MIF and MIF-2 influence macrophage polarization in opposite ways. A prolonged excess of M1 macrophages is considered as an evidence for non-healing wounds [163].

2. Aims

Wound repair is a complex process of tissue regeneration. Although cutaneous wound healing has long been studied, there are still several unclear mechanisms to be explored. Above all, wound healing disorders and chronic wounds, as they often occur in obese patients, are still a major challenge for medicine and research.

The chemokine-like protein macrophage migration inhibitor factor (MIF) is a well known pro-inflammatory atypical cytokine. MIF plays a crucial role in various inflammatory diseases such as rheumatoid arthritis, atherosclerosis, sepsis, as well as in obesity and importantly in chronic wounds. Recently a second member of the MIF protein family was discovered, the MIF homolog D-dopachrome tautomerase, also known as MIF-2. Similar to MIF, MIF-2 also is a pro-inflammatory cytokine, but less is known about its role in inflammation. MIF and MIF-2 seem to act in reciprocal ways in obesity and adipose tissue inflammation. MIF is elevated in obese patients whereas MIF-2 level is reduced. The impact of MIF on wound healing is still controversial but it appears to be dependent on the wound location and the phase of the healing process. In contrast, MIF-2 has been sparsely studied for wound healing. In previous *in vitro* data, we have shown that MIF-2 enhances fibroblast proliferation and promotes anti-inflammatory M2 macrophage polarization.

Thus, the aim of my thesis was to discover the function of MIF-2 in cutaneous wound healing and its role in obesity-induced wound healing disorders. At first, I went to investigate how a *Mif-2* knockout influences the healing process in a murine excision wound model under regular and high fat diet. Tissue samples harvested at different time points were analyzed on protein and gene level. Next, I focused on the differentiation from fibroblast into myofibroblasts under supplementation with recombinant MIF-2 protein and MIF-2 specific inhibitors. Furthermore, I questioned the pathway and the mechanism how MIF-2 interacts and exerts its function on the myofibroblasts differentiation. Finally, I questioned the therapeutic approach of recombinant MIF-2 as a potential treatment for cutaneous wound healing. Freshly isolated human fibroblasts were incubated in medium conditioned with the stroma vascular fraction from obese and lean patients and supplemented with various concentrations of MIF-2.

3. Materials

3.1 Mouse strains

Table 3.1: Mouse strains used in this thesis.

Mouse strain	Origin	Total number of used animals
C57BL/6	Charles River Laboratories Germany GmbH, Sulzfeld, Germany	29
C57BL/6 <i>Mif-2^{-/-}</i>	Animal facility LMU Munich, Germany Breeding in the BZL animal facility	29

3.2 Mouse chows

Table 3.2: Various mouse chows for the regular and high fat diet used in this thesis.

Chows	Manufacturer
Chows for high fat diet (60 kJ % fat)	ssnif Spezialdiäten GmbH, Soest, Germany
Chows for regular diet (Breeding Extrudate)	Kliba Nafag, Kaiseraugst, Switzerland

3.3 Patient characteristics

Table 3.3: Details of patient characteristics from which the stromal vascular fraction (SVF) was isolated to generate SVF conditioned media. Patients with a body mass index (BMI) > 25 were considered obese and patients with a BMI ≤ 25 were considered lean.

Obese patients				vs.	Lean patients			
Number	Age	Gender	BMI		Number	Age	Gender	BMI
PAT-52	30	f	32.7		PAT-48	38	f	22.5
PAT-54	42	f	28.6		PAT-50	45	f	22.2
PAT-56	42	f	34.9		PAT-63	29	f	21.8
PAT-57	51	f	27.5		PAT-64	33	f	24.5

3.4 Chemicals, reagents, media and drugs

Table 3.4: Chemicals, reagents, media and drugs used in this thesis.

Chemicals/reagents/media/drugs	Manufacturer
2-(4-(2-Hydroxyethyl)-1-piperazinyl)-ethansulfonsäure (HEPES)	Sigma Aldrich, Steinheim, Germany
2-Propanol, ≥ 99.8 % purity	Sigma Aldrich, Steinheim, Germany
3,3-Diaminobenzidine tetrahydrochloride (DAB)	Agilent DAKO, Santa Clara, CA, USA
4-(3-Carboxyphenyl)-2,5-pyridinedicarboxylic acid (4-CPPC)	Adipogen AG, Liestal, Switzerland
alamarBlue® Cell Viability Assay	G-Biosciences, St. Louis, MO, USA
Bepanthen® Salbe	Bayer AG, Leverkusen, Germany
bFGF	LuBioScience GmbH, Zurich, Switzerland
Bovine Serum Albumin (BSA)	VWR Life Science, Solon, OH, USA

Materials

Chloroform, 99 % purity	Sigma Aldrich, Steinheim, Germany
Clostridium histolyticum Collagenase Type II	MP Biomedicals SARL, Illkirch-Graffenstaden, France
DAB Substrate Buffer	Agilent DAKO, Santa Clara, CA, USA
Dispase® II	Sigma Aldrich, Steinheim, Germany
Dithiothreitol (DTT), 0.1 M	Invitrogen, Waltham, MA, USA
Dulbecco's Modified Eagle's Medium (DMEM) - F12 w/stable Glutamine w/15 mM HEPES	Biowest, Nuaille, France
DMEM - low glucose, 10 x	Sigma Aldrich, St. Louis, MO, USA
DMEM High Glucose w/stable Glutamine w/Sodium Pyruvate	Biowest, Nuaille, France
dNTP Mix	Invitrogen, Waltham, MA, USA
Eosin	Agilent DAKO, Santa Clara, CA, USA
Ethanol	Merck, Darmstadt, Germany
FACSClean	BD, Allschwil, Switzerland
FACSFlow	BD, Allschwil, Switzerland
FACSRinse	BD, Allschwil, Switzerland
Flex Hematoxylin	Agilent DAKO, Santa Clara, CA, USA
Flex Wash Buffer (20 x)	Agilent DAKO, Santa Clara, CA, USA
Foetal bovine serum (FBS), South American origin	Biowest, Nuaille, France
Hydrogen peroxide (30 %)	Merck, Darmstadt, Germany
Isofluran	JD Medical Distributing Co., Inc., Phoenix, AZ, USA
NaCl 0.9 % sodium chloride solution sterile, 100 mL	B.Braun, Sempach, Switzerland
Normal Goat Serum Blocking Solution	Vector Laboratories, Burlingame, CA, USA
Oligo(dT) ₁₂₋₁₈ Primer	Invitrogen, Waltham, MA, USA
Penicillin-Streptomycin Solution 100 x (pen/strep)	Biowest, Nuaille, France
Phosphate-buffered saline (PBS), pH 7.2, Gibco	Thermo Fische Scientific, Schwerte, Germany
RBC Lysis Buffer	G-Biosciences, St. Louis, MO, USA

Materials

Recombinant macrophage migration inhibitor factor 2 (rMIF-2), human	Produced in laboratory of Prof. Bernhagen at the LMU
Recombinant macrophage migration inhibitor factor 2 (rMIF-2), murine	Produced in laboratory of Prof. Bernhagen at the LMU
Recombinant transforming growth factor β 1, murine	Bio-techne, Zug, Switzerland
Rnase AWAY	Molecular BioProducts, San Diego, CA, USA
Rnase Inhibitor	Applied Biosystems Invitrogen, Waltham, MA, USA
Rotor-Gene SYBR Green PCR Kit (2000)	QIAGEN, Hilden, Germany
RPMI 1640 w/stable Glutamine	Biowest, Nuaille, France
Shutdown Solution	BD, Allschwil, Switzerland
SuperScript™ III Reverse Transcriptase	Invitrogen, Waltham, MA, USA
Target Retrieval Solution high pH 9.0	Agilent DAKO, Santa Clara, CA, USA
Target Retrieval Solution low, pH 6.0	Agilent DAKO, Santa Clara, CA, USA
TeloCol® - 3, Type I Bovine Collagen Solution	Advanced BioMatrix, Carlsbad, CA, USA
Temgesic® solution for injection, 0.3 mg/mL Amp.	Indivior Schweiz AG, Baar, Switzerland
TRIzol Reagent	Invitrogen, Waltham, MA, USA
Trypan Blue Soution, 0.4 %	VWR Life Science, Solon, OH, USA
Trypsin-EDTA (1 x), 0.25 %, phenol red	Biowest, Nuaille, France
Water Molecular biology grade (DNases/Rnases/Proteases free)	PanReac AppliChem GmbH, Darmstadt, Germany
XyloI-IVD for Microscopy	Merck, Darmstadt, Germany

3.5 Cell culture media and buffers

3.5.1 Cell culture media

Table 3.5: Components of the various media used in this thesis.

Culture media	Components
NIH/3T3 & Fibroblast culture medium/proliferation medium	<ul style="list-style-type: none"> • DMEM High Glucose • 10 % FBS • 1 % pen/strep
Fibroblast basic medium	<ul style="list-style-type: none"> • DMEM High Glucose • 1 % pen/strep
SVF culture medium	<ul style="list-style-type: none"> • DMEM – F12 • 10 % FBS • 1 % pen/strep
SVF-conditioned medium	<ul style="list-style-type: none"> • DMEM High Glucose • 1 % pen/strep • 5×10^5 SVF cells
AlamarBlue medium	<ul style="list-style-type: none"> • DMEM High Glucose • 1 % pen/strep • 10 % AlamarBlue reagent

3.5.2 Buffer for the gel contraction assay

Table 3.6: Components of the buffer for the gel contraction assay.

Buffer	Components
Buffer for gel contraction assay	<ul style="list-style-type: none"> • 20 % v/v 0.2 M HEPES solution • 4.33 % v/v 10 x DMEM - low glucose • 2.67 % v/v sterile H₂O

3.6 Primers

Table 3.7: Primers used in this thesis.

Gene Name	Forward primer (5`-3')	Reverse primer (5`-3')
CD11c	TGC CAG GAT GAC CTT AGT GTC G	CAG AGT GAC TGT GGT TCC GTA G
CD301b	GAC TGA GTT CTC GCC TCT GG	CTG GGA AGG AAT TAG AGC AAA CT
Collagen I	CTG GCG GTT CAG GTC CAA TG	GAA GCC TCG GTG TCC CTT CA
Collagen III	GAC CAA AAG GTG ATG CTG GAC AG	CAA GAC CTC GTG CTC CAG TTA G
Collagen IV	GGT GTG CGG TTT GTG AAG CA	TGG CGT GGG CTT CTT GAA CA
Elastin	TCC TGG GAT TGG AGG CAT TGC A	ACC AGG CAC TAA ACC TCC AGC A
Fibronectin	CGG ACG CTG CGA AAA GAT GA	ACT TGG CTG GCA ACC CTT CT
IL-6	TAC CAC TTC ACA AGT CGG AGG C	CTG CAA GTG CAT CAT CGT TGT TC
Keratin 10	TCG CAA GGA TGC TGA AGA GTG G	GGA CTG TAG TTC AAT CTC CAG AC
KGF1/FGF7	TGT TCT GTC GCA CCC AGT GGT A	TTC CAA CTG CCA CGG TCC TGA T
KGF2/ FGF10	CAA CTC CGA TTT CCA CTG ATG T	GCT GTT CTC CTT CAC CAA GT
MIF	CGC TTT GTA CCG TCC T	CGT GCC GCT AAA AGT CA
MIF-2/D-DT	CTC TTC TCC CGC TAA CAT GC	TCA TGC CAG GTC GTA TCG TA
MMP-9	CAG CCA ACT ATG ACC AGG AT	CTG CCA CCA GGA ACA GG
PDGF A	GCA AGA CCA GGA CGG TCA TTT AC	TGT TCA GGA ATG TCA CAC GCC
RPS29	TTC CTT TCT CCT CGT TGG GC	TTC AGC CCG TAT TTG CGG AT
TGF-β1	TGA TAC GCC TGA GTG GCT GTC T	CAC AAG AGC AGT GAG CGC TGA A
β-actin	CAT CCA GGC TGT GCT GTC CCT GTA TGC	GAT CTT CAT GGT GCT AGG AGC CAG AGC

3.7 Antibodies

Table 3.8: Primary antibodies used in this thesis.

Antibody	Host species	Dilution	Use	Manufacture
CD31	rabbit (polyclonal)	1:50	Immunohistochemistry	Abcam, Cambridge, England
CD74 (conjugated to BB700)	rat (monoclonal)	1:50	Immunofluorescence for FACS analysis	BD, Allschwil, Switzerland
F4/80	rat (monoclonal)	1:400	Immunohistochemistry	BMA Biomedicals, Augst, Switzerland
F(ab)	goat (polyclonal)	1:50	Immunohistochemistry	Abcam, Cambridge, England
Ki67	rabbit (monoclonal)	1:200	Immunohistochemistry	Abcam, Cambridge, England
α -SMA	mouse (monoclonal)	1:2	Immunohistochemistry	Abcam, Cambridge, England
TNF- α	rabbit (monoclonal)	1:100	Immunohistochemistry	Abcam, Cambridge, England

Table 3.9: Secondary antibodies used in this thesis.

Antibody	Host species	Use	Manufacture
anti-rabbit IgG	goat (polyclonal)	Immunohistochemistry	Agilent DAKO, Santa Clara, CA, USA
anti-rat IgG	rabbit (polyclonal)	Immunohistochemistry	Merck, Darmstadt, Germany
anti-mouse IgG	goat (polyclonal)	Immunohistochemistry	Agilent DAKO, Santa Clara, CA, USA

3.8 Consumables

Table 3.10: Consumables used in this thesis.

Consumables	Manufacturer
Aspirating pipette, 2 mL	Falcon Corning, Corning, NY, USA
Cell culture flasks T-75; filter cap	Sarstedt AG, Sevelen, Switzerland
Cell strainer, 70 μm , Nylon membrane	Falcon Corning, Corning, NY, USA
Centrifuge tube, 15 mL	TPP Techno Plastic Products AG, Trasadingen, Switzerland
Centrifuge tube, 50 mL	TPP Techno Plastic Products AG, Trasadingen, Switzerland
Cryotubes	VWR, Dietikon, Switzerland
Filter tips, clear, sterile, 0.5 – 10 μL	Axygen Corning, Corning, NY, USA
Filter tips, clear, sterile, 2 – 20 μL	Axygen Corning, Corning, NY, USA
Filter tips, clear, sterile, 2 – 100 μL	Axygen Corning, Corning, NY, USA
Filter tips, clear, sterile, 2 – 200 μL	Axygen Corning, Corning, NY, USA
Filter tips, clear, sterile, 100 – 1000 μL	Axygen Corning, Corning, NY, USA
Filter-Tips, 50 μL QIAgility	QIAGEN, Hilden, Germany
Insulin syringe, 1 mL	BD, Allschwil, Switzerland
Mesh woven filters 1000 μm , nylon, Spectra Mesh®	Spectrum LifeSciences, Los Angeles County, CA, USA
Microtiter plate PS, F-form (96-wells)	Semadeni AG, Ostermundigen, Switzerland
Opsite Flexifix	Smith & Nephew Orthopaedics GmbH, Tuttlingen, Germany
Parafilm "M" - Laboratory Film	American National Can, USA
Pipettes, Research™ Plus Pipettors, 0.1 – 10 μL	Research™ Plus Pipettors
Pipettes, Research™ Plus Pipettors, 0.5 – 20 μL	Research™ Plus Pipettors
Pipettes, Research™ Plus Pipettors, 1 – 100 μL	Research™ Plus Pipettors
Pipettes, Research™ Plus Pipettors, 1 – 200 μL	Research™ Plus Pipettors
Pipettes, Research™ Plus Pipettors, 100 – 1000 μL	Research™ Plus Pipettors

Materials

Reaction tube, 0.5 ml, PP	Sarstedt, Sevelen, Switzerland
Reaction tube, 1.5 ml, PP	Sarstedt, Sevelen, Switzerland
Reaction tube, 2.0 ml, PP	Sarstedt, Sevelen, Switzerland
Rotor-Disc 100	QIAGEN, Hilden, Germany
Rotor-Disc Heat Sealing Film	QIAGEN, Hilden, Germany
Scalpel blade no. 11	Swann-Morton, Sheffield, England
Scalpel blade no. 21	Swann-Morton, Sheffield, England
Serological Pipette, 5 mL	TPP Techno Plastic Products AG, Trasadingen, Switzerland
Serological Pipette, 10 mL	TPP Techno Plastic Products AG, Trasadingen, Switzerland
Serological Pipette, 25 mL	TPP Techno Plastic Products AG, Trasadingen, Switzerland
Skin biopsie punch (6 mm)	Kai medical, Seki, Japan
Surgical forceps	B.Braun, Sempach, Switzerland
Surgical scissors	B.Braun, Sempach, Switzerland
Syringe Filter, 0.22 µm pore size	TPP Techno Plastic Products AG, Trasadingen, Switzerland
Syringe, Luer-lock, sterile, 5 mL	B.Braun, Sempach, Switzerland
Syringe, Luer-lock, sterile, 10 mL	B.Braun, Sempach, Switzerland
Syringe, Luer-lock, sterile, 20 mL	B.Braun, Sempach, Switzerland
Syringe, Luer-lock, sterile, 50 mL	B.Braun, Sempach, Switzerland
Tissue culture dishes (100 mm)	VWR, Dietikon, Switzerland
Tissue culture dishes (150 mm)	VWR, Dietikon, Switzerland
Tissue culture plates (6-well)	VWR, Dietikon, Switzerland
Tissue culture plates (12-wel)	VWR, Dietikon, Switzerland
Tissue culture plates (24-wel)	VWR, Dietikon, Switzerland
Tissue grinding CKMix50-R, 2 mL tubes	bertin Instruments, Montigny-le-Bretonneux, France

3.9 Devices

Table 3.11: Devices used in this thesis.

Devices	Manufacturer
Biological Safety Cabinets, Safe 2020 Class II	Thermo Scientific, Langenselbold, Germany

Materials

-20 °C Freezer Premium NoFrost	Liebherr, Bulle, Switzerland
4 °C Fridge GRAM	GKM, Sarnen Germany
-80 °C Freezer HeraFreeze HFU T	Thermo Scientific, Asheville, NC, USA
Autostainer Link48	Agilent DAKO, Santa Clara, CA, USA
Camera stative	house intern workshop from USZ, Zurich, Switzerland
Capsulefuge (Centrifuge PMC-060)	Tomy Kogyo, Tokyo, Japan
Centrifuge 5417R	Eppendorf, Hamburg, Germany
Centrifuge Rotina 35 R	Hettich Kirchlengern, Germany
CO ₂ -Incubator, Forma™ Steri-Cult™	Thermo Fisher Scientific, Asheville, NC, USA
Digital Camera EOS 4000D	Canon, Tokyo, Japan
Electronic veterinary weighing scale for small animals	Soehnle Industriel Solution GmbH, Backnang, Germany
FACSCanto™ II	BD, Allschwil, Switzerland
Handling Tube Tunnel	ZoonLab GmbH, Castrop-Rauxel, Germany
Minilys Personal Homogenizer	bertin Instruments, Montigny-le-Bretonneux, France
NanoDrop 2000 Spectrophotometer	Thermo Scientific, Langenselbold, Germany
Pipettor Turbo-Fix	TPP Techno Plastic Products AG, Trasadingen, Switzerland
QIAgility	QIAGEN, Hilden, Germany
Rodent heating pad	Stoelting co, Wood Dale, IL, USA
Rodent shaver	AgnTho, Lidingö, Sweden
Rotor-Disc® Heat Sealer	QIAGEN, Hilden, Germany
Rotor-Gene Q	QIAGEN, Hilden, Germany
Shaking Water Baths, THERMOLAB®, Typ 1083	GFL, Burgwedel, Germany
SimpliAmp™ Thermal Cycler	Thermo Fisher Scientific, Asheville, NC, USA
Thermomixer comfort	Eppendorf, Hamburg, Germany
Vortex Genie 2™	Bender & Hobein AG, Zurich, Switzerland

3.10 Software

Table 3.12: Software used in this thesis.

Software	Use	Manufacturer
GraphPad Prism 8	<ul style="list-style-type: none"> • Data and statistical analyses • Generate graphs for publication and dissertation 	GraphPad Software, La Jolla, CA, USA
ImageJ	<ul style="list-style-type: none"> • Measurement of wound areas • Measurement of gel area • Analysis of histochemical stained tissue slights for collagen participation • Analysis of immunohistochemically stained slights 	Schneider <i>et al.</i> [164]
Adobe Photoshop CS6	Quantification of the fluorescence signal	Adobe Inc., San José, CA, USA
Zeiss Zen 3.1 Airyscan	Processing of scanned tissue slights	Carl Zeiss AG, Oberkochen, Germany
FlowJo v10	Data analysis of FACS samples	FlowJo, Becton, Dickinson & Company, Franklin Lakes, USA

4. Methods

4.1 *in vivo* techniques

C57BL/6 wild type (WT) mice were used for mouse experiments. WT mice were purchased from Charles River Laboratories. In addition, a C57BL/6 *Mif-2^{-/-}* strain was bred in the animal facility. All mice were housed under the regular 12:12 h light:dark cycle in the animal facility of the institute of Biologisches Zentrallabor (BZL) of University Hospital Zurich (USZ). The mice had access *ad libitum* to water and food. All *in vivo* experiments were approved by the Cantonal Veterinary Office, Zurich (ZH004/19) and was in accordance with the Swiss Animal Protection Law and the European Directive 2010/63/EU of the European Parliament and of the Council on the Protection of Animals used for Scientific Purposes.

4.1.1 High fat diet (HFD) and weight measurement

In order to mimic the state of obesity in humans a high fat diet (HFD) model to induce obesity using chows consisting of 60 % fat per kilocalorie was used [46, 165]. One WT mice group ($n = 15$) and one group of C57BL/6 *Mif-2^{-/-}* mice ($n = 13$) were put on HFD at an age of 4 weeks, a second WT group ($n = 14$) and a second *Mif-2^{-/-}* mice ($n = 16$) were fed with regular chows (RD, regular diet) containing 4.5 % fat per kilocalorie. Each mouse group had access *ad libitum* to chows. The weight gain was determined by weekly weight measurements with a rodent scale.

4.1.2 Wound healing model

The major focus from the *in vivo* experiments was on the well established wound healing model. Thirteen-week-old mice from each group underwent wounding. Two dorsal incision wounds and two dorsal excision wounds were set per mouse (Figure 4.1). Both wound models were chosen as Ansell *et al.* have shown that excision wounds show less variety in wound closure and planimetric measurements but high fluctuations in histological analysis, while incision wounds vary strongly in planimetry but are more stable in histology as excisional wounds [166].

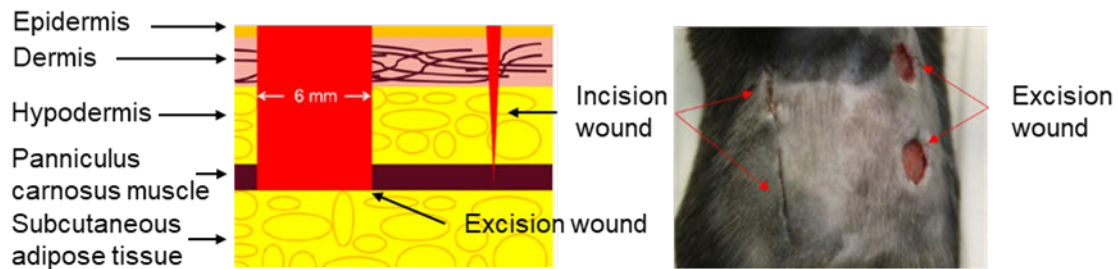


Figure 4.1: Incisional and excisional wound model. In the incision wound model, two 1 cm long wounds are created on the left side of the dorsum of mice with a scalpel blade. In the excision wound model two defined circular 6 mm wounds are created on the right side of the dorsum of mice with a standard punch biopsy device. The wounds penetrate the epidermis, dermis, hypodermis and *panniculus carnosus* muscle.

After the mouse was injected subcutaneously with buprenorphine (0.1 mg per kg body weight) as analgesic and was anaesthetized with 5 % isoflurane the back was shaved and cleaned with warm water and a tissue. During the whole surgery, the mouse laid on a heating pad set to 37 °C to keep constant body temperature. To maintain the anesthesia a rodent gas mask was placed on the nose of the mouse with a steady flow of 3 – 5 % isoflurane. Two 1 cm long incisions wounds were set on the left side of the dorsum reaching subcutaneous adipose tissue using a scalpel. Two dorsal 6 mm circular excision wounds were inflicted by a biopsy puncher. The tissue was carefully cut off with a surgical scissor including *panniculus carnosus* muscle.

After infliction of wounds they were covered by a transparent plaster and buprenorphine (0.1 mg per kg body weight) was injected for postoperative follow-up care. The mice were single housed to prevent fights between wounded mice. Furthermore, the mice were put into a warm chamber at 29 °C with a humidity of 60 % over night. Afterwards they were housed under regular conditions.

4.1.3 Macroscopic analysis of the wounds and wound scoring

To assess the healing process photos of incision and excision wounds were taken daily and closure were monitored through planimetry. The wound size was digitally determined using Adobe Photoshop and ImageJ. To ensure always the same distance between wound and camera a device was designed in collaboration with the technical service of the USZ (Figure 4.2). In short, a metal plate with a rectangle cutout (screen) was fixed on a metal rail. The camera could be fixed on the rail and the distance between camera and the metal screen was adjustable. A scale placed around the cutout was used to calculate the wound area.



Figure 4.2: Picture of the designed device to ensure always the same distance from camera to the wound.

Furthermore, the wounds and the mice respectively were monitored for wound state/inflammation, weight, activity, physical appearance and posture daily (see Appendix).

4.1.4 Sample collection

Mice were euthanized by CO₂ fumigation at day 1, 3, 7, 14 and 21 after wound infliction. Days were chosen in order to cover each wound healing phase [46]. Wound tissue including surrounding area and underlying subcutaneous tissue was collected and either flash frozen in liquid nitrogen or fixated in 4 % paraformaldehyde overnight. After the fixation, water was removed from the samples and they were embedded in paraffin for further histological analysis.

4.2 Histology and immunohistochemistry

All histological and immunohistochemical stains were carried out by Ines Kleiber-Schaaf and Andrea Garcete-Bärschi of the histology service of the Center for Surgical Research. The paraffin-tissue blocks were cut into 5 µm slides using a microtome. The tissue slides were placed on microscope slides. The stained tissue slides were scanned at 10-fold magnification and analyzed as described below.

4.2.1 Masson-Goldner's trichrome staining

In order to visualize the different skin layers of the wounds tissue slides were stained via Masson-Goldner's trichrome technique [167]. All steps were done at room

temperature (RT). First paraffin was removed incubating twice in xylene for 5 min. Subsequently the tissue was rehydrated in 100 % ethanol (EtOH) three times for 2 min, in 96 % EtOH for 2 min and finally in 70 % EtOH for 2 min. Afterwards the tissue was incubated with Weigert's haematoxylin solution for 8 min. Following washing in water for 5 min, the slide was stained in ponceau acid fuchsin solution (Goldner solution I) for 15 min. After washing briefly in 1 % acetic acid, the tissue slide was treated with phosphomolybdic acid-orange G solution (Goldner solution II) for 5 min. Consecutively the tissue slide was washed briefly with 1 % acetic acid and stained with light green solution (Goldner solution III). After the tissue was washed in 1 % acetic acid for 1 min, it was dehydrated in 96 % EtOH for 2 min and twice in 100 % EtOH for 2 min. At the end, the tissue slide was washed three times in 100 % xylene and a coverslip was mounted over the tissue.

4.2.2 Immunohistochemical staining

As described in the Masson-Goldner's trichrome staining the paraffin was eliminated from the tissue section and the tissue section was rehydrated. Afterwards the tissue was treated with 3 % H₂O₂ for 5 min and washed with distilled (d)H₂O for 5 min. Following incubation in Normal Goat Serum for 30 min and a washing step with supplied wash buffer for 3 min, the antibody solution was added onto the tissue slide and incubated for 60 min (see antibody list with appropriated dilutions in Table 4.1). A pretreatment with goat F(ab) anti-mouse immunoglobulin G (IgG) for 30 min was necessary in case of anti- α -smooth muscle actin (SMA) antibody. After washing with wash buffer for 3 min the staining procedure for all samples was as following. The tissue slide was incubated in the desired primary antibody for 30 min and washed with wash buffer for 3 min. The secondary horseradish peroxidase (HRP) conjugated antibody was added and after 20 min the slide was washed for 5 min in washing buffer. It followed an incubation in 3,3'-diaminobenzidine (DAB) solution for 10 min and a brief washing step with wash buffer. Afterwards the tissue was treated with flex hematoxylin solution for 10 min and washed with the wash buffer for 5 min. At the end, the slide was dehydrated by incubation in EtOH with increasing concentration (70 – 96 - 100 %) followed by washing three times with xylene (100 %) and mounted as described in the Masson-Goldner's trichrome technique.

Table 4.1: Antibodies used for immunohistochemical staining.

primary antibody	host species	used dilution	secondary antibody-HRP
CD31	rabbit (polyclonal)	1:50	anti-rabbit
F4/80	rat IgG (monoclonal)	1:400	anti-rat IgG
F(ab)	goat IgG (polyclonal)	1:50	-
Ki67	rabbit (monoclonal)	1:200	anti-rabbit
α -SMA	mouse (monoclonal)	1:2	anti-mouse
tumor necrosis factor- α	rabbit (monoclonal)	1:100	anti-rabbit

4.3 Molecular biological analyses of the wound tissue

4.3.1 RNA isolation from mouse wound tissue

RNA was isolated from the sampled wound tissue based on the work of P. Chomczynski and N. Sacchi [168]. After adding ceramic beads and 1 mL TRIzol the tissue was homogenized using a tissue homogenizer for 3 min at 5,000 rpm and 4 °C. After homogenization of the tissue, the samples were incubated for 15 min at 300 rpm at 23 °C in a thermomixer. The suspension was transferred into a microcentrifuge tube (tube) and centrifuged for 10 min at 12,000 x *g* and 4 °C. The cleared supernatant was transferred into a new tube, 200 μ L chloroform was added and the sample was incubated for 3 min at 300 rpm at 23 °C in a thermomixer. To separate the aqueous phase containing the RNA from the organic phase the samples were centrifuged for 15 min at 12,000 x *g* and 4 °C.

RNA was precipitated by adding 500 μ L 100 % isopropanol and centrifuged for 10 min at 12,000 x *g* and 4 °C. Supernatant was discarded. RNA pellet was washed twice with 1 mL 75 % EtOH and centrifuged 5 min at 7,500 x *g* and 4 °C. Precipitated RNA was dried at RT and afterwards resuspended in RNase-free water followed by an incubation step at 57 °C for 15 min at 1000 rpm in a thermomixer. RNA concentration was measured using a NanoDrop spectrophotometer.

4.3.2 Reverse transcription and real-time quantitative polymerase chain reaction (RT-qPCR)

Gene expression in wound tissue was analyzed by real-time quantitative polymerase chain reaction (RT-qPCR). cDNA was synthesized by reverse transcription using 500 ng of isolated total RNA. Synthesis was performed with oligo-dT primers (0.5 µg/µL), dNTP-mix (10 mM), DTT (1,4-dithiothreitol, 0.1 M), 5 x FS buffer, RNase inhibitor (20 U/µL), SuperScript® III (200 U/µL) and dH₂O using a GeneAMP PCR System (2 h 50 °C, 10 min 72 °C).

RT-qPCR was performed using a Rotor Gene PCR machine. Specific primers (Table 3.7) were premixed with dH₂O and 50 v/v % SYBR green mix to an end concentration of 0.25 µM. 2 µL of transcribed cDNA was used per analysis. Each sample was performed in triplicates. The cycling conditions were 95 °C for 5 s followed by 45 cycles of 60 °C for 30s and 72 °C for 30s. Through analysis of melting curves, unspecific amplifications and primer dimer formations were excluded. The gene expression was normalized to RPS29 and β-actin after the method of Taylor *et al.* [169].

4.4 Murine fibroblast cell line NIH/3T3 differentiation

Murine NIH/3T3 fibroblasts were used for differentiation studies of fibroblasts into myofibroblasts [170]. The cells were incubated at 37 °C in an atmosphere with 95 % humidity and 5 % CO₂. Dulbeccos's modified eagle's medium (DMEM) high glucose supplemented with 10 % fetal bovine serum (FBS) and 1 % penicillin-streptomycin (pen/strep) solution served as culture medium. Culture medium was changed twice a week. If the cells reached 80 – 90 % confluency, they were passaged. Therefore the cells were incubated with 1 x Trypsin (EDTA) for 10 – 15 min at 37 °C. The cell suspension was transferred to a centrifugation tube and centrifuged for 5 min at 500 x g. The supernatant was removed and cells were resuspended in culture medium and split 1:3.

In order to differentiate the cells into myofibroblasts, the culture medium was removed and the cells were washed with sterile phosphate buffered saline (PBS). Afterwards

the cells were incubated in myofibroblasts differentiation medium. The differentiation medium (DM) based on DMEM high glucose medium supplemented with 1 % pen/strep solution. Furthermore, recombinant mouse tumor growth factor (TGF)- β 1 was added with a final concentration of 2 ng/mL to initiate the differentiation [96, 170]. The cells were incubated under regular incubation conditions for at least one day.

4.4.1 FACS-flow cytometry

In order to analyze the CD74 receptor expression during differentiation of NIH/3T3 cells fluorescence associated cell sorting (FACS) flow cytometry was performed with undifferentiated and differentiated cells. 100'000 cells of both groups were incubated in 100 μ L anti-mouse CD74 antibody solution (4 μ g/mL in PBS) for 60 min at 4 °C in the dark. The antibody was linked to the fluorophore BD Horizon Brilliant™ Blue 700 having an excitation maximum at λ_{ex} = 476 nm and an emission maximum at λ_{em} = 695 nm.

The same amount of cells was treated equivalently lacking the antibody as the control group. After incubation the cells were washed twice with PBS, resuspended in 500 μ L PBS and filtered through a 35 μ m mesh cell strainer. The samples were excited with λ_{ex} = 488 nm and fluorescence was detected via the PerCP Cy5.5 channel at λ = 695 nm.

4.4.2 Collagen gel contraction assay

The collagen gel contraction assay was performed to examine the contractility of the differentiated NIH/3T3 cells [171]. A 24-well plate was treated with 1 % BSA solution dissolved in PBS for 30 min at 37 °C. Afterwards the BSA solution was removed. The collagen-cell-mixture consisted of 20 % v/v 0.2 M HEPES buffer (pH 8.0), 4.33 % v/v 10 x DMEM (low glucose), 2.67 % v/v sterile H₂O, 33 % v/v TeloCol® collagen solution (3 mg/mL) and 40 % v/v cell suspension (4.2 x 10⁵ cells/mL suspended in culture medium). First, HEPES was mixed with 10 x DMEM and H₂O and the mixture was transferred in 1.5 mL tubes, one tube per sample. Afterwards cells were diluted in culture medium to a concentration of 4.2 x 10⁵ cells/mL and added to the tubes. In case of gel without cells, only culture medium was added. As the final step, collagen solution, which was stored on ice, was mixed into the cell-buffer-mixture and 500 μ L of the finished collagen-cell solution was immediately transferred into one well. The

plate was incubated for 30 min at 37 °C so that the solution forms a gel. Afterwards 1 mL of the desired medium was added to the gel and the gel was softly detached from the walls of the wells using a sterile pipette tip.

As negative controls, gel without cells was incubated in DM as well as gel with cells in culture medium(basic medium, BM) without TGF- β 1. Gel with cells in DM acted as positive control. For the experiment, mouse recombinant MIF-2 (m-rMIF-2) was added in different concentrations (10 ng/mL, 50 ng/mL, 100 ng/mL, 200 ng/mL and 400 ng/mL) to DM. All samples were carried out in triplicates. The size of the gel was daily analyzed by taking pictures of each gel and calculating the gel size using Adobe Photoshop and ImageJ.

In an additional experiment the collagen-cell gel was incubated in DM supplemented with increasing concentrations (5 μ M, 10 μ M, 15 μ M, 30 μ M, 60 μ M) of 4-CPPC, a selective inhibitor for MIF-2-CD74 interaction [172]. The controls were the same as previously described.

4.5 Human primary cells

The use of patient tissue and non-personal data which were used in this work were approved by Kantonale Ethik Kommission (KEK) Zurich Swiss (KEK-ZH: StV 7-2009), the Swiss ethics (BASEC-Nr.: 2019-00389), and the international ethical guidelines (ClinicalTrials.gov; Identifier: NCT01218945).

Cell were always cultured in an incubator at 37 °C in an atmosphere with 95 % humidity and 5 % CO₂ unless otherwise stated.

4.5.1 Isolation and culture of human fibroblasts

Human fibroblasts were isolated from fresh skin received from surgeries. Subcutaneous fat tissue was removed and skin was cut in small strips (approximately 10 mm x 2 mm). The strips were incubated in Dispase II solution (5 μ g/mL in RPMI medium) for 1 h at 37 °C followed by 4 °C overnight. Next day, the solution was removed and epidermis and dermis were separated using two surgery forceps. In order to isolate the fibroblasts from the dermis the tissue pieces were incubated in

Collagenase II solution (2 mg/mL in RPMI) at 37 °C for 1 h. Afterwards the solution was filtered through a mesh filter with 1000 µm pore size to take out undigested tissue and the cell suspension was centrifuged for 10 min at 300 x *g*. Supernatant was removed and the cell pellet was resuspended in 10 mL PBS and centrifuged for 10 min at 300 x *g*. After the PBS has been removed, the cell pellet was resuspended in fibroblast culture medium (DMEM high glucose supplemented with 10 % FBS and 1% pen/strep antibiotics), transferred into a 150 mm cell culture dish and cultivated in the incubator. The culture medium was changed twice per week. When fibroblast reached 90 % confluency, they were passaged 1:3 as described above.

4.5.2 Isolation of human stromal vascular fraction (SVF)

Human stromal vascular fraction (SVF) was isolated from fat tissue received from surgeries. Fat tissue was cut into small pieces with a surgical scissor and digested in sterile 2 mg/mL collagenase II solution at 37 °C for 45 – 60 min shaking. After digestion solutions was further homogenized through pipetting up and down and undigested pieces were removed by filtering through a 200 µm mesh filter. In order to separate adipocytes and oil from isolated cells the solution was centrifuged at 300 x *g* for 10 min. The four phases (Figure 4.3) from bottom to top were as follows: SVF cell pellet ,aqueous phase containing medium, serum etc., layer of adipocytes, and on top an oily fat phase of triglycerides. All phases apart of the SVF cell pellet were discarded. Cell pellet was resuspended in 5 mL erythrocyte lysis buffer and incubated on ice for 10 min. Afterwards PBS was added *ad* 40 mL and the cell suspension was centrifuged for 10 min at 300 x *g*. The cell pellet was resuspended in 5 mL PBS and filtered through a cell strainer with 70 µm pore size. Cell suspension was centrifuged for 10 min at 300 x *g*. Isolated cells were resuspended either in 5 – 10 mL PBS to count them or directly in culture medium.

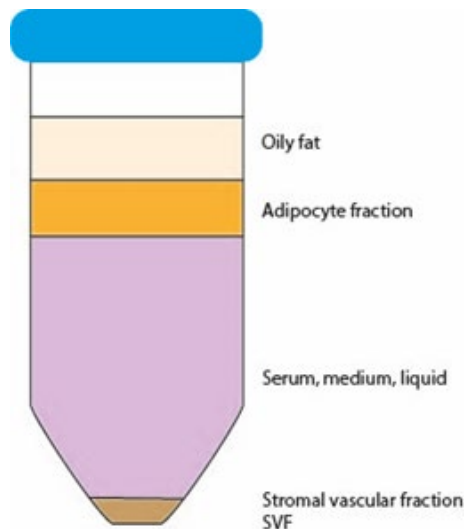


Figure 4.3: Phases of digested fat tissue after centrifugation. After collagenase II digestion of fat tissue, the solution was centrifuged to separate the different phases. On top was the oily fat phase followed by a thin layer of adipocytes. The biggest phase was the liquid phase containing medium, collagenase solution, serum etc. At the bottom, the SVF cell pellet was formed.

4.5.3 Producing of SVF-conditioned medium (SVF-CM)

SVF-conditioned medium (SVF-CM) was created from obese patients with a BMI (body mass index) >25 and lean patients with a BMI <25. In order to produce SVF-CM, freshly isolated cells were resuspended in 5 – 10 mL sterile PBS and counted using a Neubauer chamber. The cell suspension was centrifuged for 10 min at 300 x *g*. PBS was removed and the cells were resuspended in SVF culture medium (DMEM/F12 supplemented with 10 % FBS, 1 % penicillin/streptomycin antibiotics and 5 ng/mL basic fibroblast growth factor) to a cell concentration of 5×10^5 cells/mL. One milliliter of the cell suspension was transferred into a T75-cell culture flask and 9 mL SVF culture medium was added. After incubation over night in the incubator SVF culture medium was removed and cells were washed twice with PBS. Afterwards 10 mL of DMEM high glucose medium supplemented with 1 % pen/strep antibiotics were added to the cells and the cell culture flask was incubated for 3 days. SVF-CM was centrifuged for 5 min at 500 x *g*, sterile filtered through a 0.22 μm syringe filter and stored at -20 °C (for long term storage at -80 °C) [173].

4.5.4 Viability assay with SVF-CM and rMIF-2 treatment

To evaluate the effect of SVF-CM from obese and lean patients supplemented with different concentrations of human recombinant MIF-2 (h-rMIF-2) on fibroblast an

Alamar Blue viability assay was performed. Fibroblasts were seeded in a 24-well plate in a concentration of 40'000 cells/well and cultivated in fibroblast culture medium/proliferation medium (PM) overnight in the incubator. On the next day the culture medium was removed, the cells were washed with PBS and 0.5 mL SVF-CM was added to the cells. In addition, h-rMIF-2 was added to the cells in concentrations of 0 ng/mL, 50 ng/mL, 100 ng/mL, 200 ng/mL and 400 ng/mL based on the work of Kim *et al.* [162]. Cells cultured in basic medium (BM, DMEM high glucose medium with 1 % pen/strep) and PM served as negative and positive controls. Each condition was carried out in triplicate.

To assess cell viability under the different conditions at different time points, the medium was removed and cells were washed twice with PBS and incubated in 500 μ L PM with 10 % alamarBlue reagent for 3 h in the incubator. Afterwards 100 μ L supernatant was transferred into a 96-well plate to measure fluorescence with excitation at $\lambda_{exc} = 555$ nm and emission at $\lambda_{em} = 596$ nm. Each sample was measured as a technical triplicate and the average was calculated. After each alamarBlue assay cells were washed with PBS and treated as described above. Cell viability was measured at day 3 and day 7 and day 0 before the first treatment as reference.

4.6 Statistics

GraphPad Prism8 was used for statistical analysis and to plot the graphs. Graphs are shown as mean \pm SEM. Statistical variance between groups were calculated by either student's unpaired two-tailed t-test or one-way or two-way ANOVA. Tukey-test were used as *post hoc* test. A *p*-value < 0.05 was considered as statistically significant.

5. Results

5.1 *In vivo* experiments

Several clinical studies have shown that obese patients have a diminished wound repair up to formation of ulcer [37-39]. This negative effect was also investigated and verified in different *in vivo* mouse models with no conclusive results provided to this day [46, 47, 174]. It is well described, that cytokine secretion is altered in adipose tissue and causes a worsened wound healing response. One impactful cytokine is the pro-inflammatory chemokine-like mediator macrophage migration inhibitor factor (MIF)-2, whose expression and serum level is decreased in obese individuals [50, 141].

Thus, next to the impact of MIF-2 on wound healing, one focus of my dissertation was to study the impact of obesity on wound healing and the correlation with MIF-2. To evaluate specific effects of obesity on wound healing, a regular diet (RD) and a high-fat diet (HFD) model of diet-induced obesity (DIO) in wild type (WT) and *Mif-2*^{-/-} C57BL/6J male mice to mimic the state of obesity in humans [46, 165, 175]. Solely male mice were selected as the female mice in a previous pilot study did not respond to the HFD and did not develop an appropriate state of obesity. First, the course of HFD-induced obesity was followed as basis for the following *in vivo* wound healing experiments.

5.1.1 Weight gain of C57BL/6 wild type and *Mif-2*^{-/-} mice under RD or HFD

The various diets started from week 4, one week after weaning. The weight was weekly measured using a rodent scale. The data were plotted as weight gain vs age (week). On the one hand, the different diet groups were compared within the same strains (Figure 5.1) and, furthermore, the different genetic strains under the same diet (Figure 5.2) were compared. Up to week 8, the two WT mice groups showed no difference in weight gain (Figure 5.1 A). The HFD group then began to put on more weight, from week 11 on, the difference became significant. There was no increased weight gain in *Mif-2*^{-/-} mice under HFD compared to RD (Figure 5.1 B). The WT mice under RD slowly gained more weight from week 8 – 9 than *Mif-2*^{-/-} mice under RD, but the difference did not reach statistical significance until the end (Figure 5.2 A). In contrast to mice fed with HFD (Figure 5.2 B), in this case, wild type mice gained

significantly more weight than the *Mif-2^{-/-}* mice from week 8 onwards. The difference became even more significant from week to week.

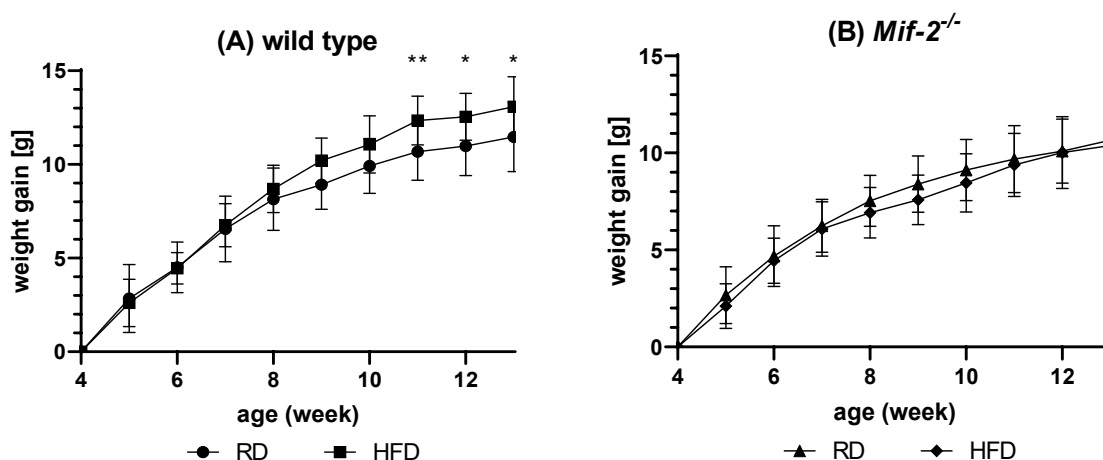


Figure 5.1: Weight gain of (A) wild type (WT) and (B) *Mif-2^{-/-}* C57BL/6 male mice under regular diet (RD) and high fat diet (HFD). Four-week-old male mice were fed either with regular chows or with high fat chows containing 60 % fat/kcal for 9 weeks. The weight gain was determined through weekly weight measurements. n (WT RD) = 14; n (WT HFD) = 15; n (*Mif-2^{-/-}* RD) = 16; n (*Mif-2^{-/-}* HFD) = 13. Statistical differences were calculated within the two groups for each day using two-way ANOVA followed by *post hoc* Tukey-test. Significance are indicated by *p < 0.05 and **p < 0.01.

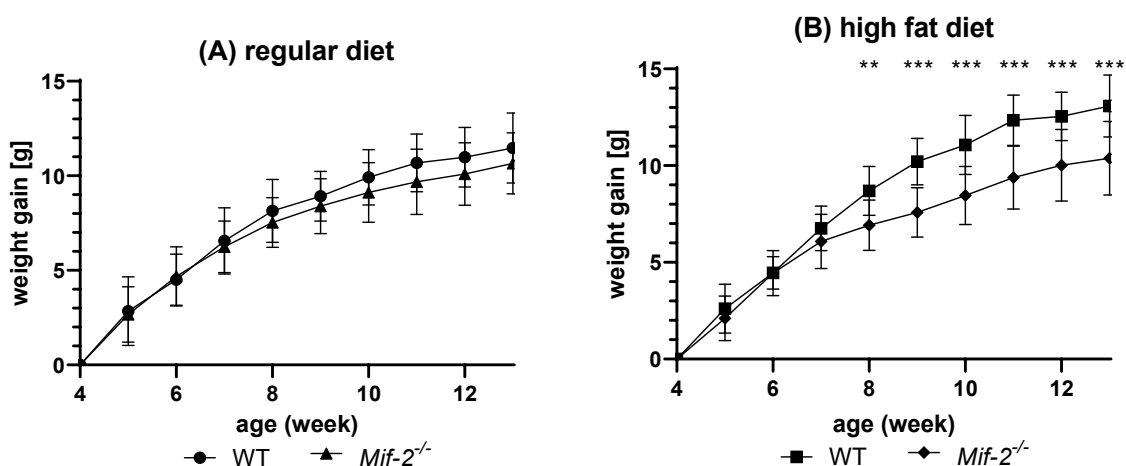


Figure 5.2: Weight gain of wild type (WT) and *Mif-2^{-/-}* C57BL/6 male mice under (A) regular diet and (B) high fat diet. Four-week-old male mice were fed either with regular chows or with high fat chows containing 60 % fat/kcal for 9 weeks. The weight gain was determined through weekly weight measurements. n (WT RD) = 14; n (*Mif-2^{-/-}* RD) = 16; n (WT HFD) = 15; n (*Mif-2^{-/-}* HFD) = 13. Statistical differences were calculated within the two groups for each day using two-way ANOVA followed by *post hoc* Tukey-test. Significance are indicated by *p < 0.05, **p < 0.01 and ***p < 0.001.

5.1.2 Wound size measurement

To investigate the impact of obesity and MIF-2 on wound healing, a well-established model of excisional wound healing was carried out [151]. Two 6 mm diameter wounds were placed on the dorsum of each mouse with a biopsy puncher. Photos of the wounds were taken on certain days to calculate the wound size. Representative sample photos for each group are shown in Figure 5.3 from day 0 to day 7. The N-numbers are shown in table. The initial wound size on day 0 was set as 100 % and served as a reference for the following days. While the wound size of WT mice continuously decreased under RD up to complete closure after 14 days, the wound size in the other groups initially increased and began to decrease again after about three days until the wounds were closed after 14 – 17 days (Figure 5.4).

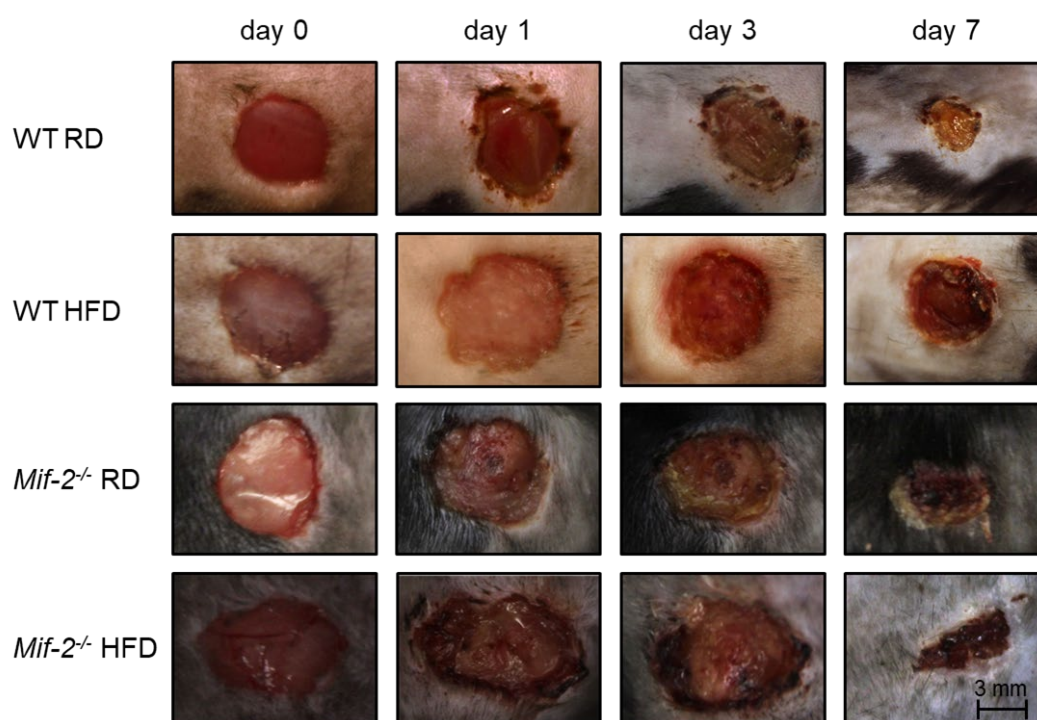


Figure 5.3: Representative wound photos from one mouse in each group in an excisional wound model. Excisional wounds were placed on the backs of WT mice and *Mif-2^{-/-}* mice fed either an RD or an HFD using a 6 mm diameter biopsy punch to assess wound healing. Wound photos were taken at day 0, 1, 3, 7, 14 and 21 to determine the wound area. Representative wound photos from one mouse for each group are shown on day 0, 1, 3 and 7.

Results

Table 5.1: n-value of wounds of each mice group on the specific days of the wound size measurement. Since mice were euthanized on days 1, 3, 7, 14 and 21 after wounding, the n-value was depending on day of experiment.

Day		0	1	3	7	10	14	17	21
WT	ND	28	28	22	16	10	10	4	4
	HFD	30	30	24	18	12	12	6	6
<i>Mif-2</i> ^{-/-}	ND	32	32	32	26	16	16	6	6
	HFD	26	26	26	26	16	16	6	6

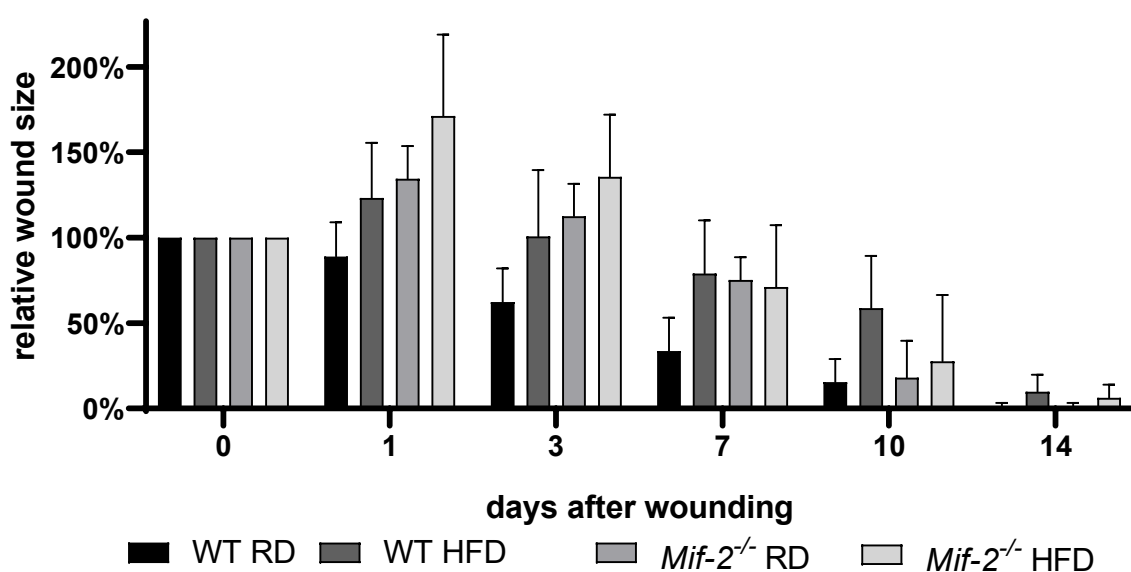


Figure 5.4: Wound area in an excisional wound model in wild type (WT) and *Mif-2*^{-/-} C57BL/6 male mice under regular diet (RD) and high fat diet (HFD). Excision wounds were set on the back of mice using a 6 mm diameter biopsy puncher to evaluate wound healing under various diets. The wound size were regularly determined photographically. The wound size was calculated in relation to the initial wound in %. Data of the days 17 and 21 are not displayed due to zero value. Statistical analysis is omitted here due to the multiple comparison and the resulting overloaded representation. They are shown in the individual separate comparisons in the following figures.

In Figure 5.5, the data of the wild type groups were plotted and compared. During the first 10 days after the wounding, the wound size of the HFD group was significantly increased compared to the WT RD mice. After three days, the wound size in the HFD group was similar to that at day 0 in the RD group. After 10 days, the HFD mice still had wounds with an area greater than 50 % of the initial wound size. While the RD mice have shown less than a third of the wound size from the HFD group. From the 10th to the 14th day, the wound size of the HFD group shrank from over 50 % to about 10 % and the wound was completely healed after 17 days.

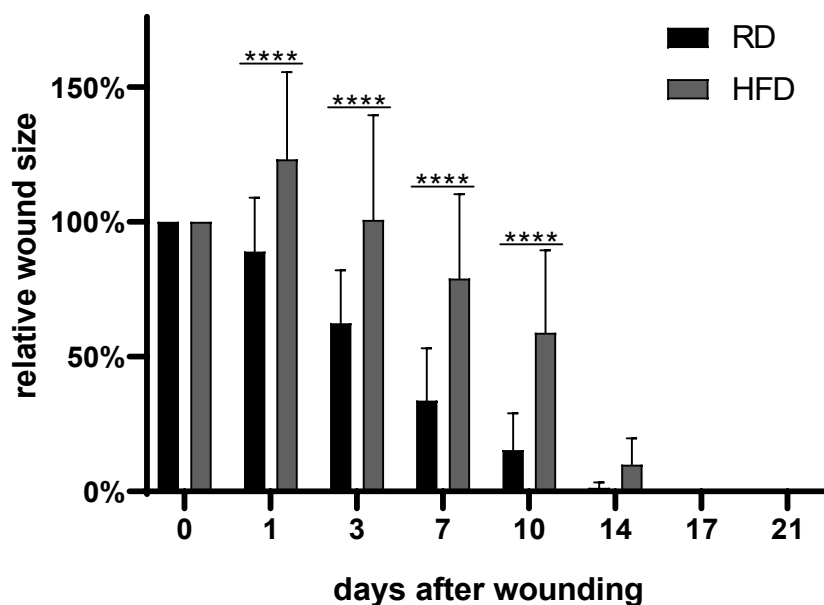


Figure 5.5: Wound size in an excisional wound model in wild type C57BL/6 male mice under regular diet (RD) and high fat diet (HFD). Excisional wounds were set on the back of mice using a 6 mm diameter biopsy puncher to evaluate wound healing under different diets. The wound size were regularly determined photographically. The wound size was calculated in relation to the initial wound in %. Statistical analysis was calculated for each day between the groups using two-way ANOVA followed by *post hoc* Tukey-test. Significance are indicated by * $p < 0.05$, ** $p < 0.01$ and **** $p < 0.001$.

In contrast to WT mice, *Mif-2^{-/-}* mice have shown a similar wound healing process under the two different diets (Figure 5.6). With the exception on day 1, where the wound size was significantly enlarged in the HFD group compared to the RD group. After 3 days, the wounds of the obese mice were still bigger although this trend did not reach statistical significance. After one week of healing, there was no difference anymore.

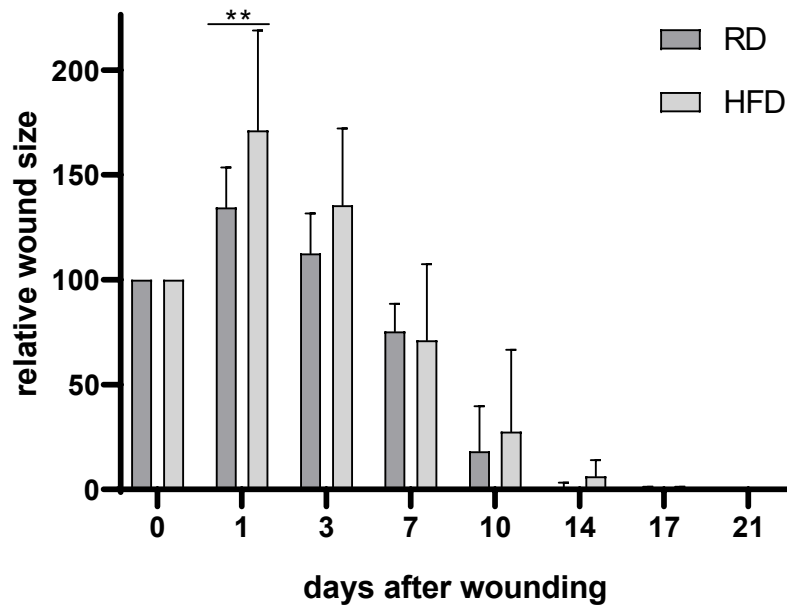


Figure 5.6: Wound size in an excisional wound model in *Mif-2^{-/-}* C57BL/6 male mice under regular diet (RD) and high fat diet (HFD). Excisional wounds were set on the back of mice using a 6 mm diameter biopsy puncher to evaluate wound healing under different diets. The wound size were regularly determined photographically. The wound size was calculated in relation to the initial wound in %. Statistical analysis was calculated within each day between the groups using two-way ANOVA followed by *post hoc* Tukey-test. Significance are indicated by * $p < 0.05$, ** $p < 0.01$ and *** $p < 0.001$.

The different mice strains were also compared under the same diet. Like the WT mice under HFD, the *Mif-2^{-/-}* RD mice showed a strongly significantly diminished wound healing compared to the WT mice under RD (Figure 5.7). Interestingly, the wound size was already at the same level after 10 days, while the WT mice that were fed with high fat chows had significantly larger wounds. After two weeks, the wounds were completely healed in both cases, the WT RD and the *Mif-2^{-/-}* RD mice.

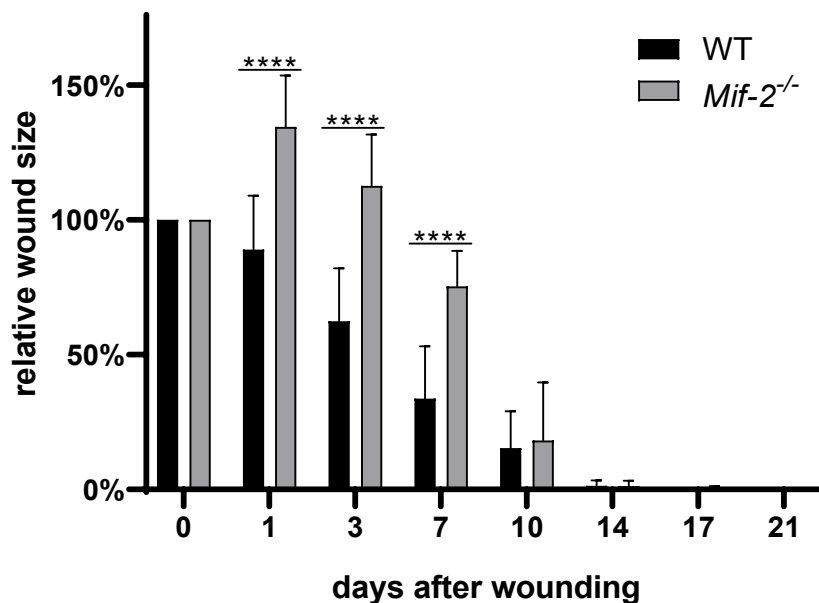


Figure 5.7: Wound area in an excisional wound model in wild type (WT) and *Mif-2*^{-/-} C57BL/6 male mice under regular diet. Excisional wounds were placed on the back of mice using a 6 mm diameter biopsy puncher to investigate the role of MIF-2 on wound healing. The wound size were regularly determined photographically. The wound size was calculated in relation to the initial wound in %. Statistical analysis was calculated within each day between the groups using two-way ANOVA followed by *post hoc* Tukey-test. Significance are indicated by **p* < 0.05, ***p* < 0.01 and ****p* < 0.001.

Under HFD the *Mif-2*^{-/-} mice had even larger wounds than the WT HFD mice at day one after wounding (Figure 5.8). Afterwards, the *Mif-2*^{-/-} mice healed faster compared to the WT group. After 3 days, the wound area of the knockout mice were still significant wider but after 7 days the wound area was on the same level. At day ten, they changed and the WT mice had the slightly larger wounds. At both groups, the wounds were closed after 17 days.

In general, the healing process of the *Mif-2*^{-/-} mice was similar to the healing process of the WT mice under HFD (Figure 5.4). There was still a difference, however. While the HFD WT mice showed continuously diminished wound healing, both *Mif-2*^{-/-} groups only had delayed healing in the first week. From day 7 to 10 the wound areas suddenly shrank, in case of the *Mif-2*^{-/-} RD group even on the WT RD size, while the HFD WT mice group still had a wound area of 50 %.

Thus, the *in vivo* excisional wound healing experiment indicates that a HFD exerted a negative effect on the wound healing, delaying healing by about 3 – 7 days. A similar conclusion in the *Mif-2*^{-/-} mice, but with an even stronger impact during the first 3 days.

This implies that MIF-2 had a crucial role in the wound healing process, especially in the first 7 days and a lacking of MIF-2 diminished the wound healing in the early state.

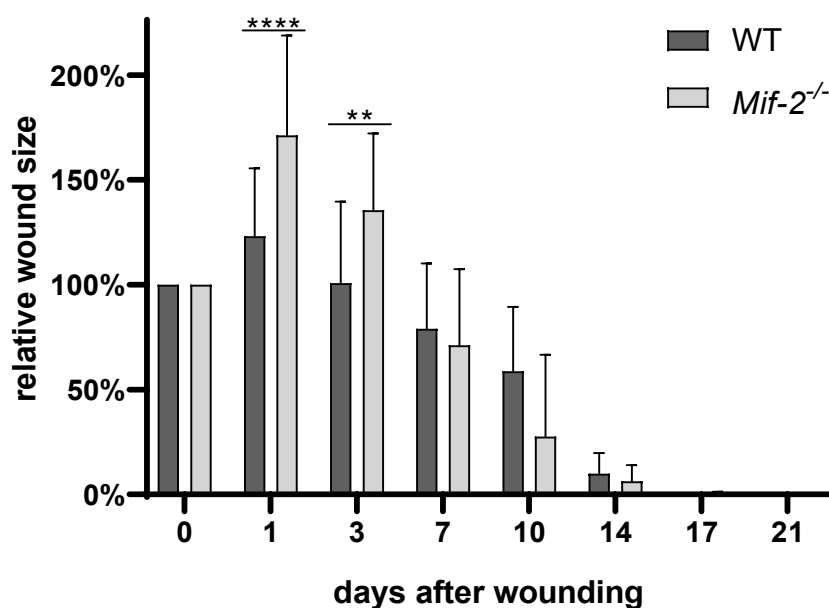


Figure 5.8: Wound area in an excisional wound model in wild type (WT) and *Mif-2*^{-/-} C57BL/6 male mice under high fat diet. Excisional wounds were set on the back of mice using a 6 mm diameter biopsy puncher to analyze the role of MIF-2 on wound healing in obese individuals. The wound size were regularly determined photographically. The wound size was calculated in relation to the initial wound in %. Statistical analysis was calculated within each day between the groups using two-way ANOVA followed by *post hoc* Tukey-test. Significance are indicated by **p* < 0.05, ***p* < 0.01 and ****p* < 0.001.

Mif-2^{-/-} mice on HFD showed a comparable healing process to *Mif-2*^{-/-} mice on a RD. Therefore, HFD *Mif-2*^{-/-} mice would not afford any additional insight into wound healing and they were omitted from the following experiments.

5.2 Immunohistochemical and immunocytochemical staining of wound tissue

In addition to the macroscopic examination of wound closure, incisional wounds were also analyzed at protein level by means of histological and immunohistochemical staining. Wound tissue was harvested at specific time points and fixed in paraformaldehyde. Tissue samples were then drained overnight and embedded in paraffin. The staining was carried out by Ines Kleiber-Schaaf and Andrea Garcete-Bärtschi from the histological laboratory of the Research Surgery Center. Since the HFD WT mice and the *Mif-2*^{-/-} mice under RD had no proper wound tissue to stain

and analyze at day 1, tissue stains were focused on wound tissue harvested three days after wounding in further analysis.

5.2.1 Collagen determination in wound tissue via Masson-Goldner's trichrome staining

The trichrome staining according to Masson-Goldner was carried out because with this method collagen, the main component of the connective tissue of the skin can be made visible [13, 167, 171]. Via this way, newly formed granulation tissue could be visualized and compared with native connective tissue in terms of its quality (Figure 5.10). In addition, I was able to determine the amount of newly regenerated tissue based on its thickness (Figure 5.11). For this reason, I analyzed wound tissue from mice, which were euthanized after 1, 3 or 7 days (Figure 5.9).

Both the WT HFD group and *Mif-2^{-/-}* RD group did not form any new tissue one day after wounding. In contrast to them, the WT mice under RD have already formed granulation tissue with about 45 – 50 % of the thickness of the original dermis. The new tissue had 20 % proper connective tissue compared to healthy tissue. On day three, the RD WT mice had already 80 % of granulation tissue thickness. It was significant in comparison to the *Mif-2^{-/-}* mice that had less than 20 % of thickness of granulation tissue. Granulation tissue of the WT HFD mice was about 45 – 50 % tissue thickness at the level of the WT mice under RD on day 1, but reduced compared to WT RD mice on day 3. The *Mif-2^{-/-}* mice built up even less granulation tissue than the WT HFD mice. The tissue quality of the WT RD group was significantly increased compared to the other two groups. The quality of the knockout group was even significantly lower than that of the HFD mice. After one week (day 7), the newly build tissue of the WT RD group was almost as thick as the surrounding healthy tissue. With regard to tissue thickness, the WT mice under RD were slightly increased compared to the other groups, while they were still significantly enhanced with regard to quality. However, the WT mice under HFD and the *Mif-2^{-/-}* mice under RD were on an equal level in terms of granulation tissue thickness and its quality on day 7. Their thickness level was similar to that of the RD WT mice at day 3.

In general, the granulation tissue of the WT mice was rapidly regenerated under RD and was of the same quality as healthy tissue after one week. In the WT HFD mice,

Results

the production of the tissue appeared to be delayed by 3 – 4 days but at the same growing speed. While in the *Mif-2*^{-/-} mice, the inhibition of tissue formation was stronger, but only at the beginning. Later it suddenly rose to the level of the control mice. The different behavior of the *Mif-2*^{-/-} strain and the wild type strains could also be observed with regard to the quality (amount of collagen) of the granulation tissue formed.

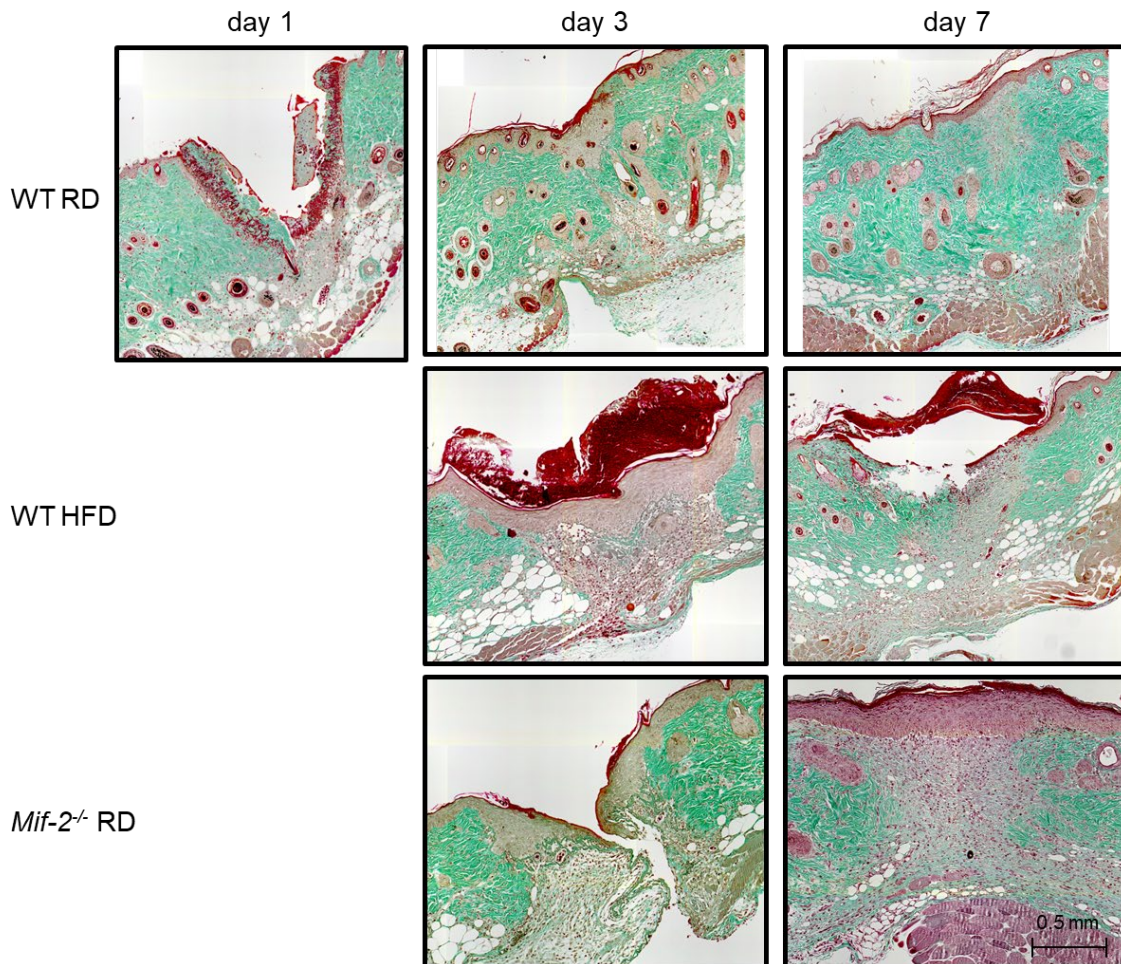


Figure 5.9: Representative tissue slights stained by the Masson-Goldner's trichrome procedure. Wound tissue from WT RD, WT HFD, and *Mif-2*^{-/-} RD mice was collected 1, 3, and 7 days after intervention and tissue slights were stained by the Masson-Goldner's trichrome procedure. WT HFD and *Mif-2*^{-/-} RD mice did not form any tissue to analyze after 1 day. Connective tissue/collagen: turquoise, keratin and muscle fibers: red, nuclei: black.

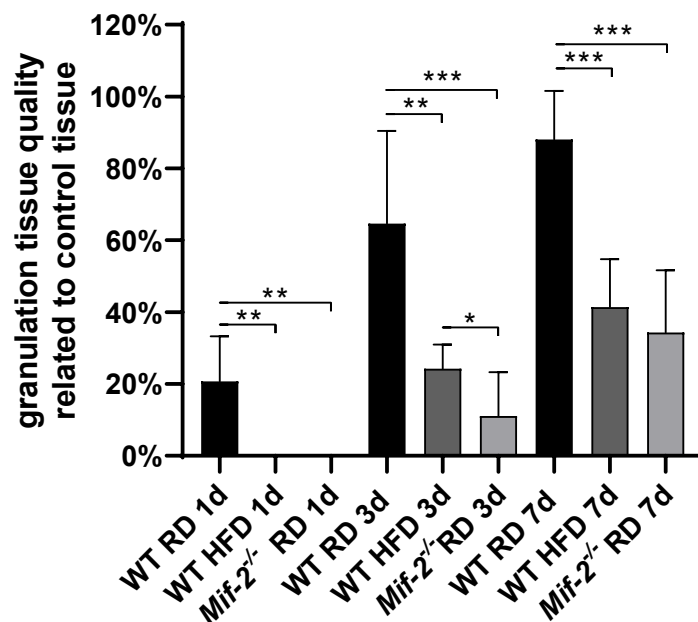


Figure 5.10: Quality of newly formed granulation tissue in an incisional murine wound model. Wound tissue from wild type C57BL/6 (WT) mice under regular diet (RD) or high fat diet (HFD) and Mif-2^{-/-} mice under RD was stained by the trichrome method according to Masson-Goldner. The tissue was sampled after 1, 3 and 7 days of wound healing. WT HFD and Mif-2^{-/-} RD mice had no tissue to stain at day 1. Healthy connective tissue consists principally of collagen types. That is why the amount of collagen is a quality indicator. The regenerated tissue was compared with healthy tissue regarding to the quality of connective tissue by measuring collagen. Statistical analysis was performed within the day of sample harvesting between the groups. Two-way ANOVA followed by *post hoc* Tukey-test was used for calculation. Significance are indicated by *p < 0.05, **p < 0.01 and ***p < 0.001.

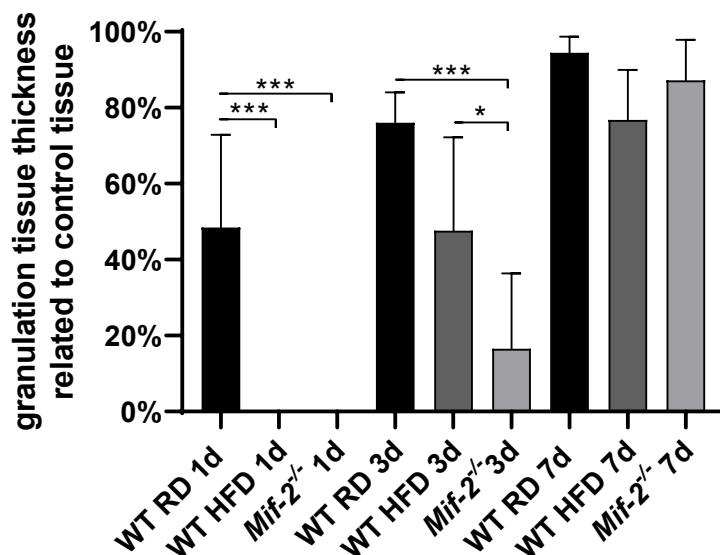


Figure 5.11: Determination of tissue thickness of newly formed granulation tissue in an incisional murine wound healing model. Wound tissue from wild type C57BL/6 (WT) mice under regular diet (RD) or high fat diet (HFD) and Mif-2^{-/-} mice under RD was stained by the trichrome method according to Masson-Goldner. The tissue was sampled after 1, 3 and 7 days of wound healing. WT HFD and Mif-2^{-/-} RD mice had no tissue to stain at day 1. The thickness was determined as formed tissue from the panniculus carnosus muscle to epidermis. The

Results

calculated distance was set in relation to healthy tissue next to the wound. Statistical calculations were done using two-way ANOVA followed by *post hoc* Tukey-test within the different days between the groups. Significance are indicated by * $p < 0.05$, ** $p < 0.01$ and *** $p < 0.001$.

Like the wound healing model, tissue analysis with Masson Goldner's trichrome stain revealed the delayed tissue regeneration caused by HFD or the absence of MIF-2. This confirms the macroscopic analysis from the wound model. In addition, the amount of collagen was strongly reduced in the new formed tissue in the WT HFD group and in the *Mif-2*^{-/-} RD group. The reduced tissue quality indicates that obesity and a lack of MIF-2 cause diminished collagen production, which leads to a delay in tissue formation.

5.2.2 Myofibroblast determination in wound tissue via expression of α -smooth muscle actin

Myofibroblasts are the primary cell type producing collagen for wound repair. They play a crucial role in the proliferation and rebuilding phase in wound healing [94]. A specific marker for myofibroblasts is alpha smooth muscle actin (α -SMA). Wound tissue was stained with anti- α -SMA antibody to determine the amount of myofibroblasts in the wound area (Figure 5.12 and Figure 5.13). Since collagen production of *Mif-2*^{-/-} and WT HFD mice on the third day was similar to that of WT RD mice on day 1, tissues from all groups after three days of wound healing and tissues from the WT RD group after one day were used.

The α -SMA levels decreased about a third within the WT RD group from day 1 to day 3. Both mice groups, the obese WT mice and the *Mif-2*^{-/-} mice under RD had no tissue to analyze at day 1. However, day 3 α -SMA expression in *Mif-2*^{-/-} mice increased rapidly to day 1 levels in WT RD mice. While WT HFD mice still showed low α -SMA levels, half of those from *Mif-2*^{-/-} mice on day 3.

The low α -SMA level in the HFD and the *Mif-2*^{-/-} group mean that the myofibroblast differentiation was reduced in these groups. This indicates a negative impact of obesity on myofibroblast differentiation and that MIF-2 plays either a direct or an indirect role in the myofibroblast differentiation pathway.

Results

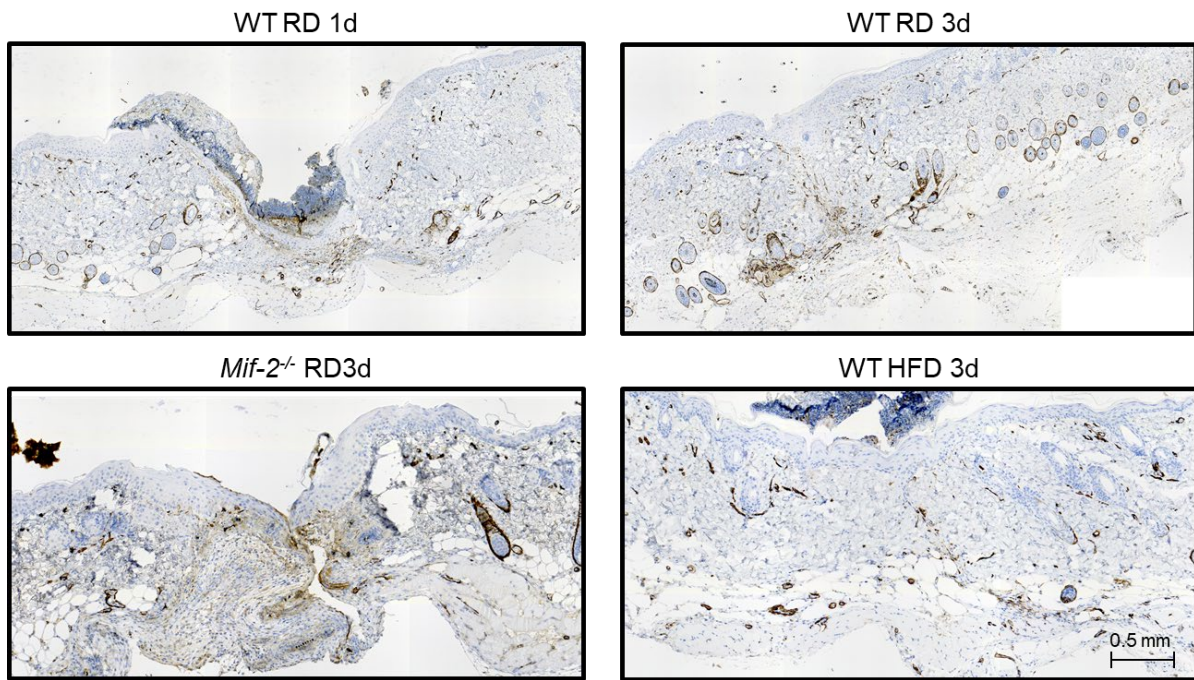


Figure 5.12: Representative tissue slides stained by anti- α -smooth muscle actin (α -SMA). Wound tissue from WT RD, WT HFD, and *Mif-2^{-/-}* RD mice was collected 1 and 3 days after intervention and tissue slights were stained by anti- α SMA antibody. WT HFD and *Mif-2^{-/-}* RD mice did not form any tissue to analyze after 1 day. α -SMA: brown; nucleus: blue.

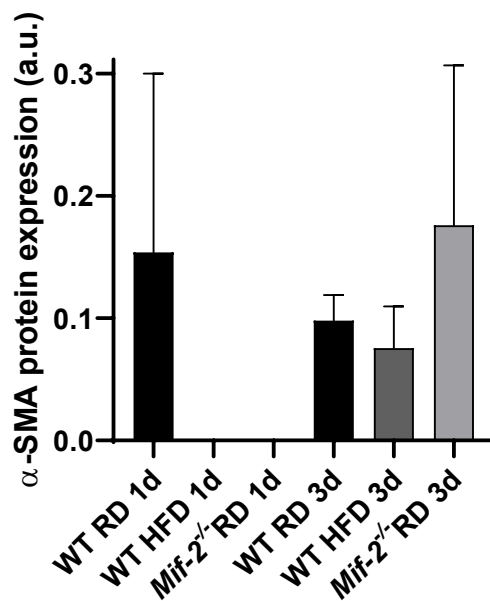


Figure 5.13: Expression of α -SMA protein in wound tissue by IHC. Wound tissue of wild type (WT) mice under regular diet (RD) and high fat diet (HFD) and *Mif-2^{-/-}* mice under RD was harvested on day 3 after wounding. Tissue samples were stained with anti- α SMA antibody to determine the amount of myofibroblasts. $n = 6$ for each group. Students unpaired two-tailed t-test was used for statistical analysis.

5.2.3 Cell proliferation in wound area via expression of Ki-67

Cell proliferation is an important step in wound healing to regenerate tissue. Ki-67 is a well-known proliferation marker and established in wound healing assays [176, 177]. The wound tissue of all three mice groups was treated with anti-Ki67 antibody and visualized with DAB (Figure 5.14). Ki67-levels were measured in wound areas and healthy tissue. The expression of Ki67 was at a similar level in healthy tissue in all groups. In *Mif-2*^{-/-} mice, Ki67 levels were slightly reduced compared to both WT groups, but without any significance. Both WT groups had same Ki67 expression in wound tissue. From this, it can be concluded that the delayed wound healing was not caused by impaired cell proliferation either in the HFD group or in the MIF-2 knockout group.

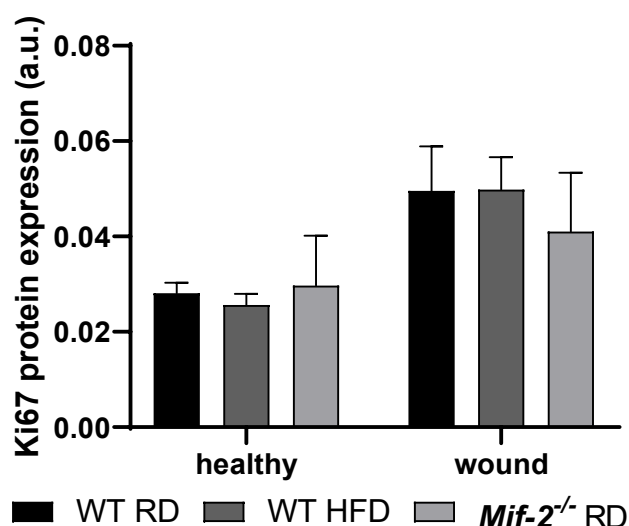


Figure 5.14: Expression of Ki67 protein in healthy skin tissue and wound tissue by IHC. Healthy skin tissue and wound tissue of wild type (WT) mice under regular diet (RD) and high fat diet (HFD) and *Mif-2*^{-/-} mice under RD was harvested on day 3 after wounding. Tissue samples were stained with anti-Ki67 antibody to determine general cell proliferation. n = 6 for each group. Students unpaired two-tailed t-test was used for statistical analysis.

5.2.4 Inflammation and macrophage infiltration via expression of TNF- α and F4/80

Inflammation plays a crucial role in the wound repair process. In the inflammatory phase, the wound area is cleaned of bacteria, cell debris and other pathogens by neutrophils and macrophages. Tumor necrosis factor (TNF)- α is a chemoattractant for macrophages and neutrophils and is involved in their activation and regulation. [21, 24]. Therefore, TNF- α is a common marker for inflammation in tissue analysis. Another typical inflammation marker is F4/80, which is specific for macrophages [178]. A

prolonged inflammation state, however, leads to a diminished wound healing or even a non-healing, chronic wound [40].

Expression of TNF- α was determined in wound tissue and healthy tissue in all three mouse groups on day 3 after wound setting (Figure 5.15). All groups showed higher TNF- α levels in the wound tissue. Thereby both groups, the WT HFD mice and the *Mif-2*^{-/-} RD mice, showed greater increase in TNF- α expression than the WT RD mice. In the *Mif-2*^{-/-} group, TNF- α levels were even higher as the WT HFD group. The differences to the WT RD mice were significantly. TNF- α levels of the healthy tissue, however, were similar in the WT RD mice and *Mif-2*^{-/-} RD mice and slightly decreased at the WT HFD.

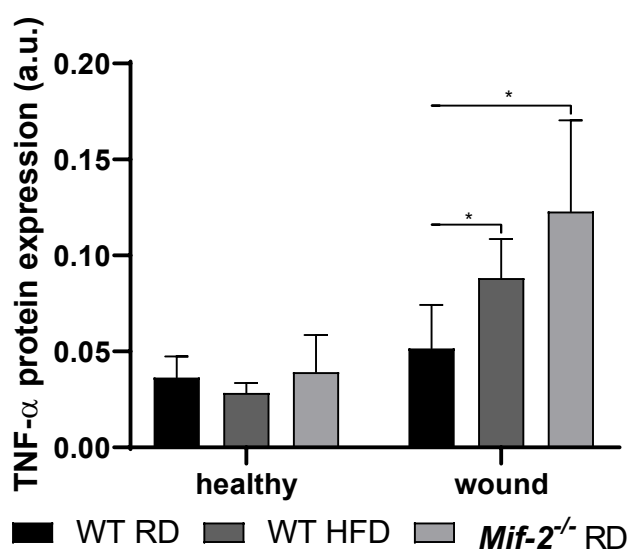


Figure 5.15: Expression of TNF- α protein in healthy skin tissue and wound tissue by IHC. Healthy skin tissue and wound tissue of wild type (WT) mice under regular diet (RD) and high fat diet (HFD) and *Mif-2*^{-/-} mice under RD was harvested on day 3 after wounding. Tissue samples were stained with anti-TNF- α antibody to determine inflammation. n = 6 for each group. Students unpaired two-tailed t-test was used for statistical analysis. Significance are indicated by *p < 0.05 and **p < 0.01.

Furthermore, tissue samples were also stained with anti-F4/80 antibody (Figure 5.16). The degree of expression of F4/80 was used to determine the number of macrophages per wound area. In contrast to TNF- α expression, WT mice showed a similar expression of F4/80 regardless of the diet. While *Mif-2*^{-/-} RD mice showed a significantly higher expression of F4/80, even though the wound area was larger.

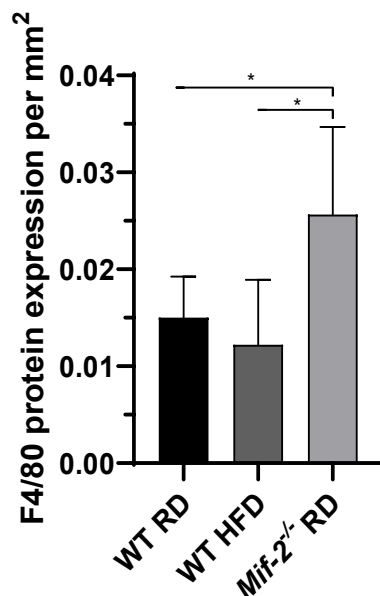


Figure 5.16: Expression of F4/80 protein in wound tissue by IHC. Wound tissue of wild type (WT) mice under regular diet (RD) and high fat diet (HFD) and *Mif-2*^{-/-} mice under RD was harvested on day 3 after wounding. Tissue samples were stained with anti-F4/80 antibody to determine indirectly the number of macrophages per wound area. n = 6 for each group. Students unpaired two-tailed t-test was used for statistical analysis. Significance are indicated by *p < 0.05.g

The increased TNF- α levels as well as the elevated macrophage recruitment in the *Mif-2*^{-/-} group imply that the *Mif-2*^{-/-} mice had an increased inflammation degree when compared to the WT RD mice and might be still in the inflammation phase. The WT HFD mice only showed an increased TNF- α levels, but less than the *Mif-2*^{-/-} mice indicating that both obesity and lack of MIF-2 have a pro-inflammatory effect, MIF-2 however even more.

5.2.5 Angiogenesis via expression of CD31

Proper angiogenesis is essential to ensure that formed granulation tissue is adequately supplied with nutrients and oxygen. Platelet endothelial cell adhesion molecule (PECAM-1), also called CD31, is a protein on the surface of endothelial cells from blood vessels [179]. Hence, wound tissue samples were stained with anti-CD31 antibody and the number of blood vessels in the newly formed tissue was counted (Figure 5.17). The number of blood vessels per newly formed tissue is given in mm². With over 40 blood vessels per wound area, the WT RD mice produced the most blood

vessels. The WT mice under HFD only had about half of newly formed blood vessels and were significantly reduced. Blood vessel production in *Mif-2*^{-/-} mice under RD was greatly decreased, less than a quarter of the WT RD mice. Even though the *Mif-2*^{-/-} group had half of the WT mice under HFD, the difference was not significant. These results imply that blood vessel production is impaired by both HFD and the absence of MIF-2.

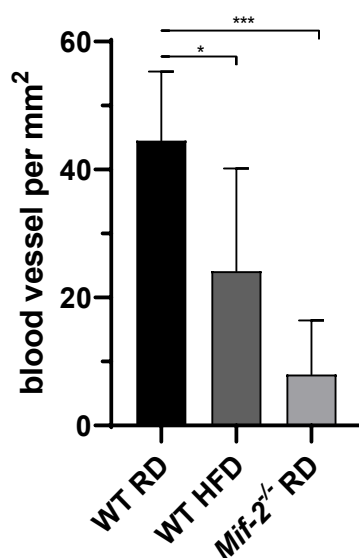


Figure 5.17: Blood vessel production in newly formed granulation tissue. Wound tissue of wild type (WT) mice under regular diet (RD) and high fat diet (HFD) and *Mif-2*^{-/-} mice under RD was harvested on day 3 after wounding. Tissue samples were stained with anti-CD31 antibody. Blood vessels were counted and indicated per area in mm² of newly formed granulation tissue. n = 6 for each group. Students unpaired two-tailed t-test was used for statistical analysis. Significance are indicated by *p < 0.05, **p < 0.01 and ***p < 0.001.

5.3 Wound tissue analysis on genetic level via RT-qPCR

Real-time quantitative polymerase chain reaction (RT-qPCR) is a technique for the quantitative measurement of gene expression. Via this way, downregulation or upregulation of certain genes due to the HFD or the MIF-2 knockout can be determined in comparison to control WT RD mice. All genes were normalized to two housekeeping genes (RPS29 and β -actin) [169].

5.3.1 Expression of genes coding for collagen types

The extracellular matrix (ECM) consists largely of different types of collagen. The composition of the different types changes during wound healing. In early wound state, type III collagen is more strongly expressed and decreases over time. While type I collagen is the principal type in healthy tissue and is at a lower level in early stages of

the healing process [4, 13]. Thus, the major types of collagen were examined in the wound tissue (Figure 5.18). Type I collagen was determined through the *Col1A*-gene and type III collagen through the *Col3A1*-gene. Both groups, the HFD WT and the RD *Mif-2^{-/-}* mice, had lower *Col1A* and *Col3A1* gene expression compared to WT mice under RD. The knockout mice even had lower expression levels than the WT HFD mice, the expression was about half of the WT RD mice. In the case of *Col3A1*, the difference between the *Mif-2^{-/-}* RD mice and the WT RD mice was significant.

In addition to collagen I and III, collagen IV is another important protein in the skin and in skin wound healing. The basal membrane connects the dermis and epidermis and consists mainly of type IV collagen. To determine the collagen IV level the expression of the *Col4A* gene was measured. In contrast to expression of type I and III collagen, the expression of type IV collagen was upregulated to a similar level in the WT mice under HFD and the *Mif-2^{-/-}* mice when compared to the WT RD group.

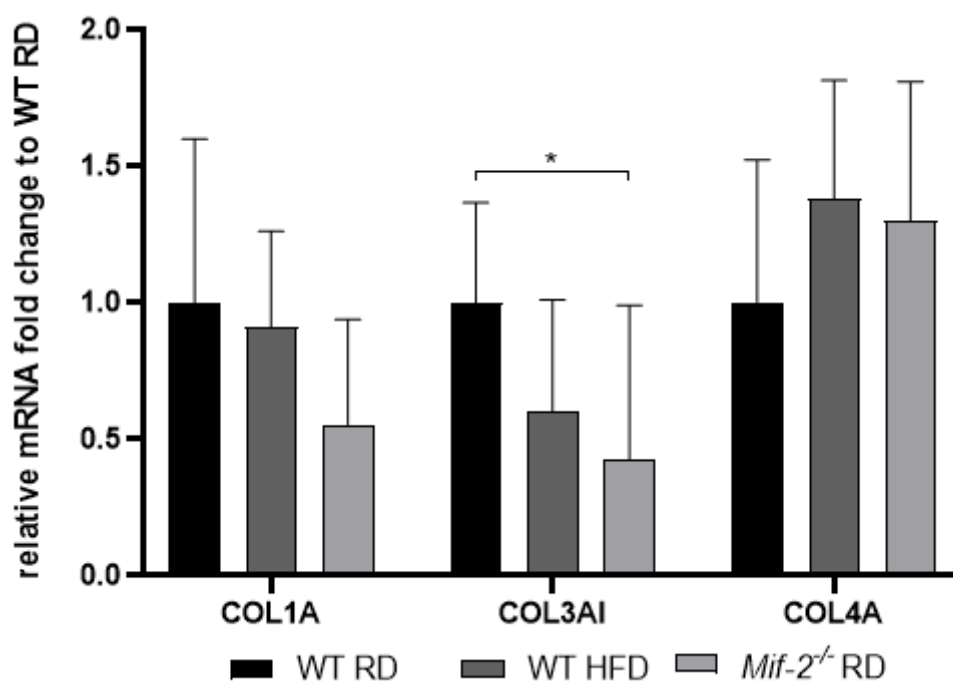


Figure 5.18: Relative mRNA expression of three collagen types in wound tissue from an incisional wound model. Wound tissue from wild type (WT) mice under regular diet (RD) or high fat diet (HFD) and *Mif-2^{-/-}* RD mice was harvested on day 3 after wounding. Tissue samples were homogenized and mRNA levels of genes coding for collagen type I (*Col1A*), type III (*Col3A1*) and type IV (*Col4A*) were measured by RT-qPCR. Genes were normalized to two housekeeping genes (*RPS29* and β -actin). Tissue samples from WT HFD mice and *Mif-2^{-/-}* RD mice were compared to WT RD mice. $n = 6$ for each group. Students unpaired two-tailed t-test was used for statistical analysis. Significance are indicated by * $p < 0.05$, ** $p < 0.01$ and *** $p < 0.001$.

Tissue analysis at the genetic level confirmed the histological results. Collagen production was diminished in the early state of wound healing in the obese WT mice and even more in the *Mif-2^{-/-}* mice. However, it appeared that collagen IV was increased in these groups to compensate for the decreased amount of collagen I and III.

5.3.2 Expression of various genes related to extracellular matrix

Beside the various types of collagen, ECM consists of elastin, which is mainly responsible for the elasticity of skin, and adhesion proteins such as fibronectin [4, 13]. Fibronectin occurs in the hemostasis phase of wound healing, as part of the clot, and in the early stages of tissue regeneration. While elastin is mainly produced at the end of the proliferation phase and in the final remodeling phase. Elastin is coded on the *Eln*-gene and fibronectin on the *Fn1*-gene. Other important proteins, which have an impact on ECM, are matrix metallo-proteases (MMPs), especially MMP9. MMP9 mainly digests collagen from damaged tissue [19].

The *Eln* expression levels of the *Mif-2^{-/-}* RD mice were similar to that of the WT RD mice, while the levels were slightly downregulated in the WT HFD mice. *Fn1*, however, was upregulated in both groups, the *Mif-2^{-/-}* RD and the WT HFD mice. In case of the WT HFD mice, the levels were seven times higher and the difference to the other two groups was significant. While the *Mif-2^{-/-}* mice had only 1.5 times higher levels than the WT RD mice, but with no significance. *Mmp9* was slightly upregulated only in the WT HFD mice. The expression was unchanged in the *Mif-2^{-/-}* mice compared to the WT mice under RD.

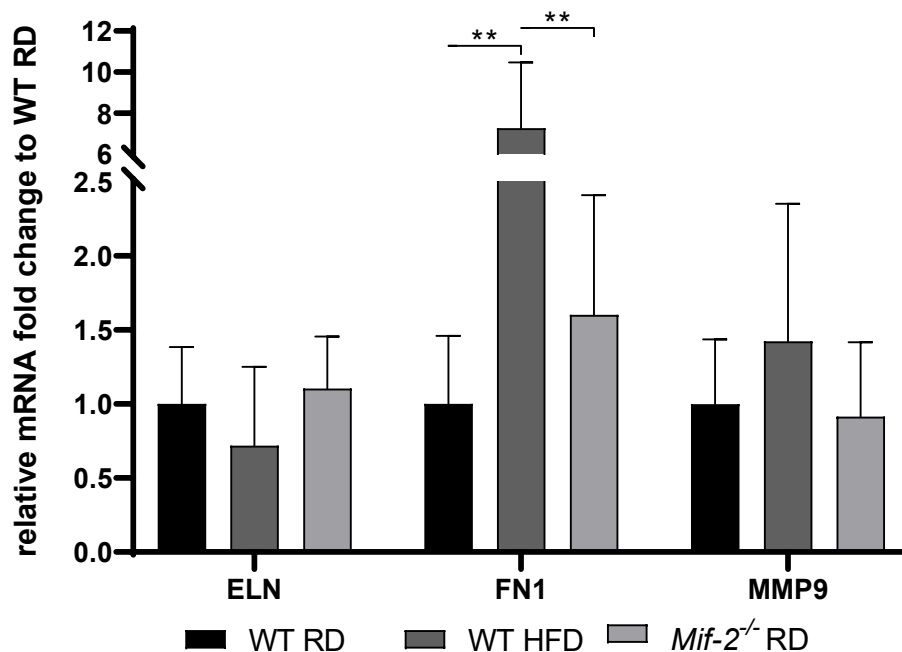


Figure 5.19: Relative mRNA expression of extracellular matrix related proteins in wound tissue from an incisional wound model. Wound tissue from wild type (WT) mice under regular diet (RD) or high fat diet (HFD) and *Mif-2*^{-/-} RD mice was harvested on day 3 after wounding. Tissue samples were homogenized and mRNA levels of genes coding for elastin (Eln), fibronectin (Fn1) and matrix metallo protease-9 (Mmp9) were measured by RT-qPCR. Genes were normalized to two housekeeping genes (RPS29 and β -actin). Tissue samples from WT HFD mice and *Mif-2*^{-/-} RD mice were compared to WT RD mice. n = 6 for each group. Students unpaired two-tailed t-test was used for statistical analysis. Significance are indicated by *p < 0.05, **p < 0.01 and ***p < 0.001.

5.3.3 Expression of genes related to growth factors that activate fibroblast differentiation

Fibroblasts play an important role in the cutaneous wound repair process, as they are the major producer for proteins forming the ECM. Therefore, they are recruited immediately after being wounded and encouraged to reproduce even more in the later course [22, 26]. Transforming growth factor (TGF)- β is a fibroblast stimulating cytokine secreted directly after an injury, while platelet-derived growth factor (PDGF) recruit fibroblast during the end of the inflammation phase of wound healing [19, 24]. In addition, both cytokines stimulate fibroblasts to differentiate. PDGF causes fibroblasts to change their phenotype to "wound fibroblasts" and TGF- β then initiates myofibroblast differentiation. Myofibroblasts have increased protein production to build new tissue [27-29]. Hence, gene expression of TGF- β was measured via the *Tgf- β 1*-gene and of PDGF via the *Pdgf-A*-gene. The gene coding for TGF- β was slightly increased in the *Mif-2*^{-/-} RD mice, while it was at a similar level in the WT HFD group compared to the WT RD mice. The *Pdgf-A* levels were also only slightly elevated in

the *Mif-2*^{-/-} RD mice compared to the WT RD mice. The WT mice under HFD, however, showed significantly upregulated *Pdgf-A* levels.

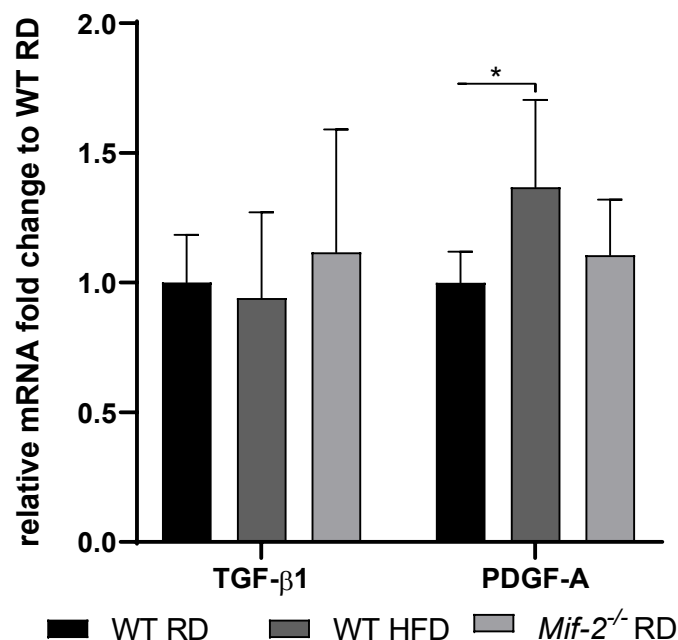


Figure 5.20: Relative mRNA expression of proteins triggering fibroblast differentiation in wound tissue from an incisional wound model. Wound tissue from wild type (WT) mice under regular diet (RD) or high fat diet (HFD) and *Mif-2*^{-/-} RD mice was harvested on day 3 after wounding. Tissue samples were homogenized and mRNA levels of genes coding for transforming growth factor-β (Tgf-β1) and platelet derived growth factor (Pdgf-A) were measured by RT-qPCR. Genes were normalized to two housekeeping genes (RPS29 and β-actin). Tissue samples from WT HFD mice and *Mif-2*^{-/-} RD mice were compared to WT RD mice. n = 6 for each group. Students unpaired two-tailed t-test was used for statistical analysis. Significance are indicated by *p < 0.05, **p < 0.01 and ***p < 0.001.

5.3.4 Expression of genes related to re-epithelization

Besides production of new connective tissue, re-epithelialization is also a crucial step in the wound healing process. Keratinocytes are recruited for re-epithelialization by released fibroblast growth factor (FGF)7 and FGF10 [3, 89]. During the formation of the upper epidermal layers, keratinocytes differentiate, lose their mitotic ability, and form robust, intercellular spine-like desmosomes. Meanwhile they also produce keratin 10, which is encoded on the *Krt10*-gene [3].

In both cases, *Fgf7* and *Fgf10*, the expression in the WT HFD group was downregulated compared to the WT mice under RD. The *Mif-2*^{-/-} mice under RD had similar *Fgf7* gene levels, but strongly downregulated *FGF10* levels compared to both

WT groups. The expression of *Krt10* was upregulated by 50 % in the *Mif-2*^{-/-} RD mice compared to the WT RD mice; the WT mice under HFD had the same *Krt10* levels as the WT RD mice.

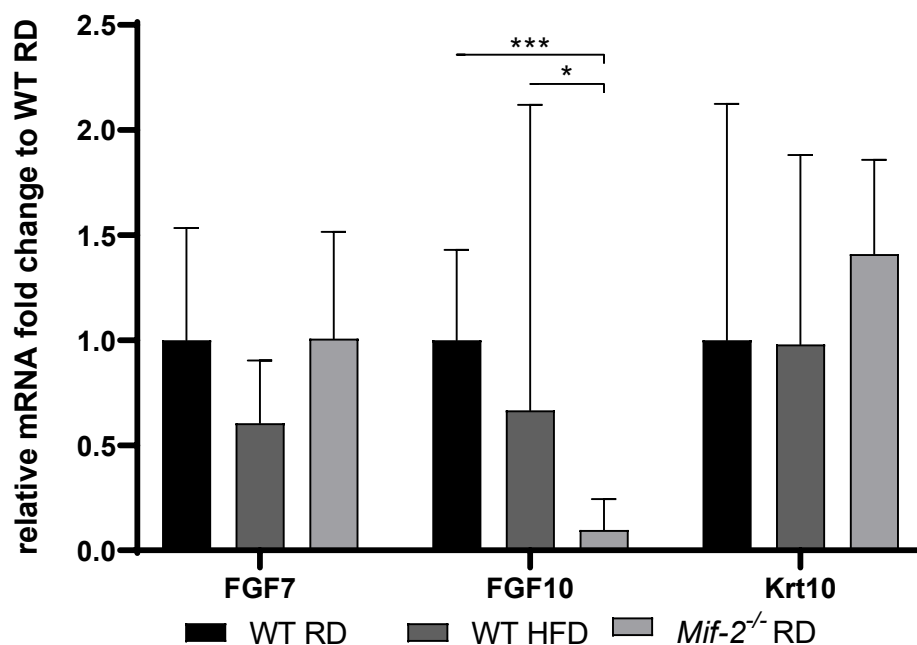


Figure 5.21: Relative mRNA expression of proteins related to re-epithelialization in wound tissue from an incisional wound model. Wound tissue from wild type (WT) mice under regular diet (RD) or high fat diet (HFD) and *Mif-2*^{-/-} RD mice was harvested on day 3 after wounding. Tissue samples were homogenized and mRNA levels of genes coding for fibroblast growth factor 7 (FGF7), FGF10 and keratin 10 (Krt10) were measured by RT-qPCR. Genes were normalized to two housekeeping genes (RPS29 and β -actin). Tissue samples from WT HFD mice and *Mif-2*^{-/-} RD mice were compared to WT RD mice. n = 6 for each group. Students unpaired two-tailed t-test was used for statistical analysis. Significance are indicated by *p < 0.05, **p < 0.01 and ***p < 0.001.

5.3.5 Expression of genes related to macrophages

Macrophages play also an important role in wound healing. They have various functions. On the one hand, they act as cleaning system and free the wound area from pathogens and cell debris and produce reactive oxygen species. These are pro-inflammatory macrophages, which have the phenotype M1. They can be detected by CD11c or IL-6. Furthermore, macrophages can be skewed towards the M2 phenotype, which is anti-inflammatory and can be detected via CD301. The M2 macrophages secrete cytokines to recruit more cells and turn off the damaging immune system [180]. Hence, the expression of M1 and M2 markers was measured.

The expression of *Il-6* was upregulated almost twice in both groups, the WT HFD and the *Mif-2*^{-/-} RD mice, compared to the WT RD group, but not significantly. *Cd11c*

expression was similar in all three groups, only slightly upregulated in the *Mif-2*^{-/-} RD mice. The *Cd301b* gene levels were strongly significantly downregulated in the *Mif-2*^{-/-} mice, less than 10 % of the WT RD group. *Cd301b* levels were also significantly reduced in the WT HFD mice, but still significantly higher than in the knockout mice.

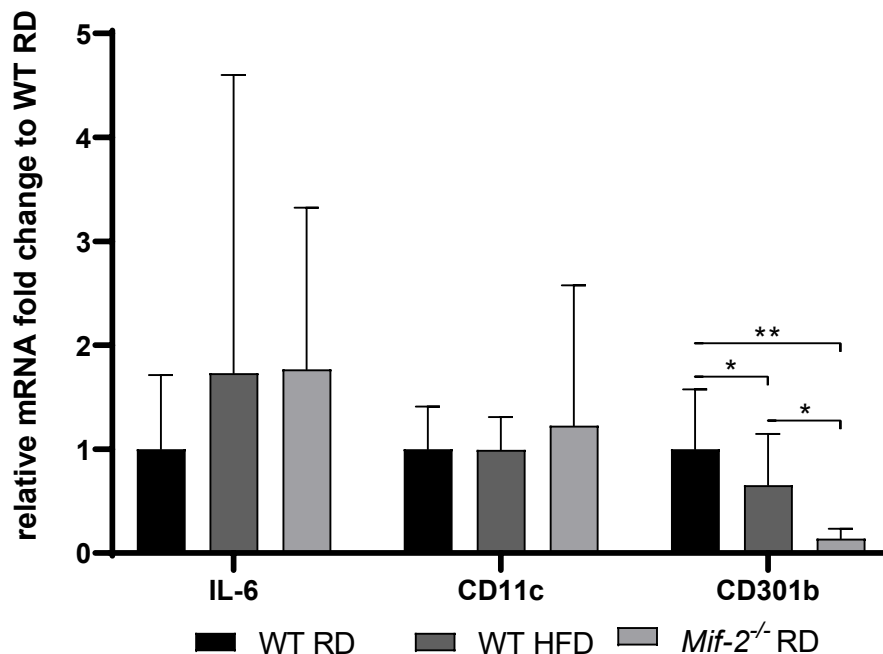


Figure 5.22: Relative mRNA expression of proteins related to macrophages in wound tissue from an incisional wound model. Wound tissue from wild type (WT) mice under regular diet (RD) or high fat diet (HFD) and *Mif-2*^{-/-} RD mice was harvested on day 3 after wounding. Tissue samples were homogenized and mRNA levels of genes coding for interleukin 6 (IL-6), CD11 (Cd11c) and CD301 (Cd301b) were measured by RT-qPCR. Genes were normalized to two housekeeping genes (RPS29 and β -actin). Tissue samples from WT HFD mice and *Mif-2*^{-/-} RD mice were compared to WT RD mice. n = 6 for each group. One-way ANOVA followed by *post hoc* Tukey-test was used for statistical analysis. Significance are indicated by *p < 0.05, **p < 0.01 and ***p < 0.001.

5.3.6 Expression of genes coding for macrophage migration inhibitor factor protein family

Since the macrophage migration inhibitor factor (MIF) -2 is the main topic of this work, the gene expression of MIF and MIF-2 in wound tissue was investigated. The MIF-2 expression was determined exclusively in the WT mice, since the *Mif-2*^{-/-} mice had a global *Mif-2* knockout. Gene levels of MIF were examined to assess whether there is a counter-upregulation in the mice, since MIF has the same receptor as MIF-2 [132]. In the WT HFD group, the *Mif* levels were greatly significantly upregulated compared to the WT RD and *Mif-2*^{-/-} RD mice. Whereas the *Mif-2* levels were significantly downregulated in less than a quarter of the WT mice under RD. The *Mif-2*^{-/-} mice

showed slightly upregulated *Mif* levels compared to the WT RD mice and no *Mif-2* expression.

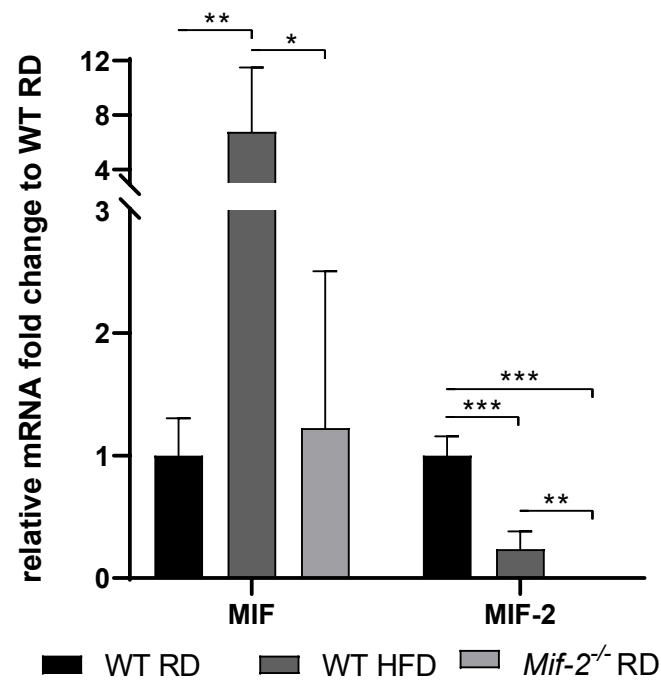


Figure 5.23: Relative mRNA expression of macrophage migration inhibitor factor (MIF) protein family in wound tissue from an incisional wound model. Wound tissue from wild type (WT) mice under regular diet (RD) or high fat diet (HFD) and *Mif-2*^{-/-} RD mice was harvested on day 3 after wounding. Tissue samples were homogenized and mRNA levels of genes coding for MIF and MIF-2 were measured by RT-qPCR. Genes were normalized to two housekeeping genes (RPS29 and β -actin). Tissue samples from WT HFD mice and *Mif-2*^{-/-} RD mice were compared to WT RD mice. $n = 6$ for each group. One-way ANOVA followed by *post hoc* Tukey-test was used for statistical analysis. Significance are indicated by * $p < 0.05$, ** $p < 0.01$ and *** $p < 0.001$.

5.4 CD74 receptor expression during differentiation of NIH/3T3 cells

To ensure that the used NIH/3T3 cells expressed the CD74 receptor and whether the expression changed during the differentiation, fluorescence associated cell sorting (FACS) flow cytometry was carried out with undifferentiated and differentiated cells (Figure 5.24). Both, the undifferentiated (Figure 5.24 A) and the differentiated (Figure 5.24 B) cells, expressed the CD74 receptor in low levels. The expression did not change during the differentiation into myofibroblasts (Figure 5.24 C).

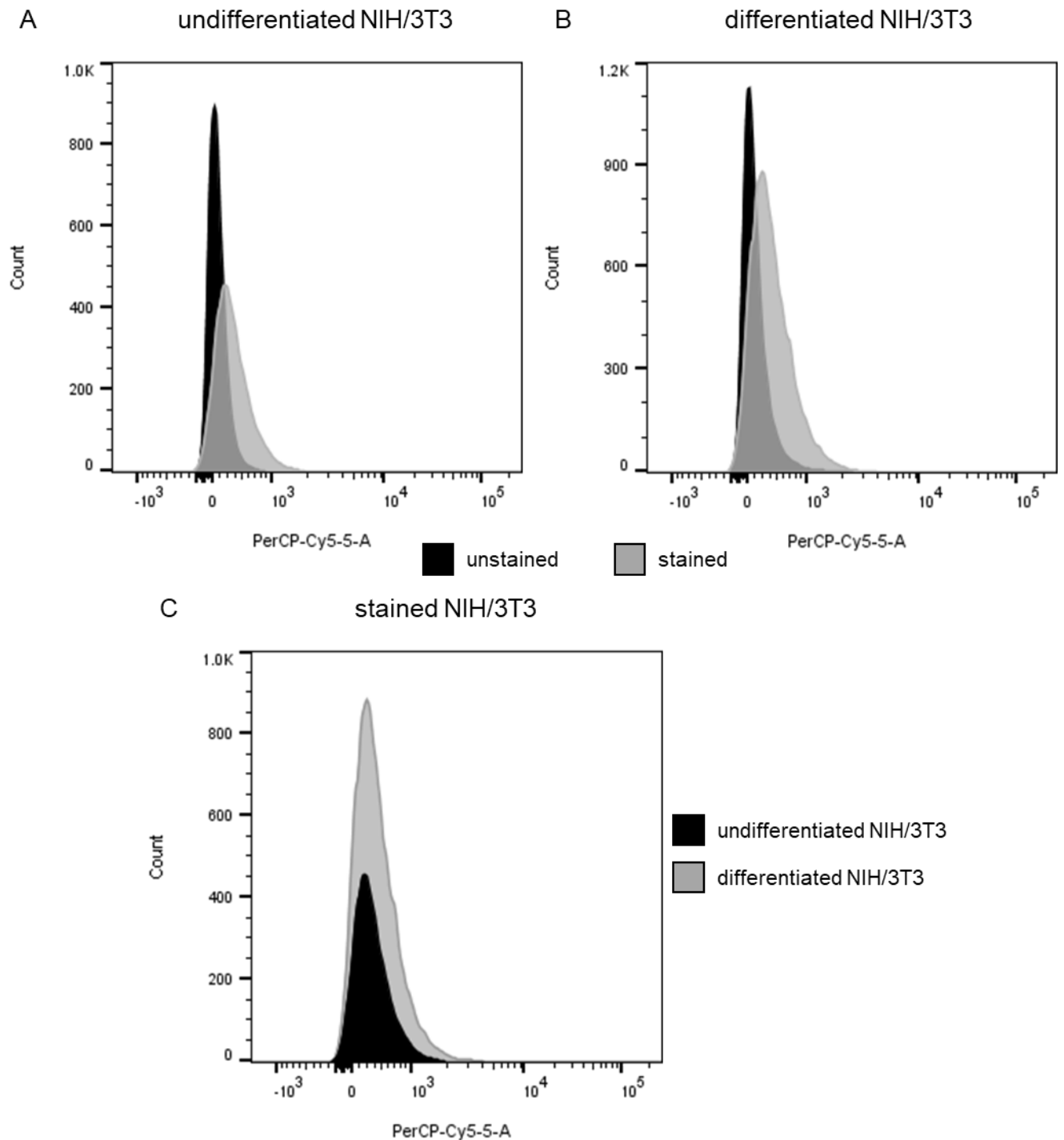


Figure 5.24: CD74 receptor on undifferentiated and differentiated NIH/3T3 cells. Cell surface expression of CD74 receptor on undifferentiated (A) and differentiated (B) NIH/3T3 cells measured via FACS flow cytometry. Cells were marked with fluorescently labelled CD74 antibody. black: unstained and grey: stained (C) Undifferentiated stained NIH/3T3 cells (black) compared to differentiated stained NIH/3T3 cells (grey).

5.5 Collagen gel contraction assay

During the wound healing process, fibroblasts differentiate into myofibroblasts, which have two main roles. On the one hand, they are the main producer of compounds for

the newly formed granulation tissue and, on the other hand, they are responsible for wound contraction [26, 27]. To investigate the differentiation of fibroblast into myofibroblasts, NIH/3T3 cells, an immortal murine fibroblast cell line, were used. The differentiation was initiated by treatment with murine TGF- β 1 [170]. The differentiation state and the contractile activity of the cells were determined by performing a collagen gel contraction assay [171]. In order to gain a more detailed insight into the role of MIF-2 in fibroblast differentiation and the contractile activity of differentiated myofibroblasts, the cells were treated with either the MIF-2-selective competitive inhibitor 4-CPPC [172] to decrease the MIF-2 levels in the cells or with additional murine recombinant MIF-2 (rMIF-2) to increase the cellular levels (Figure 5.25).

The two negative controls, collagen gel incubated in differentiation medium (DM) and cells incubated in basic medium, showed no contraction of the gel. The cells that were incubated only in DM showed the highest contractile activity and were set as 100 %. When cells were treated with DM and 4-CPPC, the contractile activity decreased in a dose-response manner. A 4-CPPC concentration of 5 μ M still showed sufficient contractile activity of 50 %. While treatment with 15 μ M 4-CPPC led almost to no contraction and 30 μ M 4-CPPC led to complete inhibition of contractile activity. Treatment with DM supplemented with murine rMIF-2 has shown an effect similar to that of 4-CPPC treatment. The supplementation of only 10 μ g/mL m-rMIF-2 resulted in a similar contractile activity as the untreated cells incubated in DM. While with increasing protein concentration, the activity decreased to a value of about 50 % activity at 400 ng/mL m-rMIF-2.

These results indicate that MIF-2 was essential for the NIH/3T3 cells to differentiate into myofibroblasts. Not only did decreased MIF-2 levels impair differentiation, but increasing MIF-2 also resulted in decreased differentiation potential. Either MIF-2 appears to play a regulatory role in myofibroblast differentiation, and alterations in MIF-2 homeostasis, by increasing or decreasing MIF-2 levels, caused reduced differentiation potential.

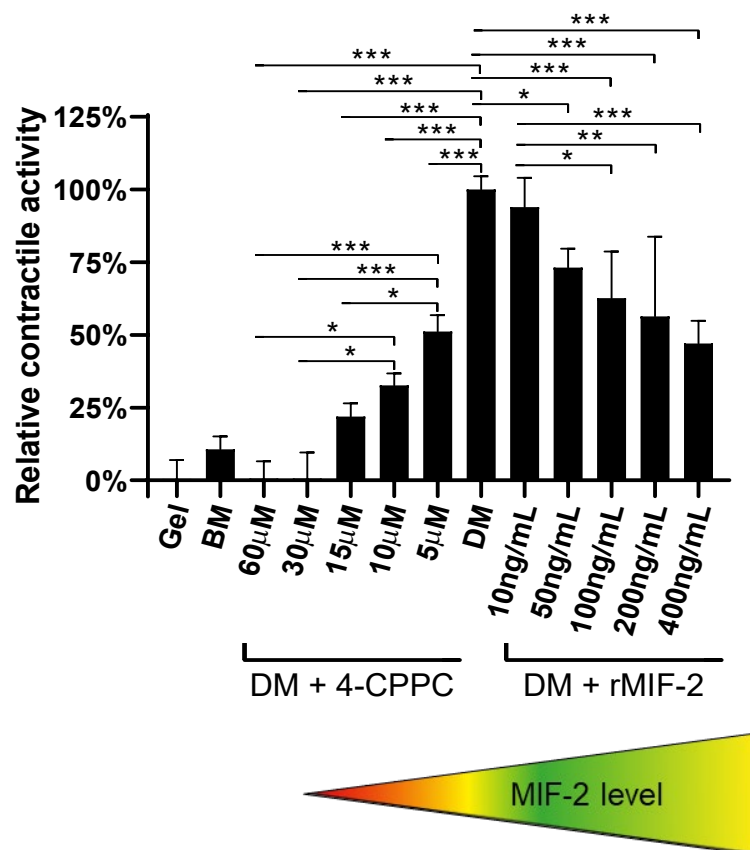


Figure 5.25: Contractile activity after myofibroblasts differentiation under different treatments. NIH/3T3 cells were mixed with collagen to form a collagen-cell gel. The cells were incubated in basic medium (BM) as control or in differentiation medium (DM). Cells in DM medium were additionally treated with either 4-CPPC, a MIF-2 inhibitor, or recombinant MIF-2 (rMIF-2). The size of the gels were determined at day 0 and day 1. The contractile activity of the cells incubated in DM without further treatment was set as 100 % contractile activity. Statistics were calculated within a treatment group and cells in DM. $n = 3$ for each treatment. One-way ANOVA followed by *post hoc* Tukey-test was used for statistical analysis. Significance are indicated by * $p < 0.05$, ** $p < 0.01$ and *** $p < 0.001$.

5.6 Impact of rMIF-2 on primary human dermal fibroblast (HDF) proliferation

In obese people, the adipose tissue is often chronically inflamed and the secretion of cytokines and growth factors is pathologically altered. Thus, cytokine secretion of the stromal vascular fraction (SVF) derived from adipose tissue is pathologically changed compared to lean patients [50, 181]. This also includes MIF and MIF-2 levels. Kim *et al.* have already shown that treatment with supernatant from inflammatory adipose tissue from chronic wounds has a negative impact on cell viability and proliferation of human dermal fibroblasts (HDFs) compared to supernatant from healthy adipose tissue. Furthermore, they showed that supplemented rMIF-2 enhanced proliferation in

a dose dependent manner after treatment with supernatant from inflammatory adipose tissue [162].

To assess whether this negative effect on cell viability also occurs in adipose tissue from obese persons, HDFs were incubated with SVF conditioned medium (SVF-CM) from obese patients (BMI > 25) with additional rMIF-2 in different concentrations based on previous works (Figure 5.26). The viability was measured via alamar Blue assay on day 0 (reference), day 3 and day 7. Cell were also treated with culture medium/proliferation medium (PM) as positive control as well as with medium without fetal bovine serum (FBS) (starvation medium, SM). The measured values are given as a percentage increase or decrease in relation to day 0 and normalized to positive control (PM treated cells).

The viability of HDFs was strongly decreased after treatment with pure SVF-CM similar to treatment with SM. After 7 days, the viability was even less than about 25 % of the initial value. The negative impact of SVF-CM appeared to be reversed after the addition of rMIF-2. After 3 days, the viability was even higher than that of PM treated cells (> 100 %). Furthermore, a slight dose dependency could be observed from 50 ng/mL rMIF-2 up to the higher concentrations. On day 7, the viability of cells that were incubated in CM plus rMIF-2 was lower compared to PM treated cells (< 100 %), but the difference to pure CM and SM was even more significant. On day 7, however, viability decreased with increasing rMIF-2 concentration, in contrast to day 3.

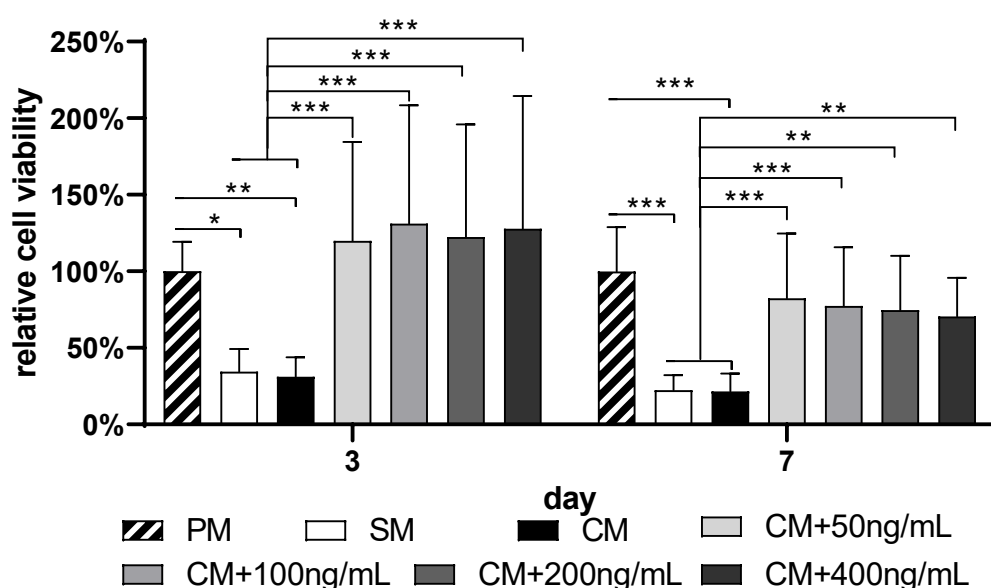


Figure 5.26: Viability assay of HDFs treated with SVF-CM derived from 4 obese patients (BMI > 25) and additional rMIF-2. HDF viability was measured by alamar Blue® assay on day 0 as base value, day 3 and day 7. The values were set in relation to that on day 0 and normalized to cells that were incubated in culture medium. Medium without FBS (starvation medium, SM) served as negative control. Fibroblasts were treated with SVF-CM derived from 4 obese patients (BMI > 25) with or without additional rMIF-2 in a concentration of 50 ng/mL, 100 ng/mL, 200 ng/mL or 400 ng/mL. n = 4 for each treatment. Statistical analysis were determined within each day between the groups using two-way ANOVA followed by Tukey's-test as post hoc test. Significance are indicated by *p < 0.05, **p < 0.01 and ***p < 0.001.

In addition, the same experiment was performed, but with SVF-CM from lean patients (BMI ≤ 25) under the same conditions, to investigate whether additional rMIF-2 had the same positive effect on viability in lean patients as in obese patients (Figure 5.27). Here, the cell viability of all treatments was reduced compared to PM treated cells. After 3 days, additional rMIF-2 diminished cell viability to similar levels to that of SM treated cells. Interestingly, 200 ng/mL and 400 ng/mL rMIF-2 showed an even worse effect than 50 ng/mL and 100 ng/mL rMIF-2. On day 7, cell viability of HDFs that were incubated with CM and rMIF-2 were decreased to about 20 – 25 %, with the value of the CM plus 50 ng/mL samples being lower than that of the samples treated with CM plus 400 ng/mL. In contrast, HDFs incubated in SM and CM were more viable with a value of about 40 %.

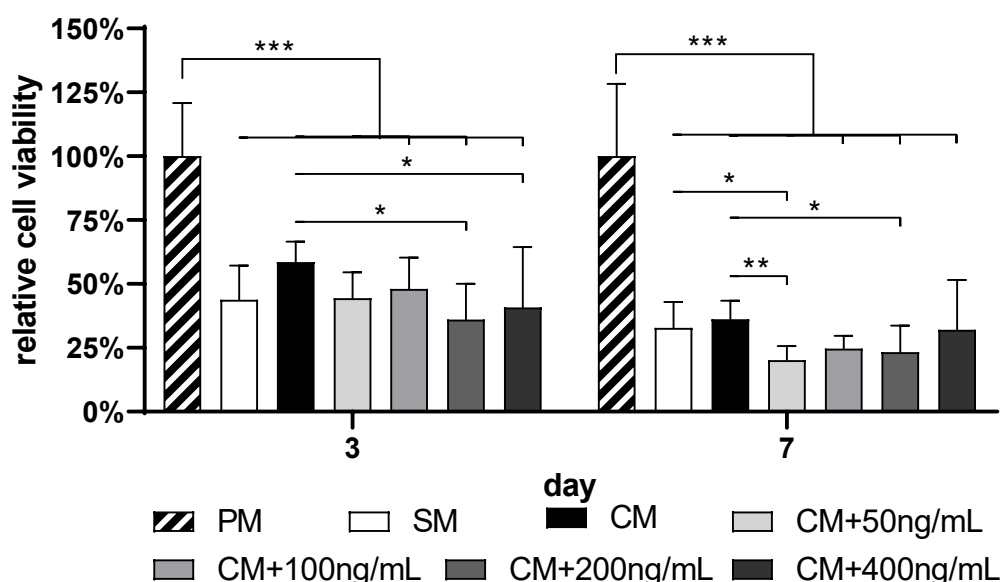


Figure 5.27: Viability assay of HDFs treated with SVF-CM derived from 4 lean patients (BMI ≤ 25) and additional rMIF-2. HDF viability was measured by alamar Blue® assay on day 0 as base values, day 3 and day 7. The values were set in relation to day 0 and normalized to cells which were incubated in culture medium. Medium without FBS (starvation medium, SM) served as negative control. Fibroblasts were treated with SVF-CM derived from 4 lean patients (BMI ≤ 25) with or without additional rMIF-2 in a concentration of 50 ng/mL, 100 ng/mL, 200 ng/mL or 400 ng/mL. n = 4 for each treatment. Statistical analysis were determined within each day between

Results

the groups using two-way ANOVA followed by Tukey's-test as post hoc test. Significance are indicated by * $p < 0.05$, ** $p < 0.01$ and *** $p < 0.001$.

To get a better overview of the different effects of SVF-CM from lean and obese patients with and without rMIF-2, results were also presented as lean vs. obese (Figure 5.28). At both time points, the viability ratio between the two CM groups was the same. The cell viability of cells incubated in pure CM was significantly higher in the lean group ($p < 0.001$). In contrast, after adding rMIF-2, the effect was reversed. SVF-CM from obese patients supplemented with rMIF 2 showed a strongly significantly better influence on cell viability compared to SVF-CM from lean individuals regardless of the rMIF-2 concentration. After 7 days, the difference was even more significant ($p < 0.001$).

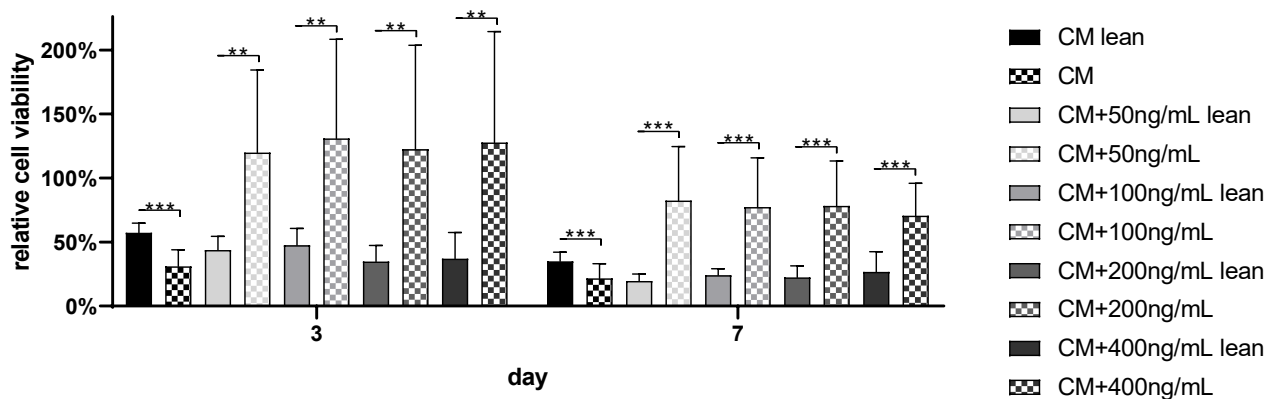


Figure 5.28: Viability assay of HDFs treated with SVF-CM derived from 4 lean patients (BMI ≤ 25) and 4 obese patients (BMI > 25) with or without additional rMIF-2. HDF viability was measured by alamar Blue[®] assay on day 0 as base values, day 3 and day 7. The values were set in relation to day 0 and normalized to cells which were incubated in culture medium. Fibroblasts were treated with SVF-CM derived either from lean patients ($n = 4$) (BMI ≤ 25) or from obese patients ($n = 4$) (BMI > 25) with or without additional rMIF-2 in a concentration of 50 ng/mL, 100 ng/mL, 200 ng/mL or 400 ng/mL. Statistical differences were calculated within each day between the lean and the obese group in the single conditions using student unpaired two-tailed t-test. Significance are indicated by * $p < 0.05$, ** $p < 0.01$ and *** $p < 0.001$.

The treatment of fibroblasts with SVF-conditioned medium with additional rMIF-2 indicates that MIF-2 has a crucial role in cell viability. SVF-CM gained from obese individuals, which had a reduced MIF-2 level, showed and decreased cell viability but as soon as rMIF-2 was added the viability elevated strongly. This supports the hypothesis that reduced MIF-2 levels are a major factor in reduced cell viability. However, too high a level of MIF-2 also leads to a deterioration in cell viability as was indicated in the treatment of fibroblast with SVF-CM gained from lean individuals with additional amount of rMIF-2. Thus, it seems MIF-2 has a regulatory role in cell viability.

6. Discussion

6.1 Obesity and *Mif-2*^{-/-} results in delayed wound healing

Wound healing disorders and chronic wounds present a major challenge in today's medicine. Since they often manifest as keloids, ulcers, fistula, or septic wounds they pose a heavy burden on the patients and the global healthcare system [34, 35, 37-39]. Several studies have shown that obese patients are more prone to wound healing disorders [36-39, 46, 47]. Obesity leads to altered secretion levels of chemokines such as macrophage migration inhibitor factor (MIF) and its structural homolog D-dopachrome tautomerase, so called MIF-2. While MIF levels are elevated in obese individuals, MIF-2 levels are decreased as compared to lean patients [141, 144, 146]. In previous studies however, first results hinted that MIF-2 has a positive influence on wound healing [152, 162]. Based on these findings, the goal of this work was to examine the role of MIF-2 in wound repair more closely and prove the hypothesis that diminished wound healing in obese patients is partially caused by a lack of MIF-2.

The effect of diminished wound healing after high fat diet (HFD) or in genetically modified obese mice has previously been shown by other groups [46, 174, 182]. In a murine wound healing model, such findings of obesity leading to delayed wound repair were reproduced. Furthermore, it was shown in this thesis that wounds in wild type (WT) mice under HFD widen before they start healing. Global *Mif-2* knockout in mice also initially resulted in enlarged wounds - even more so than in obese WT mice - before wounds began to heal and reduce in size. However, already after 10 days, unlike the obese WT mice, *Mif-2*^{-/-} mice that were fed a regular diet (RD) showed wound sizes similar to WT mice under RD and wounds of both groups were closed at the same time. This means that the delay in the wound healing process only occurred during the first days after intervention in *Mif-2*^{-/-} mice, while the delay under HFD lasted for the entire healing process.

Obesity is associated with several pathologically altered factors, resulting in reduced angiogenesis or a systemic, chronic inflammation of subcutaneous adipose tissue as previously mentioned. Altered secretion levels of several chemokines, such as MIF and MIF-2 due to obesity lead to impairment of migration, proliferation, and differentiation of cells essential for wound repair such as fibroblasts, keratinocytes,

stem cells, or monocytes [39, 46, 48, 49, 144, 146]. This may explain the difference in wound healing between knockout mice and HFD fed mice.

Knockout of *Mif-2* seems to play an important role in the early phases of wound repair as the organism finds alternative mechanisms to compensate. In a previous study, deletion of the *Mif-2* gene led to increased pro-inflammatory M1 polarization of macrophages and lower levels of the anti-inflammatory phenotype M2 macrophages [152]. A dominant M1 polarization results in an elevated pro-inflammatory cytokine expression causing a prolonged inflammation state and impaired wound healing [35]. Furthermore, mainly M2 macrophages secrete the platelet derived growth factor (PDGF) and the transforming growth factor (TGF)- β which play major roles in fibroblast activation and differentiation relating to wound healing [28, 29, 183]. It may appear that a lower M2 phenotype polarization leads to reduced TGF- β and PDGF expression, resulting in delayed or impaired activation of fibroblasts for differentiation and production of components to rebuild the extracellular matrix (ECM). However, it was shown in this work that expression levels of *Tgf- β* and *Pdgf* were not impacted.

6.2 Consequences of impaired *Mif-2* expression

6.2.1 Influence of MIF-2 on the differentiation of myofibroblasts

Granulation tissue, a transitional connective tissue present before the wound has completely healed, mostly consists of ECM. Myofibroblasts produce the individual components to form the ECM and form granulation tissue [26-28, 92]. Therefore, the wound tissue of the *Mif-2*^{-/-} mice under RD and both WT groups (RD and HFD) was analyzed for myofibroblasts. The lack of MIF-2 seemed to negatively influence the myofibroblast differentiation. *Mif-2*^{-/-} mice presented significant α -smooth muscle actin (SMA) levels only after three days, as compared to WT RD mice, which already reached high levels after one day.

Since the WT HFD mice had an even lower α -SMA level on day 3 after intervention, other factors besides reduced *Mif-2* expression must be involved in the differentiation impairment. Seitz *et al.* have shown that delayed myofibroblast differentiation in obese

mice lasts for almost the entire repair process [46]. This long-lasting delay could also be observed in the wound closure of the WT HFD group.

The major growth factors that initiate the differentiation from fibroblasts to “wound fibroblasts” and finally myofibroblasts are PDGF and TGF- β [28, 29, 90, 183]. A lack of MIF-2 does not affect the expression of these initiating growth factors themselves, since both growth factors were not downregulated but rather slightly upregulated in *Mif-2^{-/-}* mice. In case of the WT HFD mice, *Pdgf* is expressed even more compared to lean mice, analogous to Cheng *et al.* who have recently shown that obesity leads to elevated PDGF expression [184]. Hence, MIF-2 might be a previously unknown key protein within the differentiation pathway.

6.2.2 MIF-2 and the myofibroblast differentiation pathway

As MIF-2 is known to interact with CD74 which subsequently activates the extracellular signal-regulated kinase (ERK)/mitogen-activated protein kinase (MAPK) cascade, the ERK/MAPK signaling pathway is a likely mechanism for the influence of MIF-2 on myofibroblast differentiation [132]. The TGF β /Smad signaling cascade is the canonical pathway for myofibroblast differentiation [95, 96]. In addition, the differentiation triggered by TGF- β also runs through non-Smad pathways such as MAPK downstream via ERK1 and/or ERK2, among others [83, 95, 98]. The MAPK signaling cascades are not only activated by TGF- β , but also by other stimulating cytokines and growth factors [185]. However, several groups have demonstrated that inhibition of the ERK/MAPK pathway greatly diminishes myofibroblast differentiation and their contractile activity. Particularly in mesenchymal cell types like fibroblasts, ERK is critical for signaling, especially for the Smad pathway as shown by Hough *et al.* [98, 186-189]. Furthermore, Hayashida *et al.* have shown positive crosstalk between ERK/MAPK and the Smad pathway for collagen production. [190]

In this thesis, it was shown that the contractile activity of the differentiating NIH/3T3 cells was strongly inhibited in gel contraction assays when treated with 4-CPPC, a specific MIF-2 antagonist to block CD74 activation [172]. The previously mentioned studies and the results that were generated in this thesis support the hypothesis that MIF-2 is an essential protein in TGF- β initiated myofibroblast differentiation, as it may interfere within the pathway presumably through ERK1/2 signaling.

6.2.3 Direct consequences of diminished myofibroblast differentiation

As mentioned earlier, granulation tissue is a transitional connective tissue consisting mainly of ECM, myofibroblasts, stem cells, and keratinocytes [26, 27, 92]. Impaired myofibroblast differentiation means that proteins such as type 1 and 3 collagen and fibronectin for rebuilding the ECM are not produced, or are produced in insufficient quantities [98, 174, 186, 188, 191]. The diminished myofibroblast differentiation caused by a *Mif-2* knockout has been shown to lead to delayed formation of granulation tissue in the early healing phases. In later healing phases, granulation tissue was on a similar level as in control animals but with significantly lower collagen participation. In addition, mRNA levels of type 1 and 3 collagen, the major types for tissue reconstruction, were reduced to about 50 % while fibronectin expression was increased. Fibronectin is not synthesized by terminal myofibroblasts but by “wound fibroblasts”, a premature differentiation phenotype, which is triggered by PDGF [29]. I conclude that the delayed granulation tissue formation in the *Mif-2*^{-/-} mice is not caused by a general inhibition of ECM proteins, but rather the diminished collagen production and subsequent fibronectin overexpression, which seems triggered to compensate for this deficiency in collagen levels.

On the other hand, obese mice, which still showed low *Mif-2* expression, built up to three times more granulation tissue with a significantly higher participation of collagen compared to mice that did not express *Mif-2* on day 3. Nevertheless, the tissue quality, measured by collagen content, was still strongly diminished compared to lean mice. It seems that obesity leads to a general retardation of 3 – 4 days regarding tissue restoration and wound closure [46, 47, 174, 182]. Even though WT HFD mice had less granulation tissue than *Mif-2*^{-/-} mice on day 7 post intervention, they produced more collagen. On the other hand, collagen production was reduced when compared to WT RD mice. The delay of granulation tissue formation and collagen production in obese mice is only partially diminished through lower levels of MIF-2, but also by other factors since the delay persisted as has also been described in previous studies [46, 47, 174, 182, 192, 193]. Similar to the *Mif-2*^{-/-} mice, obese mice compensated for lower collagen production by an overexpression of fibronectin. Elevated fibronectin levels caused by obesity have also been shown in other studies including in humans [194-196]. However, unlike in the knockout strain fibronectin expression was abnormally

increased in obese mice, which can partly be explained by elevated PDGF levels. An excess of fibronectin may be an additional reason for the impaired wound healing in obese mice and helps to explain the difference in the healing process of *Mif-2*^{-/-} mice in the later phases [197, 198].

6.2.4 Further consequences of a delayed myofibroblast differentiation

The delay of granulation tissue formation caused by a *Mif-2* deficit results in further impairment of wound healing: The ECM serves as a scaffold for vascular endothelial cells supporting neovascularization. Newly formed blood vessels are crucial for wound healing as they supply the wound area with oxygen, nutrients, and additional cells for the repair process [199]. Reduced granulation tissue is associated with a decreased angiogenesis [46, 200]. It appears that the formation of granulation tissue and neovascularization is proportionally related, since *Mif-2*^{-/-} mice formed even fewer blood vessels than the obese mice. Nevertheless, a reduced angiogenesis is not only caused by low *Mif-2* expression and impaired granulation tissue formation. The altered chemokine secretion and the chronic inflammation state of adipose tissue also negatively influence vascularization. [39, 201, 202]

The basal membrane separates the dermis and the epidermis. Endothelial cells and podocytes synthesize collagen type IV, the major component of this layer. Although the basal membrane is just a thin separating layer, it is still essential for proper wound healing. A disorder in basal membrane formation may have a negative impact on the entire repair process [10-12]. Both mice groups, WT HFD and *Mif-2*^{-/-} expressed more collagen IV than the control group. Obesity leads to elevated collagen IV levels in subcutaneous fat tissue. Reggio *et. al.* assume that an increased TGF- β 1 and -3 level as well as insulin resistance result in increased collagen IV production. [203] Nevertheless, the underlying mechanism is not yet verified. As the collagen IV levels in *Mif-2*^{-/-} mice and obese mice are similar and the TGF- β 1 expression is not increased in either group, there must be further reasons for the excess of collagen IV. One explanation could be a compensating reaction from the organisms for the low collagen I and III production. However, more research is needed to investigate whether MIF-2 has an impact on collagen IV synthesis and how obesity disrupts it.

6.2.5 Impact on re-epithelialization and keratinocytes associated growth factors

Re-epithelialization is a critical step for sufficient wound healing, as the epidermis as the most superficial skin layer is rebuilt and serves as the outermost protection barrier of the body. The predominant cells in the epidermis are keratinocytes. They occur in different degrees of differentiation: from undifferentiated, mitotic keratinocytes in the deepest layer, to anucleate, terminally differentiated keratinocytes/corneocytes in the outermost layer [3, 4, 7, 9]. During the differentiation process, keratinocytes change the expression of keratin type from keratin 14 to keratin 10 [1, 8]. However, stromal cells particularly fibroblasts and endothelial cells secrete fibroblast growth factors (FGF)-7 and FGF-10 (previously known as keratinocyte growth factor 1 and 2) stimulating keratinocytes to migrate into the wound area and proliferate [89, 204-206]. In general, re-epithelialization as well as keratinocyte migration and differentiation did not appear to be strongly influenced neither by the HFD nor by the *Mif-2* knockout. Rather, it seems that the expression of keratin 10 was minimally elevated in the *Mif-2^{-/-}* strain. The consensus of existing literature is that obesity impairs the reepithelialization and disturbs the homeostasis of the epidermis [39, 206-208]. Nevertheless, it was found that this disturbance is not associated with a low *Mif-2* level.

Interestingly, the *Fgf-10* expression seemed to be greatly influenced by MIF-2. Although FGF-7 and -10 are homologues and bind to the same FGFR2iiib receptor, FGF-10 expression is not stimulated by inflammatory cytokines after an injury unlike FGF-7. [205, 209]. Therefore, MIF-2 might be a hitherto unknown regulator for FGF-10, as the expression levels of *Fgf-10* were similar to those of *Mif-2* in all three groups. Furthermore, several studies have reported a positive impact from FGF-10 on wound healing. In addition to its effect on re-epithelialization, it also plays a role in collagen production and granulation tissue formation. FGF-10 treatments enhanced healing in injured lungs and skin wound models of mice, rats, and rabbits [89, 210-213]. However, there is evidence that FGF-10 affects collagen production intrinsically via two MAPK pathways: ERK1/2 and PI3K/Akt [213-217]. Perl and Gale have also shown that FGF-10 is essential for α -SMA expression in myofibroblast progenitor cells during alveolar regeneration [218]. Nevertheless, nothing has been reported about the role of FGF-10 and α -SMA production during wound healing. Thus, I hypothesize that

MIF-2 might be a previously unknown regulator for *Fgf-10* expression after injury and that FGF-10 also triggers the α -SMA synthesis of myofibroblasts via ERK/MAPK and PI3K/Akt pathways as described above. Further investigation is necessary to examine this proposed signaling cascade.

6.3 Increased wound tissue inflammation caused by low MIF-2 levels

Inflammation is an important phase in the wound repair process. It is a stage of purge. Here, previously recruited neutrophils secrete proteolytic enzymes to kill bacteria and other invading pathogens as well as to digest damaged tissue. Monocytes differentiate into pro-inflammatory M1 macrophages to clean cell debris and kill pathogens [19-21]. In the late inflammatory phase monocytes differentiate into anti-inflammatory M2 macrophages, release several growth factors and cytokines such as PDGF and TGF- β to stimulate further cells which then migrate to the wound area, proliferate, and differentiate [24, 29, 183]. MIF is known to elevate the secretion of pro-inflammatory factors such tumor necrosis factor (TNF)- α and interferon (IFN)- γ resulting in an increased M1 polarization of macrophages [147, 149, 151, 152]. Our group recently discovered an M2 driving effect of MIF-2 in a murine endotoxemia model [152].

In general, the macrophage recruitment measured by F4/80 was only increased in *Mif-2^{-/-}* mice, in contrast to obese mice where this level was minimally reduced [178, 219]. In addition, TNF- α levels were slightly but not significantly reduced in uninjured skin tissue of the WT HFD group. Seitz *et al.* have demonstrated that the TNF- α serum levels in HFD mice were similar to those in lean mice; moreover, the genetically modified obese *ob/ob* mice had a reduced baseline level of TNF- α [46]. In contrast, several studies have shown an increased inflammation in obese individuals particularly after wounding [39, 47, 49, 50, 182, 220]. The results of this thesis agree with those studies, except for the chronic low-grade inflammation in healthy tissue of the obese mice model (WT under HFD). As mice of this group were set on HFD at the early age of 4 weeks at a total experimental duration of 9 weeks, the mice may have developed chronic adipose tissue inflammation at a later stage.

The HFD mice did show a shift in the ratio of MIF to MIF-2. Just like obesity changes their levels in humans, it also led to a dramatic increase in *Mif* and a decrease in *Mif-*

$2^{-/-}$ in mice. [141, 144-146]. Only one M1 marker was upregulated in the WT HFD mice, while the *CD301b* gene, a M2 marker, was downregulated. Lumeng *et al.* demonstrate the general shift towards M1 macrophages correlated with obesity.[220] The same was observed for *Mif-2^{-/-}* mice, which showed minimal *Mif* increase compared to lean WT mice, but in the knockout strain both M1 markers were elevated and the M2 marker was even more downregulated than in the HFD mice. Thus, I propose that obesity causes a disturbed MIF-MIF-2 relationship, which in turn skews macrophages towards the pro-inflammatory M1 phenotype, which subsequently secrete more pro-inflammatory cytokines like TNF- α .

6.4 Obesity-induced secretion changes without MIF-2 influence

As already mentioned, obesity alters several different cytokines, growth factors, and other proteins. The secretion of matrix metallo-proteases (MMPs), collagen digesting enzymes, is increased in obese individuals. MMP-9 is one major protease responsible for the digestion of ECM [19, 221-223]. Various stromal cell types such as fibroblasts, adipocytes, neutrophils, and M1 macrophages secrete MMPs through TNF- α stimulation. [14, 19, 180, 222, 223]. However, the increase in MMP-9 in the obese (HFD) mice in the wound healing model could not be attributed to the M1-shifted macrophage polarization caused by low MIF-2 level, as the *Mif-2^{-/-}* mice had the same MMP-9 levels as the lean control WT mice. Therefore, I conclude that neither fibroblast- nor neutrophil-secretion are responsible for the elevated MMP-9 level, since TNF- α levels were even higher in *Mif-2^{-/-}* mice than in obese (HFD) mice. Rather, I propose that the obesity-induced excess is related to adipocytes, whose number in adipose tissue is increased due to the HFD, but not in the genetically modified group [224]. Further studies are required to verify this hypothesis.

Elastin is an additional protein important in the repair process. It is produced by fibroblasts and myofibroblasts during the remodeling phase when the wound is already closed. The inelastic, collagen rich granulation tissue is slowly exchanged with elastic elastin fibers to enhance the tension strength and elasticity. [19, 20, 225]. As the analyzed wound tissue had been sampled 3 days after intervention, during the inflammation and proliferation phase, a proper statement about the influence of elastin

synthesis during wound healing is not possible. However, obesity diminishes the general elastin secretion especially in the subcutaneous adipose tissue. Lin *et al.* showed that the decrease of elastin in adipose tissue is due to an upregulation of MMPs caused by obesity. [226-228]. The downregulation of elastin in the obese mice in their study appears to result from the elevated MMPs production in adipose tissue.

6.5 The right amount of MIF-2

In addition, treatment of myfibroblasts and fibroblasts with recombinant MIF-2 (rMIF-2) also has been examined to evaluate a potential therapeutic effect of MIF-2. An improved myfibroblast differentiation was assumed from additional rMIF-2, as a reduction in MIF-2 diminishes differentiation. In previous studies, our group demonstrated a positive impact of rMIF-2 treatment on the viability of primary human dermal fibroblasts [162]. Building on this, we further analyzed whether rMIF-2 improved viability, when dermal fibroblasts were treated with medium conditioned with stromal vascular fraction (SVF) obtained from obese or lean patients.

6.5.1 Inhibitory alternative pathway of MIF-2 in myfibroblast differentiation

Supplementary rMIF-2 decreased the contractile activity in the collagen gel contraction assay in a dose dependent manner. Thus, MIF-2 not only supports myfibroblast differentiation as mentioned previously. In contrast, at higher dosage MIF-2 appears to partially inhibit the differentiation via an alternative pathway. Oncogenic cells show counter regulation of the phosphorylated receptor-activated Smad2/3 complex [229-231]. In these studies, not only TGF- β phosphorylated Smad proteins: Smad2 and Smad3 also contain a MAPK/CDK (cyclin-dependent kinase) phosphorylation site, at which Erk1/2 is able to transfer phosphate groups. In that case, the activity of the Smad complex is inhibited. Hence, I propose that, while excess of MIF-2 leads to an elevated ERK activity, not only does ERK activity support differentiation but also a second effect occurs: the inhibition of the TGF- β /Smad pathway (Figure 6.1). To verify this proposed side effect, further investigation into the TGF- β /Smad pathway are essential.

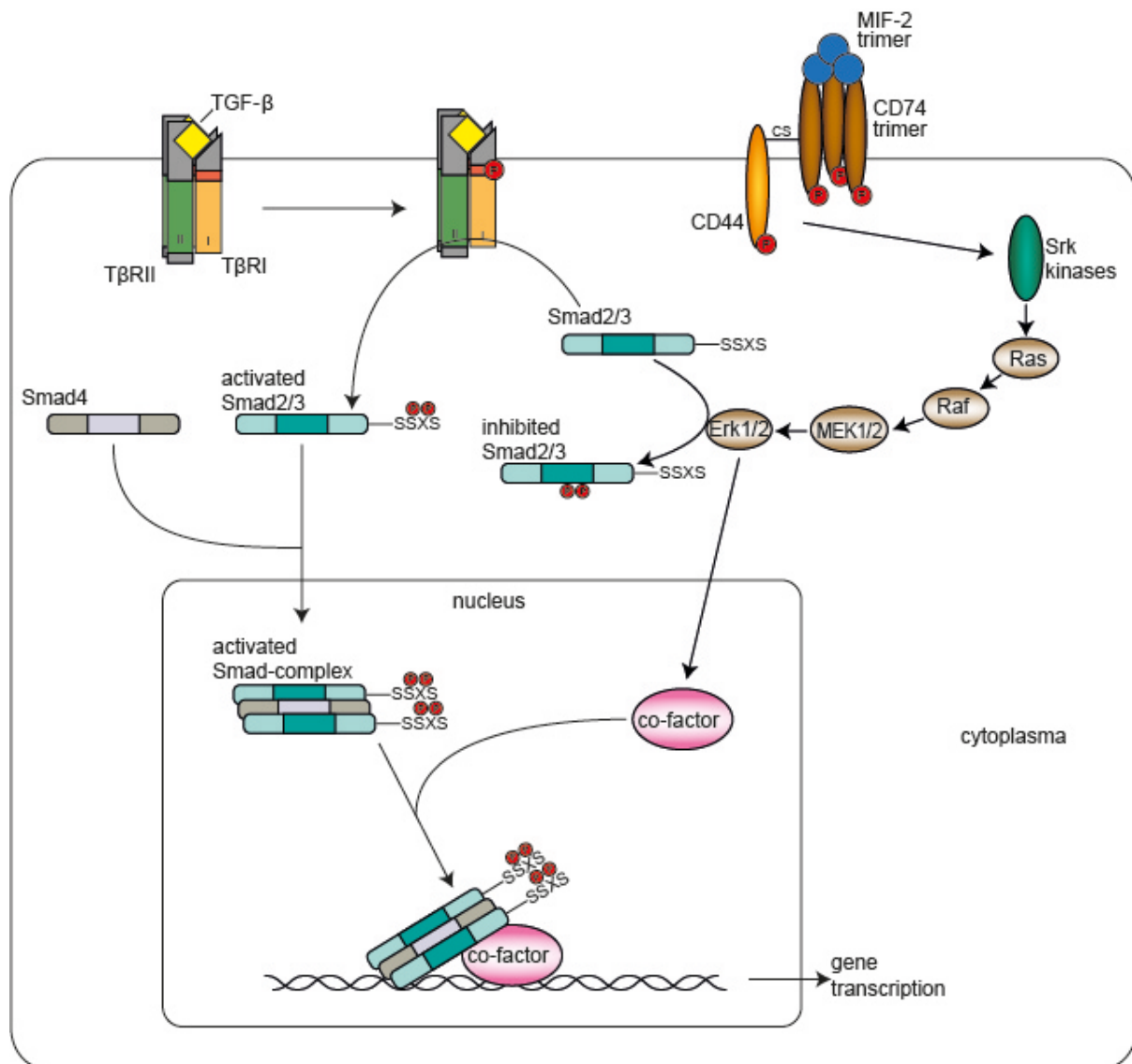


Figure 6.1: Two postulated mechanisms for the regulation of the TGF- β /Smad signaling pathway by MIF-2 via Erk1/2. MIF-2 binds to the CD74 receptor initiating an intracellular phosphorylation of CD74. CD44 is subsequently recruited and phosphorylated followed by the activation of Src kinases. This in turn activates the Ras downstream MAPK cascade ending in Erk1/2 phosphorylation. With an adequate amount of phosphorylated Erk, a cofactor is formed downstream which, together with the activated Smad complex, regulates gene transcription. If Erk1/2 is excessively activated, Smad2/3 are phosphorylated and thus inhibited. Adapted from Zhang [83, 232].

6.5.2 The positive and negative influence of MIF-2 on cell viability

The subcutaneous tissue contains a heterogeneous cell population. These include mesenchymal progenitor cells, pericytes, pre-adipocytes, endothelial cells, M2 macrophages, and T cells. Through secretion of many cytokines and growth factors, it is responsible for homeostasis of the skin. Thus, the stromal cells play a crucial role

during wound healing as they stimulate fibroblast migration and neovascularization, among other things. [233-235] However, in obese individuals, cytokine and growth factor secretion of the SVF is altered, such that the positive impact on wound healing is diminished. [50, 181, 236]. It has also been shown that the viability of dermal fibroblasts is reduced when cells are treated with SVF conditioned medium (CM) obtained from obese patients compared to that of lean patients. Since MIF-2 levels are decreased in obese individuals and our group showed a positive impact of MIF-2 on fibroblast viability [141, 162], rMIF-2 was added to the SVF-CM. The viability of the cells treated by SVF-CM from obese individuals strongly increased, but interestingly, when added to the lean SVF-CM treated cells, the viability decreased in a dose depend manner. In addition, the long-term treatment with SVF-CM of obese individuals still showed a positive effect but this effect was slowly diminished with higher rMIF-2 concentrations. So, it seems that MIF-2 only has a positive influence on cell viability in the "correct concentration" as a negative influence was observed in the event of an "overdose", similar to its effect on fibroblast differentiation.

How MIF-2 exerts its function in cell viability is not yet clear, but; as already mentioned, it could bind to the CD74 receptor and most likely the thus activated mechanism acts via the ERK/MAPK pathway. Erk1/2 are involved in the regulation of cell proliferation, in contrast, it is shown that excessive Erk1/2 phosphorylation also triggers cell apoptosis [237-240]. Various signaling cascades are described for Erk initiation of intrinsic and extrinsic apoptotic pathways [241]. Tang *et al.* demonstrated that a DNA damage induced overactivation of ERK results in cell arrest or apoptosis [242]. However, more detailed investigations are needed to make a clear statement about the MIF-2 induced pathway.

6.6 Conclusion and outlook

In my thesis, I could verify the hypothesis that macrophage migration inhibitor factor (MIF)-2 plays a crucial role in wound healing. Furthermore, I showed that the decreased MIF-2 levels in obese individuals are partially responsible for obesity-induced wound healing disorders. Deletion or reduction of MIF-2 decrease and inhibit "wound fibroblasts" to differentiate into myofibroblasts. Myofibroblasts are the major

protein producer for formation of granulation tissue. Wound contraction is another role of myofibroblasts. In mice, it is essential for a sufficient healing process, but in human, this function is not as dominant as in the mouse. Diminished wound contraction caused mainly the delayed wound closure in *Mif-2^{-/-}* and HFD fed mice. Nevertheless, reconstruction of granulation tissue and especially contribution of collagen is identical in both species. Myofibroblast secretion of proteins to rebuild the renewable tissue was also strongly impaired in both mice groups as compared to lean control mice and caused the diminished wound healing. These results can be transferred to humans. Obesity-related low MIF-2 levels lead to impaired myofibroblast differentiation and, subsequently, to insufficient formation of granulation tissue.

MIF-2 primarily interact via the CD74 receptor activating mitogen-activated protein kinase downstream cascades including the extracellular signal-regulated kinase (ERK)1/2 pathway. Furthermore, ERK1/2 interacts and regulates the transforming growth factor (TGF)- β /Smad pathway, which is the canonical signaling cascade that triggers myofibroblast differentiation. Therefore, I propose that MIF-2 is a still unknown essential regulatory cytokine for TGF- β /Smad initiating differentiation of myofibroblasts and their homeostasis. MIF-2 activates ERK1/2 via CD74 and MAPK downstream. Either phosphorylated ERK1/2 results in an unknown cofactor needed for gene transcription or it phosphorylates and inhibits Smad2/3, whereby the cascade is blocked.

Nevertheless, interaction between ERK1/2 and Smad proteins are sparsely investigated and the mechanisms is not completely identified. The proposed pathway in which MIF-2 functions is based on initial results from this work and previous studies on the mechanism of MIF-2 downstream via ERK1/2 and ERK1/2 and Smad interactions. In particular, the mentioned cofactor for gene transcription is still unknown and a “black box”. Thus in order to verify the hypothesized pathway, more detailed analysis on both downstream cascades, TGF- β /Smad and MIF-2 initiated ERK/MAPK, are necessary, especially the interaction between them. There were no direct evidence about the correct concentration on MIF-2 or phosphorylated ERK1/2, when the second inhibitory function is addressed. Furthermore, fibroblast growth factor (FGF)-10 appeared to be directly influenced by MIF-2 levels. Several studies proved the critical role of FGF-10 on formation of granulation tissue. As underlying mechanism, they also

assumed MAPK downstream cascades. Even though, there is no reported connection between MIF-2/CD74 and FGF-10, the downregulation may give evidence that MIF-2 plays a role in FGF-10 expression. However, further investigations for the underlying pathway are needed.

Since I have mainly focused on wound healing including the mechanisms in mice and the results cannot be transferred one-to-one to humans, it is necessary to prove the results on humans and human cells. Treatment with MIF-2 requires additional *in vivo* experiments on mice in addition to the previous *in vitro* experiments. The question arises whether topical or systemic treatment with recombinant MIF-2 can improve the diminished wound healing caused by obesity. In general, my model and work only partially explain obesity-induced wound healing disorder. Even though this complex field has been studied for a long time, much is still missing to fully understand the pathological mechanisms behind it.

ReferencesBibliography

1. Roger, M., N. Fullard, L. Costello, S. Bradbury, E. Markiewicz, S. O'Reilly, N. Darling, P. Ritchie, A. Määttä, I. Karakesisoglou, G. Nelson, T. von Zglinicki, T. Dicolandrea, R. Isfort, C. Bascom, and S. Przyborski, Bioengineering the microanatomy of human skin. *J Anat*, 2019. **234**(4), 438-455.
2. Romanovsky, A.A., Skin temperature: its role in thermoregulation. *Acta Physiol (Oxf)*, 2014. **210**(3), 498-507.
3. Brandner, J.M., M. Zorn-Kruppa, T. Yoshida, I. Moll, L.A. Beck, and A. De Benedetto, Epidermal tight junctions in health and disease. *Tissue Barriers*, 2015. **3**(1-2), e974451.
4. Arda, O., N. Göksügür, and Y. Tüzün, Basic histological structure and functions of facial skin. *Clinics in Dermatology*, 2014. **32**(1), 3-13.
5. Bowden, J.L., G.G. Lin, and P.A. McNulty, The prevalence and magnitude of impaired cutaneous sensation across the hand in the chronic period post-stroke. *PLoS One*, 2014. **9**(8), e104153.
6. Proksch, E., J.M. Brandner, and J.M. Jensen, The skin: an indispensable barrier. *Exp Dermatol*, 2008. **17**(12), 1063-72.
7. Odland, G.F., A Submicroscopic Granular Component in Human Epidermis**From the Department of Anatomy, University of Washington, Seattle, Washington. *Journal of Investigative Dermatology*, 1960. **34**(1), 11-15.
8. Fuchs, E. and H. Green, Changes in keratin gene expression during terminal differentiation of the keratinocyte. *Cell*, 1980. **19**(4), 1033-1042.
9. Menon, G.K., G.W. Cleary, and M.E. Lane, The structure and function of the stratum corneum. *Int J Pharm*, 2012. **435**(1), 3-9.
10. Abreu-Velez, A.M. and M.S. Howard, Collagen IV in Normal Skin and in Pathological Processes. *North American journal of medical sciences*, 2012. **4**(1), 1-8.
11. Betz, P., A. Nerlich, J. Wilske, J. Tübel, I. Wiest, R. Penning, and W. Eisenmenger, The time-dependent rearrangement of the epithelial basement membrane in human skin wounds — immunohistochemical localization of Collagen IV and VII. *International Journal of Legal Medicine*, 1992. **105**(2), 93-97.
12. Wick, G., R.W. Glanville, and R. Timpl, Characterization of Antibodies to Basement Membrane(Type IV) Collagen in Immunohistological Studies. *Immunobiology*, 1980. **156**(4), 372-381.
13. Green, E.M., J.C. Mansfield, J.S. Bell, and C.P. Winlove, The structure and micromechanics of elastic tissue. *Interface Focus*, 2014. **4**(2), 20130058.
14. McAnulty, R.J., Fibroblasts and myofibroblasts: Their source, function and role in disease. *The International Journal of Biochemistry & Cell Biology*, 2007. **39**(4), 666-671.
15. McAnulty, R.J., J.S. Campa, A.D. Cambrey, and G.J. Laurent, The effect of transforming growth factor β on rates of procollagen synthesis and degradation in vitro. *Biochimica et Biophysica Acta (BBA) - Molecular Cell Research*, 1991. **1091**(2), 231-235.
16. Prost-Squarcioni, C., S. Freitag, M. Heller, and N. Boehm, [Functional histology of dermis]. *Ann Dermatol Venereol*, 2008. **135**(1 Pt 2), 1s5-20.
17. Cinti, S., The adipose organ at a glance. *Dis Model Mech*, 2012. **5**(5), 588-94.
18. Kershaw, E.E. and J.S. Flier, Adipose tissue as an endocrine organ. *J Clin Endocrinol Metab*, 2004. **89**(6), 2548-56.
19. Rittié, L., Cellular mechanisms of skin repair in humans and other mammals. *J Cell Commun Signal*, 2016. **10**(2), 103-20.
20. Stadelmann, W.K., A.G. Digenis, and G.R. Tobin, Physiology and healing dynamics of chronic cutaneous wounds. *Am J Surg*, 1998. **176**(2A Suppl), 26s-38s.
21. Smith, O.J., G. Jell, and A. Mosahebi, The use of fat grafting and platelet-rich plasma for wound healing: A review of the current evidence. *Int Wound J*, 2019. **16**(1), 275-285.
22. Witte, M.B. and A. Barbul, General principles of wound healing. *Surg Clin North Am*, 1997. **77**(3), 509-28.
23. Weeks, J.R., Prostaglandins. 1972. **12**(1), 317-336.
24. Witte, M.B. and A. Barbul, Role of nitric oxide in wound repair. *Am J Surg*, 2002. **183**(4), 406-12.
25. Wu, B., G. Mottola, M. Schaller, G.R. Upchurch, Jr., and M.S. Conte, Resolution of vascular injury: Specialized lipid mediators and their evolving therapeutic implications. *Molecular aspects of medicine*, 2017. **58**, 72-82.

26. Baum, J. and H.S. Duffy, Fibroblasts and myofibroblasts: what are we talking about? *J Cardiovasc Pharmacol*, 2011. **57**(4), 376-9.
27. Hinz, B., The role of myofibroblasts in wound healing. *Curr Res Transl Med*, 2016. **64**(4), 171-177.
28. Desmoulière, A., A. Geinoz, F. Gabbiani, and G. Gabbiani, Transforming growth factor-beta 1 induces alpha-smooth muscle actin expression in granulation tissue myofibroblasts and in quiescent and growing cultured fibroblasts. *J Cell Biol*, 1993. **122**(1), 103-11.
29. Glim, J.E., F.B. Niessen, V. Everts, M. van Egmond, and R.H. Beelen, Platelet derived growth factor-CC secreted by M2 macrophages induces alpha-smooth muscle actin expression by dermal and gingival fibroblasts. *Immunobiology*, 2013. **218**(6), 924-9.
30. Midwood, K.S., L.V. Williams, and J.E. Schwarzbauer, Tissue repair and the dynamics of the extracellular matrix. *Int J Biochem Cell Biol*, 2004. **36**(6), 1031-7.
31. Przekora, A., A Concise Review on Tissue Engineered Artificial Skin Grafts for Chronic Wound Treatment: Can We Reconstruct Functional Skin Tissue In Vitro? *Cells*, 2020. **9**.
32. Dissemont, J., in *Blickdiagnose chronischer Wunden. Über die klinische Inspektion zur Diagnose*. 2016, Viavital Verlag. p. 11.
33. Li, S., A.H. Mohamedi, J. Senkowsky, A. Nair, and L. Tang, Imaging in Chronic Wound Diagnostics. *Adv Wound Care (New Rochelle)*, 2020. **9**(5), 245-263.
34. Olsson, M., K. Järbrink, U. Divakar, R. Bajpai, Z. Upton, A. Schmidtchen, and J. Car, The humanistic and economic burden of chronic wounds: A systematic review. *Wound Repair Regen*, 2019. **27**(1), 114-125.
35. Frykberg, R.G. and J. Banks, Challenges in the Treatment of Chronic Wounds. *Advances in wound care*, 2015. **4**(9), 560-582.
36. Mudge, E.J., Recent accomplishments in wound healing. *Int Wound J*, 2015. **12**(1), 4-9.
37. Hyun, S., X. Li, B. Vermillion, C. Newton, M. Fall, P. Kaewprag, S. Moffatt-Bruce, and E.R. Lenz, Body mass index and pressure ulcers: improved predictability of pressure ulcers in intensive care patients. *Am J Crit Care*, 2014. **23**(6), 494-500; quiz 501.
38. Abdel-Moneim, R.I., The hazards of surgery in the obese. *Int Surg*, 1985. **70**(2), 101-3.
39. Pierpont, Y.N., T.P. Dinh, R.E. Salas, E.L. Johnson, T.G. Wright, M.C. Robson, and W.G. Payne, Obesity and surgical wound healing: a current review. *ISRN Obes*, 2014. **2014**, 638936.
40. Schreml, S., R.M. Szeimies, L. Prantl, S. Karrer, M. Landthaler, and P. Babilas, Oxygen in acute and chronic wound healing. *Br J Dermatol*, 2010. **163**(2), 257-68.
41. McCarty, S.M. and S.L. Percival, Proteases and Delayed Wound Healing. *Adv Wound Care (New Rochelle)*, 2013. **2**(8), 438-447.
42. Bourguignon, L.Y., Matrix hyaluronan-activated CD44 signaling promotes keratinocyte activities and improves abnormal epidermal functions. *Am J Pathol*, 2014. **184**(7), 1912-9.
43. Cook, H., K.J. Davies, K.G. Harding, and D.W. Thomas, Defective extracellular matrix reorganization by chronic wound fibroblasts is associated with alterations in TIMP-1, TIMP-2, and MMP-2 activity. *J Invest Dermatol*, 2000. **115**(2), 225-33.
44. Telgenhoff, D. and B. Shroot, Cellular senescence mechanisms in chronic wound healing. *Cell Death Differ*, 2005. **12**(7), 695-8.
45. Wall, I.B., R. Moseley, D.M. Baird, D. Kipling, P. Giles, I. Laffafian, P.E. Price, D.W. Thomas, and P. Stephens, Fibroblast dysfunction is a key factor in the non-healing of chronic venous leg ulcers. *J Invest Dermatol*, 2008. **128**(10), 2526-40.
46. Seitz, O., C. Schürmann, N. Hermes, E. Müller, J. Pfeilschifter, S. Frank, and I. Goren, Wound healing in mice with high-fat diet- or ob gene-induced diabetes-obesity syndromes: a comparative study. *Exp Diabetes Res*, 2010. **2010**, 476969.
47. Siebert, A., I. Goren, J. Pfeilschifter, and S. Frank, Anti-Inflammatory Effects of Rosiglitazone in Obesity-Impaired Wound Healing Depend on Adipocyte Differentiation. *PLOS ONE*, 2016. **11**(12), e0168562.
48. Sugihara, H., S. Toda, N. Yonemitsu, and K. Watanabe, Effects of fat cells on keratinocytes and fibroblasts in a reconstructed rat skin model using collagen gel matrix culture. *Br J Dermatol*, 2001. **144**(2), 244-53.
49. Schmidt, B.A. and V. Horsley, Intradermal adipocytes mediate fibroblast recruitment during skin wound healing. *Development*, 2013. **140**(7), 1517-27.
50. Pence, B.D. and J.A. Woods, Exercise, Obesity, and Cutaneous Wound Healing: Evidence from Rodent and Human Studies. *Adv Wound Care (New Rochelle)*, 2014. **3**(1), 71-79.
51. Eming, S.A., P. Martin, and M. Tomic-Canic, Wound repair and regeneration: mechanisms, signaling, and translation. *Sci Transl Med*, 2014. **6**(265), 265sr6.

52. Gerber, P.A., B.A. Buhren, H. Schruppf, B. Homey, A. Zlotnik, and P. Hevezi, The top skin-associated genes: a comparative analysis of human and mouse skin transcriptomes. *Biol Chem*, 2014. **395**(6), 577-91.
53. Lindblad, W.J., Considerations for selecting the correct animal model for dermal wound-healing studies. *J Biomater Sci Polym Ed*, 2008. **19**(8), 1087-96.
54. Wong, V.W., M. Sorkin, J.P. Glotzbach, M.T. Longaker, and G.C. Gurtner, Surgical approaches to create murine models of human wound healing. *J Biomed Biotechnol*, 2011. **2011**, 969618.
55. Solanas, G. and S.A. Benitah, Regenerating the skin: a task for the heterogeneous stem cell pool and surrounding niche. *Nature Reviews Molecular Cell Biology*, 2013. **14**(11), 737-748.
56. Watt, F.M., Mammalian skin cell biology: at the interface between laboratory and clinic. *Science*, 2014. **346**(6212), 937-40.
57. Adams, E.D.M., G.G. Goss, and S.P. Leys, Freshwater Sponges Have Functional, Sealing Epithelia with High Transepithelial Resistance and Negative Transepithelial Potential. *PLOS ONE*, 2010. **5**(11), e15040.
58. Waterston, R.H., K. Lindblad-Toh, E. Birney, J. Rogers, J.F. Abril, P. Agarwal, R. Agarwala, R. Ainscough, M. Alexandersson, P. An, S.E. Antonarakis, J. Attwood, R. Baertsch, J. Bailey, K. Barlow, S. Beck, E. Berry, B. Birren, T. Bloom, P. Bork, M. Botcherby, N. Bray, M.R. Brent, D.G. Brown, S.D. Brown, C. Bult, J. Burton, J. Butler, R.D. Campbell, P. Carninci, S. Cawley, F. Chiaromonte, A.T. Chinwalla, D.M. Church, M. Clamp, C. Clee, F.S. Collins, L.L. Cook, R.R. Copley, A. Coulson, O. Couronne, J. Cuff, V. Curwen, T. Cutts, M. Daly, R. David, J. Davies, K.D. Delehaunty, J. Deri, E.T. Dermitzakis, C. Dewey, N.J. Dickens, M. Diekhans, S. Dodge, I. Dubchak, D.M. Dunn, S.R. Eddy, L. Elnitski, R.D. Emes, P. Eswara, E. Eyas, A. Felsenfeld, G.A. Fewell, P. Flicek, K. Foley, W.N. Frankel, L.A. Fulton, R.S. Fulton, T.S. Furey, D. Gage, R.A. Gibbs, G. Glusman, S. Gnerre, N. Goldman, L. Goodstadt, D. Grafham, T.A. Graves, E.D. Green, S. Gregory, R. Guigó, M. Guyer, R.C. Hardison, D. Haussler, Y. Hayashizaki, D.W. LaHillier, A. Hinrichs, W. Hlavina, T. Holzer, F. Hsu, A. Hua, T. Hubbard, A. Hunt, I. Jackson, D.B. Jaffe, L.S. Johnson, M. Jones, T.A. Jones, A. Joy, M. Kamal, E.K. Karlsson, D. Karolchik, A. Kasprzyk, J. Kawai, E. Keibler, C. Kells, W.J. Kent, A. Kirby, D.L. Kolbe, I. Korf, R.S. Kucherlapati, E.J. Kulbokas Iii, D. Kulp, T. Landers, J.P. Leger, S. Leonard, I. Letunic, R. Levine, J. Li, M. Li, C. Lloyd, S. Lucas, B. Ma, D.R. Maglott, E.R. Mardis, L. Matthews, E. Mauceli, J.H. Mayer, M. McCarthy, W.R. McCombie, S. McLaren, K. McLay, J.D. McPherson, J. Meldrim, B. Meredith, J.P. Mesirov, W. Miller, T.L. Miner, E. Mongin, K.T. Montgomery, M. Morgan, R. Mott, J.C. Mullikin, D.M. Muzny, W.E. Nash, J.O. Nelson, M.N. Nhan, R. Nicol, Z. Ning, C. Nusbaum, M.J. O'Connor, Y. Okazaki, K. Oliver, E. Overton-Larty, L. Pachter, G. Parra, K.H. Pepin, J. Peterson, P. Pevzner, R. Plumb, C.S. Pohl, A. Poliakov, T.C. Ponce, C.P. Ponting, S. Potter, M. Quail, A. Reymond, B.A. Roe, K.M. Roskin, E.M. Rubin, A.G. Rust, R. Santos, V. Sapojnikov, B. Schultz, J. Schultz, M.S. Schwartz, S. Schwartz, C. Scott, S. Seaman, S. Searle, T. Sharpe, A. Sheridan, R. Shownkeen, S. Sims, J.B. Singer, G. Slater, A. Smit, D.R. Smith, B. Spencer, A. Stabenau, N. Stange-Thomann, C. Sugnet, M. Suyama, G. Tesler, J. Thompson, D. Torrents, E. Trevaskis, J. Tromp, C. Ucla, A. Ureta-Vidal, J.P. Vinson, A.C. von Niederhausern, C.M. Wade, M. Wall, R.J. Weber, R.B. Weiss, M.C. Wendl, A.P. West, K. Wetterstrand, R. Wheeler, S. Whelan, J. Wierzbowski, D. Willey, S. Williams, R.K. Wilson, E. Winter, K.C. Worley, D. Wyman, S. Yang, S.P. Yang, E.M. Zdobnov, M.C. Zody and E.S. Lander, Initial sequencing and comparative analysis of the mouse genome. *Nature*, 2002. **420**(6915), 520-562.
59. Bronaugh, R.L., R.F. Stewart, and E.R. Congdon, Methods for in vitro percutaneous absorption studies II. Animal models for human skin. *Toxicology and Applied Pharmacology*, 1982. **62**(3), 481-488.
60. Menon, G.K., New insights into skin structure: Scratching the surface. *Advanced Drug Delivery Reviews*, 2002. **54**(SUPPL.), S3.
61. Pasparakis, M., I. Haase, and F.O. Nestle, Mechanisms regulating skin immunity and inflammation. *Nature Reviews Immunology*, 2014. **14**(5), 289-301.
62. Chen, L., R. Mirza, Y. Kwon, L.A. DiPietro, and T.J. Koh, The murine excisional wound model: Contraction revisited. *Wound Repair and Regeneration*, 2015. **23**(6), 874-877.
63. Gurtner, G.C., S. Werner, Y. Barrandon, and M.T. Longaker, Wound repair and regeneration. *Nature*, 2008. **453**(7193), 314-321.
64. Fang, R.C. and T.A. Mustoe, Animal models of wound healing: utility in transgenic mice. *J Biomater Sci Polym Ed*, 2008. **19**(8), 989-1005.
65. Witte, M.B. and A. Barbul, GENERAL PRINCIPLES OF WOUND HEALING. *Surgical Clinics of North America*, 1997. **77**(3), 509-528.

66. Mascré, G., S. Dekoninck, B. Drogat, K.K. Youssef, S. Brohée, P.A. Sotiropoulou, B.D. Simons, and C. Blanpain, Distinct contribution of stem and progenitor cells to epidermal maintenance. *Nature*, 2012. **489**(7415), 257-262.
67. Enzo, E., A. Secone Seconetti, M. Forcato, E. Tenedini, M.P. Polito, I. Sala, S. Carulli, R. Contin, C. Peano, E. Tagliafico, S. Biciato, S. Bondanza, and M. De Luca, Single-keratinocyte transcriptomic analyses identify different clonal types and proliferative potential mediated by FOXM1 in human epidermal stem cells. *Nature Communications*, 2021. **12**(1), 2505.
68. Kretzschmar, K. and F.M. Watt, Markers of epidermal stem cell subpopulations in adult mammalian skin. *Cold Spring Harb Perspect Med*, 2014. **4**(10).
69. Rittié, L., D.L. Sachs, J.S. Orringer, J.J. Voorhees, and G.J. Fisher, Eccrine Sweat Glands are Major Contributors to Reepithelialization of Human Wounds. *The American Journal of Pathology*, 2013. **182**(1), 163-171.
70. Evans, N.D., R.O.C. Oreffo, E. Healy, P.J. Thurner, and Y.H. Man, Epithelial mechanobiology, skin wound healing, and the stem cell niche. *Journal of the Mechanical Behavior of Biomedical Materials*, 2013. **28**, 397-409.
71. Doeing, D.C., J.L. Borowicz, and E.T. Crockett, Gender dimorphism in differential peripheral blood leukocyte counts in mice using cardiac, tail, foot, and saphenous vein puncture methods. *BMC Clinical Pathology*, 2003. **3**(1), 3.
72. Smithey, M.J., J.L. Uhrlaub, G. Li, M. Vukmanovic-Stejic, A.N. Akbar, and J. Nikolich-Zugich, Lost in translation: mice, men and cutaneous immunity in old age. *Biogerontology*, 2015. **16**(2), 203-208.
73. Gay, D., O. Kwon, Z. Zhang, M. Spata, M.V. Plikus, P.D. Holler, M. Ito, Z. Yang, E. Treffeisen, C.D. Kim, A. Nace, X. Zhang, S. Baratono, F. Wang, D.M. Ornitz, S.E. Millar, and G. Cotsarelis, Fgf9 from dermal $\gamma\delta$ T cells induces hair follicle neogenesis after wounding. *Nature Medicine*, 2013. **19**(7), 916-923.
74. Ganz, T., Defensins: antimicrobial peptides of innate immunity. *Nature Reviews Immunology*, 2003. **3**(9), 710-720.
75. Mangoni, M.L., A.M. McDermott, and M. Zasloff, Antimicrobial peptides and wound healing: biological and therapeutic considerations. *Experimental Dermatology*, 2016. **25**(3), 167-173.
76. Kim, K.K., M.C. Kugler, P.J. Wolters, L. Robillard, M.G. Galvez, A.N. Brumwell, D. Sheppard, and H.A. Chapman, Alveolar epithelial cell mesenchymal transition develops *in vivo* during pulmonary fibrosis and is regulated by the extracellular matrix. 2006. **103**(35), 13180-13185.
77. Xue, Y.M., C.Y. Deng, W. Wei, F.Z. Liu, H. Yang, Y. Liu, X. Li, Z. Wang, S.J. Kuang, S.L. Wu, and F. Rao, Macrophage migration inhibitory factor promotes cardiac fibroblast proliferation through the Src kinase signaling pathway. *Mol Med Rep*, 2018. **17**(2), 3425-3431.
78. Abe, R., S.C. Donnelly, T. Peng, R. Bucala, and C.N. Metz, Peripheral Blood Fibrocytes: Differentiation Pathway and Migration to Wound Sites. 2001. **166**(12), 7556-7562.
79. Opalenik, S.R. and J.M. Davidson, Fibroblast differentiation of bone marrow-derived cells during wound repair. *Faseb j*, 2005. **19**(11), 1561-3.
80. Meirelles, L.d.S., P.C. Chagastelles, and N.B. Nardi, Mesenchymal stem cells reside in virtually all post-natal organs and tissues. *Journal of Cell Science*, 2006. **119**(11), 2204-2213.
81. Zavadil, J. and E.P. Böttinger, TGF-beta and epithelial-to-mesenchymal transitions. *Oncogene*, 2005. **24**(37), 5764-74.
82. Kendall, R.T. and C.A. Feghali-Bostwick, Fibroblasts in fibrosis: novel roles and mediators. 2014. **5**(123).
83. Zhang, Y.E., Non-Smad pathways in TGF- β signaling. *Cell Research*, 2009. **19**(1), 128-139.
84. Wiig, H., K. Rubin, and R.K. Reed, New and active role of the interstitium in control of interstitial fluid pressure: Potential therapeutic consequences. *Acta Anaesthesiologica Scandinavica*, 2003. **47**(2), 111-121.
85. Broughton, G., 2nd, J.E. Janis, and C.E. Attinger, The basic science of wound healing. *Plast Reconstr Surg*, 2006. **117**(7 Suppl), 12s-34s.
86. Fibbe, W.E., J. Van Damme, A. Billiau, N. Duinkerken, E. Lurvink, P. Ralph, B.W. Altrock, K. Kaushansky, R. Willemze, and J.H. Falkenburg, Human fibroblasts produce granulocyte-CSF, macrophage-CSF, and granulocyte-macrophage-CSF following stimulation by interleukin-1 and poly(rI).poly(rC). *Blood*, 1988. **72**(3), 860-6.
87. Mustafa, M., B. Wondimu, M. Bakhtiet, and T. Modéer, Induction of interferon gamma in human gingival fibroblasts challenged with phytohaemagglutinin. *Cytokine*, 2000. **12**(4), 368-73.
88. Smola, H., G. Thiekötter, and N.E. Fusenig, Mutual induction of growth factor gene expression by epidermal-dermal cell interaction. *J Cell Biol*, 1993. **122**(2), 417-29.

89. Xia, Y.P., Y. Zhao, J. Marcus, P.A. Jimenez, S.M. Ruben, P.A. Moore, F. Khan, and T.A. Mustoe, Effects of keratinocyte growth factor-2 (KGF-2) on wound healing in an ischaemia-impaired rabbit ear model and on scar formation. *J Pathol*, 1999. **188**(4), 431-8.
90. Pierce, G.F., T.A. Mustoe, B.W. Altmann, T.F. Deuel, and A. Thomason, Role of platelet-derived growth factor in wound healing. *J Cell Biochem*, 1991. **45**(4), 319-26.
91. Regan, M.C., S.J. Kirk, H.L. Wasserkrug, and A. Barbul, The wound environment as a regulator of fibroblast phenotype. *J Surg Res*, 1991. **50**(5), 442-8.
92. Darby, I.A. and T.D. Hewitson, Fibroblast differentiation in wound healing and fibrosis. *Int Rev Cytol*, 2007. **257**, 143-79.
93. Goldman, R., Growth factors and chronic wound healing: past, present, and future. *Adv Skin Wound Care*, 2004. **17**(1), 24-35.
94. Hinz, B., Myofibroblasts. *Exp Eye Res*, 2016. **142**, 56-70.
95. Sandbo, N. and N. Dulin, Actin cytoskeleton in myofibroblast differentiation: ultrastructure defining form and driving function. *Transl Res*, 2011. **158**(4), 181-96.
96. Scharenberg, M.A., B.E. Pippenger, R. Sack, D. Zingg, J. Ferralli, S. Schenk, I. Martin, and R. Chiquet-Ehrismann, TGF- β -induced differentiation into myofibroblasts involves specific regulation of two MKL1 isoforms. *J Cell Sci*, 2014. **127**(Pt 5), 1079-91.
97. Zhang, Y., T. Musci, and R. Derynck, The tumor suppressor Smad4/DPC 4 as a central mediator of Smad function. *Curr Biol*, 1997. **7**(4), 270-6.
98. Carthy, J.M., A. Sundqvist, A. Heldin, H. van Dam, D. Kleetsas, C.H. Heldin, and A. Moustakas, Tamoxifen Inhibits TGF- β -Mediated Activation of Myofibroblasts by Blocking Non-Smad Signaling Through ERK1/2. *J Cell Physiol*, 2015. **230**(12), 3084-92.
99. Bloom, B.R. and B. Bennett, Mechanism of a reaction in vitro associated with delayed-type hypersensitivity. *Science*, 1966. **153**(3731), 80-2.
100. David, J.R., Delayed hypersensitivity in vitro: its mediation by cell-free substances formed by lymphoid cell-antigen interaction. *Proc Natl Acad Sci U S A*, 1966. **56**(1), 72-7.
101. Bauters, D., I. Scroyen, M. Van Hul, and H.R. Lijnen, Gelatinase A (MMP-2) promotes murine adipogenesis. *Biochim Biophys Acta*, 2015. **1850**(7), 1449-56.
102. Sun, H.W., J. Bernhagen, R. Bucala, and E. Lolis, Crystal structure at 2.6-Å resolution of human macrophage migration inhibitory factor. *Proc Natl Acad Sci U S A*, 1996. **93**(11), 5191-6.
103. Mischke, R., R. Kleemann, H. Brunner, and J. Bernhagen, Cross-linking and mutational analysis of the oligomerization state of the cytokine macrophage migration inhibitory factor (MIF). *FEBS Lett*, 1998. **427**(1), 85-90.
104. Mühlhahn, P., J. Bernhagen, M. Czisch, J. Georgescu, C. Renner, A. Ross, R. Bucala, and T.A. Holak, NMR characterization of structure, backbone dynamics, and glutathione binding of the human macrophage migration inhibitory factor (MIF). *Protein Sci*, 1996. **5**(10), 2095-103.
105. Sugimoto, H., M. Suzuki, A. Nakagawa, I. Tanaka, and J. Nishihira, Crystal structure of macrophage migration inhibitory factor from human \bar{A} lymphocyte at 2.1 Å resolution. *FEBS Letters*, 1996. **389**(2), 145-148.
106. Sun, H.W., M. Swope, C. Cinquina, S. Bedarkar, J. Bernhagen, R. Bucala, and E. Lolis, The subunit structure of human macrophage migration inhibitory factor: evidence for a trimer. *Protein Eng*, 1996. **9**(8), 631-5.
107. Suzuki, M., H. Sugimoto, A. Nakagawa, I. Tanaka, J. Nishihira, and M. Sakai, Crystal structure of the macrophage migration inhibitory factor from rat liver. *Nat Struct Biol*, 1996. **3**(3), 259-66.
108. Bacher, M., A. Meinhardt, H.Y. Lan, W. Mu, C.N. Metz, J.A. Chesney, T. Calandra, D. Gemsa, T. Donnelly, R.C. Atkins, and R. Bucala, Migration inhibitory factor expression in experimentally induced endotoxemia. *Am J Pathol*, 1997. **150**(1), 235-46.
109. Baugh, J.A. and R. Bucala, Macrophage migration inhibitory factor. *Crit Care Med*, 2002. **30**(1 Supp), S27-s35.
110. Calandra, T., J. Bernhagen, R.A. Mitchell, and R. Bucala, The macrophage is an important and previously unrecognized source of macrophage migration inhibitory factor. *J Exp Med*, 1994. **179**(6), 1895-902.
111. Fingerle-Rowson, G., P. Koch, R. Bikoff, X. Lin, C.N. Metz, F.S. Dhabhar, A. Meinhardt, and R. Bucala, Regulation of macrophage migration inhibitory factor expression by glucocorticoids in vivo. *Am J Pathol*, 2003. **162**(1), 47-56.
112. Lue, H., R. Kleemann, T. Calandra, T. Roger, and J. Bernhagen, Macrophage migration inhibitory factor (MIF): mechanisms of action and role in disease. *Microbes Infect*, 2002. **4**(4), 449-60.
113. Calandra, T. and T. Roger, Macrophage migration inhibitory factor: a regulator of innate immunity. *Nat Rev Immunol*, 2003. **3**(10), 791-800.

114. Bernhagen, J., T. Calandra, R.A. Mitchell, S.B. Martin, K.J. Tracey, W. Voelter, K.R. Manogue, A. Cerami, and R. Bucala, MIF is a pituitary-derived cytokine that potentiates lethal endotoxaemia. *Nature*, 1993. **365**(6448), 756-759.
115. Bucala, R. and S.C. Donnelly, Macrophage Migration Inhibitory Factor: A Probable Link between Inflammation and Cancer. *Immunity*, 2007. **26**(3), 281-285.
116. Hudson, J.D., M.A. Shoabi, R. Maestro, A. Carnero, G.J. Hannon, and D.H. Beach, A proinflammatory cytokine inhibits p53 tumor suppressor activity. *J Exp Med*, 1999. **190**(10), 1375-82.
117. Meyer-Siegler, K. and P.B. Hudson, Enhanced expression of macrophage migration inhibitory factor in prostatic adenocarcinoma metastases. *Urology*, 1996. **48**(3), 448-452.
118. Su, H., N. Na, X. Zhang, and Y. Zhao, The biological function and significance of CD74 in immune diseases. *Inflamm Res*, 2017. **66**(3), 209-216.
119. Alampour-Rajabi, S., O. El Bounkari, A. Rot, G. Müller-Newen, F. Bachelier, M. Gawaz, C. Weber, A. Schober, and J. Bernhagen, MIF interacts with CXCR7 to promote receptor internalization, ERK1/2 and ZAP-70 signaling, and lymphocyte chemotaxis. 2015. **29**(11), 4497-4511.
120. Bernhagen, J., R. Krohn, H. Lue, J.L. Gregory, A. Zerneck, R.R. Koenen, M. Dewor, I. Georgiev, A. Schober, L. Leng, T. Kooistra, G. Fingerle-Rowson, P. Ghezzi, R. Kleemann, S.R. McColl, R. Bucala, M.J. Hickey, and C. Weber, MIF is a noncognate ligand of CXC chemokine receptors in inflammatory and atherogenic cell recruitment. *Nat Med*, 2007. **13**(5), 587-96.
121. Binsky, I., M. Haran, D. Starlets, Y. Gore, F. Lantner, N. Harpaz, L. Leng, D.M. Goldenberg, L. Shvidel, A. Berrebi, R. Bucala, and I. Shachar, IL-8 secreted in a macrophage migration-inhibitory factor- and CD74-dependent manner regulates B cell chronic lymphocytic leukemia survival. *Proc Natl Acad Sci U S A*, 2007. **104**(33), 13408-13.
122. Tillmann, S., J. Bernhagen, and H. Noels, Arrest Functions of the MIF Ligand/Receptor Axes in Atherogenesis. *Front Immunol*, 2013. **4**, 115.
123. Weber, C., S. Kraemer, M. Drechsler, H. Lue, R.R. Koenen, A. Kapurniotu, A. Zerneck, and J. Bernhagen, Structural determinants of MIF functions in CXCR2-mediated inflammatory and atherogenic leukocyte recruitment. *Proc Natl Acad Sci U S A*, 2008. **105**(42), 16278-83.
124. Leng, L., C.N. Metz, Y. Fang, J. Xu, S. Donnelly, J. Baugh, T. Delohery, Y. Chen, R.A. Mitchell, and R. Bucala, MIF signal transduction initiated by binding to CD74. *J Exp Med*, 2003. **197**(11), 1467-76.
125. Naujokas, M.F., M. Morin, M.S. Anderson, M. Peterson, and J. Miller, The chondroitin sulfate form of invariant chain can enhance stimulation of T cell responses through interaction with CD44. *Cell*, 1993. **74**(2), 257-68.
126. Shi, X., L. Leng, T. Wang, W. Wang, X. Du, J. Li, C. McDonald, Z. Chen, J.W. Murphy, E. Lolis, P. Noble, W. Knudson, and R. Bucala, CD44 is the signaling component of the macrophage migration inhibitory factor-CD74 receptor complex. *Immunity*, 2006. **25**(4), 595-606.
127. Nasser, M.W., S.K. Raghuvanshi, D.J. Grant, V.R. Jala, K. Rajarathnam, and R.M. Richardson, Differential activation and regulation of CXCR1 and CXCR2 by CXCL8 monomer and dimer. *J Immunol*, 2009. **183**(5), 3425-32.
128. Crump, M.P., J.H. Gong, P. Loetscher, K. Rajarathnam, A. Amara, F. Arenzana-Seisdedos, J.L. Virelizier, M. Baggiolini, B.D. Sykes, and I. Clark-Lewis, Solution structure and basis for functional activity of stromal cell-derived factor-1; dissociation of CXCR4 activation from binding and inhibition of HIV-1. *Embo j*, 1997. **16**(23), 6996-7007.
129. Lacy, M., C. Kontos, M. Brandhofer, K. Hille, S. Gröning, D. Sinitski, P. Bourilhon, E. Rosenberg, C. Krammer, T. Thavayogarah, G. Pantouris, M. Bakou, C. Weber, E. Lolis, J. Bernhagen, and A. Kapurniotu, Identification of an Arg-Leu-Arg tripeptide that contributes to the binding interface between the cytokine MIF and the chemokine receptor CXCR4. *Sci Rep*, 2018. **8**(1), 5171.
130. Rajasekaran, D., S. Gröning, C. Schmitz, S. Zierow, N. Drucker, M. Bakou, K. Kohl, A. Mertens, H. Lue, C. Weber, A. Xiao, G. Luker, A. Kapurniotu, E. Lolis, and J. Bernhagen, Macrophage Migration Inhibitory Factor-CXCR4 Receptor Interactions: EVIDENCE FOR PARTIAL ALLOSTERIC AGONISM IN COMPARISON WITH CXCL12 CHEMOKINE. *J Biol Chem*, 2016. **291**(30), 15881-95.
131. Schwartz, V., H. Lue, S. Kraemer, J. Korbil, R. Krohn, K. Ohl, R. Bucala, C. Weber, and J. Bernhagen, A functional heteromeric MIF receptor formed by CD74 and CXCR4. *FEBS Lett*, 2009. **583**(17), 2749-57.
132. Merk, M., S. Zierow, L. Leng, R. Das, X. Du, W. Schulte, J. Fan, H. Lue, Y. Chen, H. Xiong, F. Chagnon, J. Bernhagen, E. Lolis, G. Mor, O. Lesur, and R. Bucala, The D-dopachrome

- tautomerase (DDT) gene product is a cytokine and functional homolog of macrophage migration inhibitory factor (MIF). 2011. **108**(34), E577-E585.
133. Sugimoto, H., M. Taniguchi, A. Nakagawa, I. Tanaka, M. Suzuki, and J. Nishihira, Crystal structure of human D-dopachrome tautomerase, a homologue of macrophage migration inhibitory factor, at 1.54 Å resolution. *Biochemistry*, 1999. **38**(11), 3268-79.
 134. Merk, M., R. Mitchell, S. Endres, and R.J.C. Bucala, D-dopachrome tautomerase (D-DT or MIF-2): doubling the MIF cytokine family. 2012. **59** 1, 10-7.
 135. Odh, G., A. Hindemith, A.M. Rosengren, E. Rosengren, and H. Rorsman, Isolation of a New Tautomerase Monitored by the Conversion of D-Dopachrome to 5,6-Dihydroxyindole. *Biochemical and Biophysical Research Communications*, 1993. **197**(2), 619-624.
 136. Rosengren, E., P. Aman, S. Thelin, C. Hansson, S. Ahlfors, P. Björk, L. Jacobsson, and H. Rorsman, The macrophage migration inhibitory factor MIF is a phenylpyruvate tautomerase. *FEBS Lett*, 1997. **417**(1), 85-8.
 137. Jankauskas, S.S., D.W.L. Wong, R. Bucala, S. Djudjaj, and P. Boor, Evolving complexity of MIF signaling. *Cellular Signalling*, 2019. **57**, 76-88.
 138. Hirokawa, J., S. Sakaue, S. Tagami, Y. Kawakami, M. Sakai, S. Nishi, and J. Nishihira, Identification of macrophage migration inhibitory factor in adipose tissue and its induction by tumor necrosis factor- α . *Biochem Biophys Res Commun*, 1997. **235**(1), 94-8.
 139. Skurk, T., C. Herder, I. Kräfft, S. Müller-Scholze, H. Hauner, and H. Kolb, Production and release of macrophage migration inhibitory factor from human adipocytes. *Endocrinology*, 2005. **146**(3), 1006-11.
 140. Karastergiou, K., I. Evans, N. Ogston, N. Miheisi, D. Nair, J.C. Kaski, M. Jahangiri, and V. Mohamed-Ali, Epicardial adipokines in obesity and coronary artery disease induce atherogenic changes in monocytes and endothelial cells. *Arterioscler Thromb Vasc Biol*, 2010. **30**(7), 1340-6.
 141. Iwata, T., H. Taniguchi, M. Kuwajima, T. Taniguchi, Y. Okuda, A. Sukeno, K. Ishimoto, N. Mizusawa, and K. Yoshimoto, The Action of D-Dopachrome Tautomerase as an Adipokine in Adipocyte Lipid Metabolism. *PLOS ONE*, 2012. **7**(3), e33402.
 142. Ishimoto, K., T. Iwata, H. Taniguchi, N. Mizusawa, E. Tanaka, and K. Yoshimoto, D-dopachrome tautomerase promotes IL-6 expression and inhibits adipogenesis in preadipocytes. *Cytokine*, 2012. **60**(3), 772-7.
 143. Ikeda, D., S. Sakaue, M. Kamigaki, H. Ohira, N. Itoh, Y. Ohtsuka, I. Tsujino, and M. Nishimura, Knockdown of macrophage migration inhibitory factor disrupts adipogenesis in 3T3-L1 cells. *Endocrinology*, 2008. **149**(12), 6037-42.
 144. Church, T.S., M.S. Willis, E.L. Priest, M.J. LaMonte, C.P. Earnest, W.J. Wilkinson, D.A. Wilson, and B.P. Giroir, Obesity, macrophage migration inhibitory factor, and weight loss. *International Journal of Obesity*, 2005. **29**(6), 675-681.
 145. Fain, J.N., D.S. Tichansky, and A.K. Madan, Most of the interleukin 1 receptor antagonist, cathepsin S, macrophage migration inhibitory factor, nerve growth factor, and interleukin 18 release by explants of human adipose tissue is by the non-fat cells, not by the adipocytes. *Metabolism*, 2006. **55**(8), 1113-21.
 146. Kim, H., S. Lee, H.J. Kim, M.H. Kong, Y.R. Kim, S.H. Kang, K. Lee, L. Leng, B. Lee, C.G. Park, Y. Kook, B. Kim, and R. Bucala, Elevated levels of macrophage migration inhibitory factor in women with metabolic syndrome. *Horm Metab Res*, 2011. **43**(9), 642-5.
 147. Lolis, E. and R. Bucala, Macrophage migration inhibitory factor. *Expert Opin Ther Targets*, 2003. **7**(2), 153-64.
 148. Heinrichs, D., M.L. Berres, M. Coeuru, M. Knauel, A. Nellen, P. Fischer, C. Philippeit, R. Bucala, C. Trautwein, H.E. Wasmuth, and J. Bernhagen, Protective role of macrophage migration inhibitory factor in nonalcoholic steatohepatitis. *Faseb j*, 2014. **28**(12), 5136-47.
 149. Verschuren, L., T. Kooistra, J. Bernhagen, P.J. Voshol, D.M. Ouwens, M. van Erk, J. de Vries-van der Weij, L. Leng, J.H. van Bockel, K.W. van Dijk, G. Fingerle-Rowson, R. Bucala, and R. Kleemann, MIF deficiency reduces chronic inflammation in white adipose tissue and impairs the development of insulin resistance, glucose intolerance, and associated atherosclerotic disease. *Circ Res*, 2009. **105**(1), 99-107.
 150. Calandra, T., J. Bernhagen, C.N. Metz, L.A. Spiegel, M. Bacher, T. Donnelly, A. Cerami, and R. Bucala, MIF as a glucocorticoid-induced modulator of cytokine production. *Nature*, 1995. **377**(6544), 68-71.
 151. Kim, B.-S., B. Breuer, K. Arnke, T. Ruhl, T. Hofer, D. Simons, M. Knobe, B. Ganse, M. Guidi, J. Beier, P. Fuchs, N. Pallua, J. Bernhagen, and G. Grieb, The effect of the macrophage

- migration inhibitory factor (MIF) on excisional wound healing in vivo. *Journal of Plastic Surgery and Hand Surgery*, 2020. **54**, 1-8.
152. Kim, B.S., P.V. Tilstam, K. Arnke, L. Leng, T. Ruhl, M. Piecychna, W. Schulte, M. Sauler, F.S. Frueh, G. Storti, N. Lindenblatt, P. Giovanoli, N. Pallua, J. Bernhagen, and R. Bucala, Differential regulation of macrophage activation by the MIF cytokine superfamily members MIF and MIF-2 in adipose tissue during endotoxemia. *Faseb j*, 2020. **34**(3), 4219-4233.
 153. Calandra, T., B. Echtenacher, D.L. Roy, J. Pugin, C.N. Metz, L. Hültner, D. Heumann, D. Männel, R. Bucala, and M.P. Glauser, Protection from septic shock by neutralization of macrophage migration inhibitory factor. *Nat Med*, 2000. **6**(2), 164-70.
 154. Gilliver, S.C., E. Emmerson, J. Bernhagen, and M.J. Hardman, MIF: a key player in cutaneous biology and wound healing. 2011. **20**(1), 1-6.
 155. Abe, R., T. Shimizu, A. Ohkawara, and J. Nishihira, Enhancement of macrophage migration inhibitory factor (MIF) expression in injured epidermis and cultured fibroblasts. *Biochim Biophys Acta*, 2000. **1500**(1), 1-9.
 156. Zhao, Y., T. Shimizu, J. Nishihira, Y. Koyama, T. Kushibiki, A. Honda, H. Watanabe, R. Abe, Y. Tabata, and H. Shimizu, Tissue regeneration using macrophage migration inhibitory factor-impregnated gelatin microbeads in cutaneous wounds. *Am J Pathol*, 2005. **167**(6), 1519-29.
 157. Kitaichi, N., T. Shimizu, K. Yoshida, A. Honda, Y. Yoshihisa, S. Kase, K. Ohgami, O. Norisugi, T. Makino, J. Nishihira, S.-i. Yamagishi, and S. Ohno, Macrophage migration inhibitory factor ameliorates UV-induced photokeratitis in mice. *Experimental Eye Research*, 2008. **86**(6), 929-935.
 158. Marsh, L.M., L. Cakarova, G. Kwapiszewska, W. von Wulffen, S. Herold, W. Seeger, and J. Lohmeyer, Surface expression of CD74 by type II alveolar epithelial cells: a potential mechanism for macrophage migration inhibitory factor-induced epithelial repair. *Am J Physiol Lung Cell Mol Physiol*, 2009. **296**(3), L442-52.
 159. Ashcroft, G.S., S.J. Mills, K. Lei, L. Gibbons, M.J. Jeong, M. Taniguchi, M. Burow, M.A. Horan, S.M. Wahl, and T. Nakayama, Estrogen modulates cutaneous wound healing by downregulating macrophage migration inhibitory factor. *J Clin Invest*, 2003. **111**(9), 1309-18.
 160. Kim, B.-S., N. Pallua, J. Bernhagen, and R. Bucala, The macrophage migration inhibitory factor protein superfamily in obesity and wound repair. *Experimental & Molecular Medicine*, 2015. **47**(5), e161-e161.
 161. Sonesson, B., E. Rosengren, A.S. Hansson, and C. Hansson, UVB-induced inflammation gives increased d-dopachrome tautomerase activity in blister fluid which correlates with macrophage migration inhibitory factor. *Exp Dermatol*, 2003. **12**(3), 278-82.
 162. Kim, B.S., P.V. Tilstam, S.S. Hwang, D. Simons, W. Schulte, L. Leng, M. Sauler, B. Ganse, L. Averdunk, R. Kopp, C. Stoppe, J. Bernhagen, N. Pallua, and R. Bucala, D-dopachrome tautomerase in adipose tissue inflammation and wound repair. *J Cell Mol Med*, 2017. **21**(1), 35-45.
 163. Sindrilaru, A., T. Peters, S. Wieschalka, C. Baican, A. Baican, H. Peter, A. Hainzl, S. Schatz, Y. Qi, A. Schlecht, J.M. Weiss, M. Wlaschek, C. Sunderkötter, and K. Scharffetter-Kochanek, An unrestrained proinflammatory M1 macrophage population induced by iron impairs wound healing in humans and mice. *J Clin Invest*, 2011. **121**(3), 985-97.
 164. Schneider, C.A., W.S. Rasband, and K.W. Eliceiri, NIH Image to ImageJ: 25 years of image analysis. *Nature Methods*, 2012. **9**(7), 671-675.
 165. Lutz, T.A. and S.C. Woods, Overview of animal models of obesity. *Curr Protoc Pharmacol*, 2012. **Chapter 5**, Unit5.61.
 166. Ansell, D.M., L. Campbell, H.A. Thomason, A. Brass, and M.J. Hardman, A statistical analysis of murine incisional and excisional acute wound models. *Wound repair and regeneration : official publication of the Wound Healing Society [and] the European Tissue Repair Society*, 2014. **22**(2), 281-287.
 167. Goldner, J., A modification of the masson trichrome technique for routine laboratory purposes. *The American journal of pathology*, 1938. **14**(2), 237-243.
 168. Chomczynski, P. and N. Sacchi, Single-step method of RNA isolation by acid guanidinium thiocyanate-phenol-chloroform extraction. *Anal Biochem*, 1987. **162**(1), 156-9.
 169. Taylor, S.C., K. Nadeau, M. Abbasi, C. Lachance, M. Nguyen, and J. Fenrich, The Ultimate qPCR Experiment: Producing Publication Quality, Reproducible Data the First Time. *Trends in Biotechnology*, 2019. **37**(7), 761-774.
 170. Negmadjanov, U., Z. Godic, F. Rizvi, L. Emelyanova, G. Ross, J. Richards, E.L. Holmuhamedov, and A. Jahangir, TGF- β 1-mediated differentiation of fibroblasts is associated

- with increased mitochondrial content and cellular respiration. *PLoS one*, 2015. **10**(4), e0123046-e0123046.
171. Thorey, I.S., B. Hinz, A. Hoeflich, S. Kaesler, P. Bugnon, M. Elmlinger, R. Wanke, E. Wolf, and S. Werner, Transgenic mice reveal novel activities of growth hormone in wound repair, angiogenesis, and myofibroblast differentiation. *J Biol Chem*, 2004. **279**(25), 26674-84.
 172. Tilstam, P.V., G. Pantouris, M. Corman, M. Andreoli, K. Mahboubi, G. Davis, X. Du, L. Leng, E. Lolis, and R. Bucala, A selective small-molecule inhibitor of macrophage migration inhibitory factor-2 (MIF-2), a MIF cytokine superfamily member, inhibits MIF-2 biological activity. *The Journal of biological chemistry*, 2019. **294**(49), 18522-18531.
 173. Yuan, B., J.A. Broadbent, J. Huan, and H. Yang, The Effects of Adipose Stem Cell-Conditioned Media on Fibrogenesis of Dermal Fibroblasts Stimulated by Transforming Growth Factor- β 1. *Journal of burn care & research : official publication of the American Burn Association*, 2018. **39**(1), 129-140.
 174. Goodson, W.H., 3rd and T.K. Hunt, Deficient collagen formation by obese mice in a standard wound model. *Am J Surg*, 1979. **138**(5), 692-4.
 175. Kleinert, M., C. Clemmensen, S.M. Hofmann, M.C. Moore, S. Renner, S.C. Woods, P. Huypens, J. Beckers, M.H. de Angelis, A. Schürmann, M. Bakhti, M. Klingenspor, M. Heiman, A.D. Cherrington, M. Ristow, H. Lickert, E. Wolf, P.J. Havel, T.D. Müller, and M.H. Tschöp, Animal models of obesity and diabetes mellitus. *Nature Reviews Endocrinology*, 2018. **14**(3), 140-162.
 176. Gerdes, J., H. Lemke, H. Baisch, H.H. Wacker, U. Schwab, and H. Stein, Cell cycle analysis of a cell proliferation-associated human nuclear antigen defined by the monoclonal antibody Ki-67. *J Immunol*, 1984. **133**(4), 1710-5.
 177. Noguchi, F., T. Nakajima, S. Inui, J.K. Reddy, and S. Itami, Alteration of Skin Wound Healing in Keratinocyte-Specific Mediator Complex Subunit 1 Null Mice. *PLOS ONE*, 2014. **9**(8), e102271.
 178. Lin, H.-H., D.E. Faunce, M. Stacey, A. Terajewicz, T. Nakamura, J. Zhang-Hoover, M. Kerley, M.L. Mucenski, S. Gordon, and J. Stein-Streilein, The macrophage F4/80 receptor is required for the induction of antigen-specific efferent regulatory T cells in peripheral tolerance. *The Journal of experimental medicine*, 2005. **201**(10), 1615-1625.
 179. Shih, S.-C., G.S. Robinson, C.A. Perruzzi, A. Calvo, K. Desai, J.E. Green, I.U. Ali, L.E.H. Smith, and D.R. Senger, Molecular profiling of angiogenesis markers. *The American journal of pathology*, 2002. **161**(1), 35-41.
 180. Hesketh, M., K.B. Sahin, Z.E. West, and R.Z. Murray, Macrophage Phenotypes Regulate Scar Formation and Chronic Wound Healing. *Int J Mol Sci*, 2017. **18**(7).
 181. Silva, K.R., S. Liechocki, J.R. Carneiro, C. Claudio-da-Silva, C.M. Maya-Monteiro, R. Borojevic, and L.S. Baptista, Stromal-vascular fraction content and adipose stem cell behavior are altered in morbid obese and post bariatric surgery ex-obese women. *Stem Cell Res Ther*, 2015. **6**(1), 72.
 182. Kopcewicz, M., K. Walenzik, J. Bukowska, A. Kur-Piotrowska, S. Machcinska, J.M. Gimble, and B. Gawronska-Kozak, Cutaneous wound healing in aged, high fat diet-induced obese female or male C57BL/6 mice. *Aging*, 2020. **12**(8), 7066-7111.
 183. Xiao, X., I. Gaffar, P. Guo, J. Wiersch, S. Fischbach, L. Peirish, Z. Song, Y. El-Gohary, K. Prasad, C. Shiota, and G.K. Gittes, M2 macrophages promote beta-cell proliferation by up-regulation of SMAD7. 2014. **111**(13), E1211-E1220.
 184. Cheng, Y.W., Z.B. Zhang, B.D. Lan, J.R. Lin, X.H. Chen, L.R. Kong, L. Xu, C.C. Ruan, and P.J. Gao, PDGF-D activation by macrophage-derived uPA promotes AngII-induced cardiac remodeling in obese mice. *J Exp Med*, 2021. **218**(9).
 185. Javelaud, D. and A. Mauviel, Crosstalk mechanisms between the mitogen-activated protein kinase pathways and Smad signaling downstream of TGF- β : implications for carcinogenesis. *Oncogene*, 2005. **24**(37), 5742-5750.
 186. Cheng, X., W. Gao, Y. Dang, X. Liu, Y. Li, X. Peng, and X. Ye, Both ERK/MAPK and TGF-Beta/Smad Signaling Pathways Play a Role in the Kidney Fibrosis of Diabetic Mice Accelerated by Blood Glucose Fluctuation. *Journal of Diabetes Research*, 2013. **2013**, 463740.
 187. Hough, C., M. Radu, and J.J. Doré, Tgf-beta induced Erk phosphorylation of smad linker region regulates smad signaling. *PLoS One*, 2012. **7**(8), e42513.
 188. Liu, X., S.Q. Sun, A. Hassid, and R.S. Ostrom, cAMP inhibits transforming growth factor-beta-stimulated collagen synthesis via inhibition of extracellular signal-regulated kinase 1/2 and Smad signaling in cardiac fibroblasts. *Mol Pharmacol*, 2006. **70**(6), 1992-2003.

189. Derynck, R. and Y.E. Zhang, Smad-dependent and Smad-independent pathways in TGF- β family signalling. *Nature*, 2003. **425**(6958), 577-584.
190. Hayashida, T., M. Decaestecker, and H.W. Schnaper, Cross-talk between ERK MAP kinase and Smad signaling pathways enhances TGF-beta-dependent responses in human mesangial cells. *Faseb j*, 2003. **17**(11), 1576-8.
191. Krassovka, J.M., C.V. Suschek, M. Prost, V. Grotheer, J.L. Schiefer, E. Demir, P.C. Fuchs, J. Windolf, E.K. Stürmer, and C. Opländer, The impact of non-toxic blue light (453 nm) on cellular antioxidative capacity, TGF- β 1 signaling, and myofibrogenesis of human skin fibroblasts. *J Photochem Photobiol B*, 2020. **209**, 111952.
192. Wang, X.-Q., S. Lee, H. Wilson, M. Seeger, H. Iordanov, N. Gatla, A. Whittington, D. Bach, J.-Y. Lu, and A.S. Paller, Ganglioside GM3 depletion reverses impaired wound healing in diabetic mice by activating IGF-1 and insulin receptors. *The Journal of investigative dermatology*, 2014. **134**(5), 1446-1455.
193. Xu, P., F. Gärtner, A. Gihring, C. Liu, T. Burster, M. Wabitsch, U. Knippschild, and S. Paschke, Influence of obesity on remodeling of lung tissue and organization of extracellular matrix after blunt thorax trauma. *Respiratory Research*, 2020. **21**(1), 238.
194. Andersen, T., A. Dejgaard, A. Astrup, and C. Gluud, Increased plasma fibronectin concentrations in obesity: normalization during weight loss. *Acta Med Scand*, 1987. **222**(3), 275-9.
195. Ekaidem, I.S., D.M. Bolarin, A.E. Udoh, S.J. Etuk, and C.E.J. Udiog, Plasma fibronectin concentration in obese/overweight pregnant women: a possible risk factor for preeclampsia. *Indian journal of clinical biochemistry : IJCB*, 2011. **26**(2), 187-192.
196. Jiang, T., Z. Wang, G. Proctor, S. Moskowitz, S.E. Liebman, T. Rogers, M.S. Lucia, J. Li, and M. Levi, Diet-induced obesity in C57BL/6J mice causes increased renal lipid accumulation and glomerulosclerosis via a sterol regulatory element-binding protein-1c-dependent pathway. *J Biol Chem*, 2005. **280**(37), 32317-25.
197. Ongenaes, K.C., T.J. Phillips, and H.-Y. Park, Level of Fibronectin mRNA Is Markedly Increased in Human Chronic Wounds. *Dermatologic Surgery*, 2000. **26**(5).
198. Stoffels, J.M.J., C. Zhao, and W. Baron, Fibronectin in tissue regeneration: timely disassembly of the scaffold is necessary to complete the build. *Cellular and Molecular Life Sciences*, 2013. **70**(22), 4243-4253.
199. Tonnesen, M.G., X. Feng, and R.A. Clark, Angiogenesis in wound healing. *J Investig Dermatol Symp Proc*, 2000. **5**(1), 40-6.
200. Streit, M., P. Velasco, L. Riccardi, L. Spencer, L.F. Brown, L. Janes, B. Lange-Asschenfeldt, K. Yano, T. Hawighorst, L. Iruela-Arispe, and M. Detmar, Thrombospondin-1 suppresses wound healing and granulation tissue formation in the skin of transgenic mice. *The EMBO Journal*, 2000. **19**(13), 3272-3282.
201. Corvera, S. and O. Gealekman, Adipose tissue angiogenesis: impact on obesity and type-2 diabetes. *Biochimica et biophysica acta*, 2014. **1842**(3), 463-472.
202. Wagner, I.J., C. Szpalski, R.J. Allen, Jr., E.H. Davidson, O. Canizares, P.B. Saadeh, and S.M. Warren, Obesity impairs wound closure through a vasculogenic mechanism. *Wound Repair Regen*, 2012. **20**(4), 512-22.
203. Reggio, S., C. Rouault, C. Poitou, J.C. Bichet, E. Prifti, J.L. Bouillot, S. Rizkalla, D. Lacasa, J. Tordjman, and K. Clément, Increased Basement Membrane Components in Adipose Tissue During Obesity: Links With TGF β and Metabolic Phenotypes. *J Clin Endocrinol Metab*, 2016. **101**(6), 2578-87.
204. Danilenko, D.M., B.D. Ring, J.E. Tarpley, B. Morris, G.Y. Van, A. Morawiecki, W. Callahan, M. Goldenberg, S. Hershenson, and G.F. Pierce, Growth factors in porcine full and partial thickness burn repair. Differing targets and effects of keratinocyte growth factor, platelet-derived growth factor-BB, epidermal growth factor, and neu differentiation factor. *Am J Pathol*, 1995. **147**(5), 1261-77.
205. Jimenez, P., Keratinocyte growth factor-2: A wound healing agent with epidermal and dermal activity. *Wound Rep Regen*, 1997. **5**, A115.
206. Werner, S., M. Breeden, G. Hübner, D.G. Greenhalgh, and M.T. Longaker, Induction of Keratinocyte Growth Factor Expression Is reduced and Delayed During Wound Healing in the Genetically Diabetic Mouse. *Journal of Investigative Dermatology*, 1994. **103**(4), 469-473.
207. Aoki, M. and T. Murase, Obesity-associated insulin resistance adversely affects skin function. *PLOS ONE*, 2019. **14**(10), e0223528.

208. Taylor, K.R., A.E. Costanzo, and J.M. Jameson, Dysfunctional $\gamma\delta$ T Cells Contribute to Impaired Keratinocyte Homeostasis in Mouse Models of Obesity. *Journal of Investigative Dermatology*, 2011. **131**(12), 2409-2418.
209. Sanale, A.R., J.D. Firth, V.J. Uitto, and E.E. Putnins, Keratinocyte growth factor (KGF)-1 and -2 protein and gene expression in human gingival fibroblasts. *J Periodontal Res*, 2002. **37**(1), 66-74.
210. Fang, X., L. Wang, L. Shi, C. Chen, Q. Wang, C. Bai, and X. Wang, Protective effects of keratinocyte growth factor-2 on ischemia-reperfusion-induced lung injury in rats. *Am J Respir Cell Mol Biol*, 2014. **50**(6), 1156-65.
211. Jimenez, P.A. and M.A. Rampy, Keratinocyte growth factor-2 accelerates wound healing in incisional wounds. *J Surg Res*, 1999. **81**(2), 238-42.
212. Pan, H., C. Shi, R. Yang, G. Xi, C. Lu, X. Wang, J. Chen, L. Chen, and J. Pan, Controlled release of KGF-2 for regulation of wound healing by KGF-2 complexed with "lotus seedpod surface-like" porous microsphere. *Journal of Materials Chemistry B*, 2021. **9**.
213. Tong, L., J. Bi, X. Zhu, G. Wang, J. Liu, L. Rong, Q. Wang, N. Xu, M. Zhong, D. Zhu, Y. Song, and C. Bai, Keratinocyte growth factor-2 is protective in lipopolysaccharide-induced acute lung injury in rats. *Respir Physiol Neurobiol*, 2014. **201**, 7-14.
214. Corson, L.B., Y. Yamanaka, K.M. Lai, and J. Rossant, Spatial and temporal patterns of ERK signaling during mouse embryogenesis. *Development*, 2003. **130**(19), 4527-37.
215. Nakao, Y., T. Mitsuyasu, S. Kawano, N. Nakamura, S. Kanda, and S. Nakamura, Fibroblast growth factors 7 and 10 are involved in ameloblastoma proliferation via the mitogen-activated protein kinase pathway. *Int J Oncol*, 2013. **43**(5), 1377-84.
216. Upadhyay, D., E. Correa-Meyer, J.I. Sznajder, and D.W. Kamp, FGF-10 prevents mechanical stretch-induced alveolar epithelial cell DNA damage via MAPK activation. *Am J Physiol Lung Cell Mol Physiol*, 2003. **284**(2), L350-9.
217. Watson, J. and C. Francavilla, Regulation of FGF10 Signaling in Development and Disease. *Frontiers in genetics*, 2018. **9**, 500-500.
218. Perl, A.-K.T. and E. Gale, FGF signaling is required for myofibroblast differentiation during alveolar regeneration. *American journal of physiology. Lung cellular and molecular physiology*, 2009. **297**(2), L299-L308.
219. Zhou, Y., S. Yoshida, Y. Kubo, T. Yoshimura, Y. Kobayashi, T. Nakama, M. Yamaguchi, K. Ishikawa, Y. Oshima, and T. Ishibashi, Different distributions of M1 and M2 macrophages in a mouse model of laser-induced choroidal neovascularization. *Molecular medicine reports*, 2017. **15**(6), 3949-3956.
220. Lumeng, C.N., J.L. Bodzin, and A.R. Saltiel, Obesity induces a phenotypic switch in adipose tissue macrophage polarization. *J Clin Invest*, 2007. **117**(1), 175-84.
221. Allott, E.H., J. Lysaght, M.C. Cathcart, C.L. Donohoe, R. Cummins, S.A. McGarrigle, E. Kay, J.V. Reynolds, and G.P. Pidgeon, MMP9 expression in oesophageal adenocarcinoma is upregulated with visceral obesity and is associated with poor tumour differentiation. *Molecular Carcinogenesis*, 2013. **52**(2), 144-154.
222. Chavey, C., B. Mari, M.N. Monthouel, S. Bonnafous, P. Anglard, E. Van Obberghen, and S. Tartare-Deckert, Matrix metalloproteinases are differentially expressed in adipose tissue during obesity and modulate adipocyte differentiation. *J Biol Chem*, 2003. **278**(14), 11888-96.
223. Unal, R., A. Yao-Borengasser, V. Varma, N. Rasouli, C. Labbate, P.A. Kern, and G. Ranganathan, Matrix metalloproteinase-9 is increased in obese subjects and decreases in response to pioglitazone. *The Journal of clinical endocrinology and metabolism*, 2010. **95**(6), 2993-3001.
224. Longo, M., F. Zatterale, J. Naderi, L. Parrillo, P. Formisano, G.A. Raciti, F. Beguinot, and C. Miele, Adipose Tissue Dysfunction as Determinant of Obesity-Associated Metabolic Complications. *International journal of molecular sciences*, 2019. **20**(9), 2358.
225. Almine, J.F., S.G. Wise, and A.S. Weiss, Elastin signaling in wound repair. *Birth Defects Res C Embryo Today*, 2012. **96**(3), 248-57.
226. Lin, D., T.H. Chun, and L. Kang, Adipose extracellular matrix remodelling in obesity and insulin resistance. *Biochem Pharmacol*, 2016. **119**, 8-16.
227. Ruiz-Ojeda, F.J., A. Méndez-Gutiérrez, C.M. Aguilera, and J. Plaza-Díaz, Extracellular Matrix Remodeling of Adipose Tissue in Obesity and Metabolic Diseases. *International journal of molecular sciences*, 2019. **20**(19), 4888.
228. Spencer, M., R. Unal, B. Zhu, N. Rasouli, R.E. McGehee, Jr., C.A. Peterson, and P.A. Kern, Adipose tissue extracellular matrix and vascular abnormalities in obesity and insulin resistance. *The Journal of clinical endocrinology and metabolism*, 2011. **96**(12), E1990-E1998.

Discussion

229. Hough, C. and J.J. Doré, TGF- β induced activation of ERK regulates Smad degradation. *Cancer Research*, 2006. **66**(8 Supplement), 634-635.
230. Kretzschmar, M., J. Doody, I. Timokhina, and J. Massagué, A mechanism of repression of TGFbeta/ Smad signaling by oncogenic Ras. *Genes Dev*, 1999. **13**(7), 804-16.
231. Matsuura, I., G. Wang, D. He, and F. Liu, Identification and characterization of ERK MAP kinase phosphorylation sites in Smad3. *Biochemistry*, 2005. **44**(37), 12546-53.
232. Bucala, R. and I. Shachar, The Integral Role of CD74 in Antigen Presentation, MIF Signal Transduction, and B Cell Survival and Homeostasis. *Mini reviews in medicinal chemistry*, 2015. **14**.
233. Bi, H., H. Li, C. Zhang, Y. Mao, F. Nie, Y. Xing, W. Sha, X. Wang, D.M. Irwin, and H. Tan, Stromal vascular fraction promotes migration of fibroblasts and angiogenesis through regulation of extracellular matrix in the skin wound healing process. *Stem Cell Res Ther*, 2019. **10**(1), 302.
234. Chae, D.S., S. Han, M. Son, and S.W. Kim, Stromal vascular fraction shows robust wound healing through high chemotactic and epithelialization property. *Cytotherapy*, 2017. **19**(4), 543-554.
235. Han, S., H.M. Sun, K.C. Hwang, and S.W. Kim, Adipose-Derived Stromal Vascular Fraction Cells: Update on Clinical Utility and Efficacy. *Crit Rev Eukaryot Gene Expr*, 2015. **25**(2), 145-52.
236. Trevor, L.V., K. Riches-Suman, A.L. Mahajan, and M.J. Thornton, Adipose Tissue: A Source of Stem Cells with Potential for Regenerative Therapies for Wound Healing. *Journal of Clinical Medicine*, 2020. **9**(7), 2161.
237. Mebratu, Y. and Y. Tesfaigzi, How ERK1/2 activation controls cell proliferation and cell death: Is subcellular localization the answer? *Cell cycle (Georgetown, Tex.)*, 2009. **8**(8), 1168-1175.
238. Pearson, G., F. Robinson, T. Beers Gibson, B.E. Xu, M. Karandikar, K. Berman, and M.H. Cobb, Mitogen-activated protein (MAP) kinase pathways: regulation and physiological functions. *Endocr Rev*, 2001. **22**(2), 153-83.
239. Schevzov, G., A.J. Kee, B. Wang, V.B. Sequeira, J. Hook, J.D. Coombes, C.A. Lucas, J.R. Stehn, E.A. Musgrove, A. Cretu, R. Assoian, T. Fath, T. Hanoch, R. Seger, I. Pleines, B.T. Kile, E.C. Hardeman, and P.W. Gunning, Regulation of cell proliferation by ERK and signal-dependent nuclear translocation of ERK is dependent on Tm5NM1-containing actin filaments. *Molecular biology of the cell*, 2015. **26**(13), 2475-2490.
240. Sever, R. and J.S. Brugge, Signal transduction in cancer. *Cold Spring Harb Perspect Med*, 2015. **5**(4).
241. Cagnol, S. and J.C. Chambard, ERK and cell death: mechanisms of ERK-induced cell death--apoptosis, autophagy and senescence. *Febs j*, 2010. **277**(1), 2-21.
242. Tang, D., D. Wu, A. Hirao, J.M. Lahti, L. Liu, B. Mazza, V.J. Kidd, T.W. Mak, and A.J. Ingram, ERK activation mediates cell cycle arrest and apoptosis after DNA damage independently of p53. *J Biol Chem*, 2002. **277**(15), 12710-7.

Appendix

Score Sheet

Projekt: Die Rolle der MIF Proteinsuperfamilie bei Adipositas, Diabetes mellitus und Wundheilung

Lizenznummer des Projekts: ZH004/19

Überwachungsprotokoll während der Versuchsdauer: Wundheilungsverlauf

Kontaktpersonen für Nordsee		E-Mail		Telefon		Privat	
Kevin Arnke (Laborant)	kevin.arnke@uzh.ch	044 252 6052	076 236 61 31				
Dr. med. Bong-Sung Kim	bong-sung.kim@uzh.ch	044 252 2132	-				

Experimentator	Kfz-Nr.	Tier-ID	Datum der Wundsetzung		Iniboles KG	
			Start	Ende	Start	Ende
Kevin Arnke						

10% KG-Verlust	16% KG-Verlust

Euthanasie	
Datum:	
KG:	

Verlaufs-Körpergewicht direkt vor der Operation

Datum	Verwechslung / KG der Beobachtung	Zeit	Gewicht KG	Ø Exzelsorenwunden [mm ²]		Inzelsorenwunden		Wundstatus	Körperhaltung	Kollagen	Kollagen/Sonstige
				Start	Ende	Start	Ende				
	-3										
	-4										
	-5										
	0 (Heilung der Wunden)										
	1 (H)										
	2 (H)										
	3 (H)										
	4 (H)										
	5 (H)										
	6										
	7										
	8										
	9										
	10										
	11										
	12										
	13										
	14										
	15										
	16										
	17										
	18										
	19										
	20										
	21										

Score Legend

Score Legende

	0	1	2	3
Aktivität	Unauffällige / spontane Bewegungen und Striegeln	Langsame Reaktionen auf Stimulierungen	Bewegung erst nach mittlerer Störung. Anzeichen einer Apathie	Hyperaktives, sich wiederholendes und zwanghaftes Verhalten. Apathisch: immobil, auch bei Stimulation.
körperliches Erscheinen	Keine Veränderungen	Anzeichen von Kratzern und übermäßiger Pflege. Alopezie mit normaler Haut (keine oder geringfügige Wunden)	Kratzen und Anzeichen von Psychopathologie (Automutilation/-aggression, Alopezie mit offenen Stellen/ Dermatitis)	Psychopathologie - Automutilation/-aggression. *Offene Stellen heilen auch nach Behandlung mit Salbe nicht.
KG-Verlust	Keine Gewichtsverlust	Gewichtsverlust von <10% des initialen KG ¹	Gewichtsverlust zwischen 10% und 15% des initialen KG ¹	Gewichtsverlust von >15% des initialen KG ¹
Körperhaltung	Normal	Leicht gebeugt	Abnormale Körperhaltung und leicht gebeugter Gang	Stark gebeugt/zusammen gekauert. Atmungsprobleme.
Wundstatus	Keine sichtlichen Entzündungen	Geringe Entzündung/ Rötung des Wundbereiches (Teil der Wundheilung)	übermäßige Entzündung der Wundregion. Schwellung der Wunde.	Nekrose

¹initiales KG: Körpergewicht direkt vor der Operation

Ein Veterinär wird kontaktiert, sobald mindestens ein Score bei 2 beobachtet wird. Wenn nötig wird das Tier euthanasiert.
 Wenn ein Score von 1 oder 2 bei "körperliches Erscheinen" beobachtet wird, werden die betroffenen Stellen zweimal täglich mit Salbe (Bepanthen, Merfen, o.ä.)² behandelt. Sofern nötig, wird unter Absprache mit dem Veterinär das Tier zusätzlich mit Buprenorphin (0,1 mg/kg KG) analgetisch behandelt. Nach 2 h wird das betroffene Tier erneut begutachtet. Ist keine Besserung zu erkennen, wird das entsprechende Tier euthanasiert.

Wenn ein Score von 1 oder 2 bei "Aktivität" oder "Körperhaltung" beobachtet wird, wird das betroffene Tier alle 3 h über den Tag kontrolliert und genauer dokumentiert. Gegebenenfalls wird Rat eines Veterinärs hinzugezogen. Zusätzlich werden Schüsseln mit aufgeweichtem Futter und Wasser in den Käfig gestellt. Ebenfalls bekommt es eine zusätzliche Analgesie mittels subkutaner Injektion von Buprenorphin (0,1 mg/kg KG). Sollte sich dabei nach 2 h keine Besserung zeigen, wird das Tier euthanasiert.
 Wenn ein Score von 1 oder 2 bei "Wundstatus" beobachtet wird, wird die Wunde mit frischer, steriler Saline von aussen behandelt und mit einem neuen, transparentem Pflaster abgedeckt.

Das Tier wird euthanasiert, sobald ein Score von 2 in einem Bereich über drei Tage lang trotz entsprechenden Gegenmassnahmen anhält.

Das Tier wird sofort euthanasiert, sobald ein Bereich ein Score von 3 aufweist.

Acknowledgements

First of all, I would like to thank Bong (PD Dr. med. Bong-Sung Kim), not only for giving me the opportunity to do my thesis, but also for his motivation, supervision, support throughout my thesis, and especially for the collegial relationship. He taught me to critically question myself and the results and to move on from them.

I would like also to thank Prof. Dr. Jürgen Bernhagen, for the opportunity to do my thesis under his supervision and for his support.

A big thank goes to PD Dr. Paolo Cinelli and the working group (Giulia Bortoli, Yannik Kalbas, Sonja Märsmann, Yvonne Neldner, Florencia Vonaburg, Tina Wentz, Dr. Stefan Wolf) for the friendly acceptance into the working group and the weekly lab meetings, for the scientific support, and particularly for the family atmosphere in the laboratory and during lunch. The fun we had made me daily come back to the laboratory again and again, even in tough times.




A very special thanks goes to Yvonne, who was not only a good lab colleague, moreover a really good friend, who gave me not only scientific support in the lab, but also emotional support.

I want to express my sincere gratitude to the whole BZL team, who supported me during all my animal experiments.

My warmest thanks goes to my best friends Ann-Ka, Axel, Lisa, Max, Moe and Steve. They have always been there for me and have been supportive.

Finally yet importantly, I would like to thank my parents and their partners, my older sister Denise with her husband Lukas and their children, as well as my little brother Justin.

Affidavit

	LUDWIG- MAXIMILIANS- UNIVERSITÄT MÜNCHEN	Promotionsbüro Medizinische Fakultät		
Affidavit				

Arnke, Kevin

Surname, first name

Street

Zip code, town, country

I hereby declare, that the submitted thesis entitled:

The Role of MIF-2 in Obesity-induced Wound Healing Disorder

is my own work. I have only used the sources indicated and have not made unauthorized use of services of a third party. Where the work of others has been quoted or reproduced, the source is always given.

I further declare that the submitted thesis or parts thereof have not been presented as part of an examination degree to any other university.

Zurich, 28.07.2022
place, date

Kevin Arnke
Signature doctoral candidate

Curriculum vitae

Personal Details

Kevin Arnke

Education

- Since 01/2022 **Research assistant, Center for Surgical Research**
09/2018 – 01/2022 **Doctoral thesis, Department of Plastic Surgery and Hand Surgery, USZ, Switzerland and Institute for Stroke and Dementia Research, LMU University Hospital, Germany**
“The Role of Macrophage Migration Inhibitory Factor (MIF) Family Proteins in Wound Repair and Obesity”
- 10/2015 – 01/2018 **MSc in Chemistry, WWU Münster, Germany**
08/2017 – 01/2018 **Master thesis, Institute of Pharmaceutical and Medicinal Chemistry, WWU Germany**
“Cell Surface Display of Laccase BcoCotA on *E. coli* and Development of Activity Assays”
- 10/2012 – 08/2015 **BSc in Chemistry, WWU Münster, Germany**
05/2015 – 07/2015 **Bachelor thesis, Institute of Inorganic and Analytical Chemistry, WWU Münster, Germany**
“Crystal growth experiments on intermetallic cerium compounds”
- 07/2003 – 06/2012 **Abitur, Arnold-Janssen-Gymnasium, Neuenkirchen, Germany**

Practical Experience

- 01/2018 – 07/2018 **Research Assistant, Institute of Biochemistry, WWU Münster, Germany**
 - Modification of the 5' and 3' ends of mRNAs
 - Transfection and injection of mRNA into cells and zebrafish embryos with subsequent microscopic analysis
- 10/2017 – 01/2018 **Tutor for „Allgemeine Chemie“ (BSc Chemie), WWU Münster, Germany**
- 02/2017 – 08/2017 **Research Internship, Autodisplay Biotech GmbH, Düsseldorf, Germany**
*Cell Surface Display of Laccase BcoCotA on *E. coli* and *P. putida**
- 09/2016 – 02/2017 **Erasmus, Institute of Pharmaceutical Chemistry and Biology, Università degli Studi di Palermo, Sicily, Italy**
Synthesis of new anti-inflammatory Drugs based on Betaxanthines
- 02/2016 – 04/2016 **Research Internship, Institute of Pharmaceutical and Medicinal Chemistry, WWU Germany**
Synthesis of new Inhibitors of the NMFA Receptor Subunit NR 2B
- 08/2015 – 10/2015 **Tutor for „Vorbereitungskurs in Chemie für Nebenfächler“, WWU Münster, Germany**
- seit 01/2014 **Employee at „Tanzträume“, Münster, Germany**
- 04/2011 – 12/2015 **Employee at „ADTV Tanzschule Jobmann“, Rheine, Germany**

04/2012 – 09/2012 **Employee at Temporary Employment Agency “I-Tegra”,
Osnabrück, Germany**

Languages

German	Native speaker
English	Proficient
French	Advanced knowledge (DELF B1)
Italian	Advanced knowledge (B1)
Latin	Latinum

Methods and Other Qualifications

Education for Persons Responsible for Directing Animal Experiments (study directors; LTK2)
Basic education for study directors for animal experiments
Handling of laboratory rodents including obesity and wound healing models
Good Clinical Practice (GCP) 1 – 3
Cultivation of bacteria
Isolation and cultivation of primary human skin and fat cells
Various microbiological and cytological analysis (transformation and transfection of DNA/mRNA, different activity assays, proliferation and migration assays, live/dead staining, cell differentiation)
Molecular biological methods (Western Blot, SDS-PAGE, agarose gel electrophoresis, ELISA, qPCR, error-prone PCR)
Microscopy (Fluorescence, confocal LASER-scanning)
Histology and Immunhistology
Flow cytometry
Mass spectrometry

Computer Skills

MS-Office, GraphPad Prism, Adobe Illustrator, Adobe Photoshop, Image J

Zurich, 28.07.2022

List of publications

Kim BS, Tilstam PV, Arnke K, Leng L, Ruhl T, Piecychna M, Schulte W, Sauler M, Frueh FS, Storti G, Lindenblatt N, Giovanoli P, Pallua N, Bernhagen J, Bucala R. Differential regulation of macrophage activation by the MIF cytokine superfamily members MIF and MIF-2 in adipose tissue during endotoxemia. *FASEB J.* 2020 Mar;34(3):4219-4233.

Kim BS, Breuer B, Arnke K, Ruhl T, Hofer T, Simons D, Knobe M, Ganse B, Guidi M, Beier JP, Fuchs PC, Pallua N, Bernhagen J, Grieb G. The effect of the macrophage migration inhibitory factor (MIF) on excisional wound healing *in vivo*. *J Plast Surg Hand Surg.* 2020 Jun;54(3):137-144.